# Characterization of Bacteriophage λ Displaying Epidermal Growth Factor in the Uptake, Infiltration and Formation of HT29 Spheroids

by

Haein Huh

A thesis
presented to the University of Waterloo
in fulfilment of the
thesis requirement for the degree of
Master of Science
in
Pharmacy

Waterloo, Ontario, Canada, 2019

## AUTHOR'S DECLARATION

I hereby declare that I am the sole author of this thesis. This is a true copy of this thesis, including any required final revisions, as accepted by my examiners. I understand that my thesis may be made electronically available to the public.

# Abstract

Solid tumours are characterized by a complex structure comprised of extracellular matrix, neoplastic cells and stromal cells, each presenting a barrier to conventional anticancer chemotherapy as well as carrier-mediated drug delivery. Poor penetration of therapeutics into the interstitial tumour microenvironment remains a challenge, with drugs accumulating primarily in the regions of tumours that are situated closer to blood vessels. Bacteriophages do not infect eukaryotic cells, yet they have been shown to penetrate mucosal barriers, including multiple layers of epithelial cells and endothelium. In this work, we used NIH3T3 fibroblast and HT29 colon adenocarcinoma multicellular spheroids to represent the stroma and parenchyma of solid tumours and then to examine infiltration of bacteriophages as a means of delivering therapeutic cargo. By using phage display technology to decorate the surface of λ bacteriophage with epidermal growth factor (EGF), we compared the cell-phage interactions between wildtype phages and EGF-displaying phages, including the assessment of phages' capacity to traverse the tumour interstitium, to be subjected to cell internalization and their effects on spheroid growth. Both wildtype and EGF-displaying λ phages were observed to adhere to the HT29 and NIH3T3 spheroids and to internalize into cells as early as 30 min following administration. EGF-phage treatment also slowed HT29 spheroid growth – demonstrating a delay in initial aggregation and formation of loosely-organized structures that led to much smaller spheroid formation in the latter stages of growth. These results support the potential for the therapeutic employment of bacteriophages as nanocarriers for targeted delivery.

# ACKNOWLEDGEMENTS:

I wish to thank both my supervisors Drs. Jonathan Blay & Roderick Slavcev for their endless support and patience. I was extremely fortunate to receive guidance from two supervisors that believed in me and have given me opportunities to grow as a researcher.

I would also like to thank my advisory committee members, Dr. Brenda Coomber, Dr. Praveen Nekkar and Dr. Marc Aucoin for providing me with valuable insight throughout the duration of my project. I am also thankful for Roger Chen and Dr. Marianna Foldvari for their assistance with the confocal microscope. I would also like to thank Julia Fux for all her help in the lab and ensuring everything ran smoothly.

I am fortunate to have had wonderful lab mates: Shirley, Deep, Heba, Jesse, Jessica, Heather, Bogdan and Alex. They provided me with endless laughs, shoulders to cry on and pastries – my graduate studies would not have been possible without them.

Lastly, I would like to thank my parents, brother and my best friends for their unconditional love and support. Thank you for everything you do, you guys are truly my world.

# TABLE OF CONTENTS

List of Tables ..... viii
List of Figures ..... ix
Table of Abbreviations ..... xi
Chapter 1: Introduction ..... 1
1.0 Perspective ..... 1
1.1 Solid tumours and the tumour microenvironment ..... 2
1.1.1 Extracellular matrix (ECM) ..... 3
1.1.2 Interstitial fluid pressure ..... 4
1.1.3 Hypoxic core ..... 5
1.2 Solid tumour therapy ..... 6
1.3 Cell receptors ..... 7
1.3.1 Epidermal growth factor receptor and other ErbB family members ..... 8
1.3.2 EGFR in cancer therapy ..... 11
1.3.3 HT29 colon adenocarcinoma and EGFR expression ..... 12
1.4 3D Cultures ..... 14
1.4.1 Multicellular spheroids ..... 14
1.4.2 Parameters affecting drug penetration into solid tumours ..... 17
1.5 Bacteriophages ..... 20
1.5.1 Phage internalization and cellular trafficking in eukaryotic cells ..... 23
1.5.2 Phage display ..... 24
1.5.3 Tuneable λ phage display ..... 26
1.5.4 Phages and cancer ..... 27
1.5.5 Immune response to phage therapy ..... 28
1.5.6 Phage penetration of solid tumours ..... 30
Chapter 2: Rationale, Objectives and Hypothesis ..... 32
2.1 Rationale ..... 32
2.2 Hypothesis ..... 33
2.3 Objectives ..... 33
Chapter 3: Materials and Methods ..... 34
3.1 Buffers and solutions ..... 34
3.2 Cell culture ..... 37

3.3 Spheroid culture ..... 37
3.4 Phage display ..... 38
3.4.1 Transformation ..... 38
3.4.2 Phage lysate preparation ..... 39
3.5 Phage purification ..... 40
3.6 Phage titration and standard plaque forming unit assays ..... 40
3.7 Assessing phage viability ..... 40
3.8 EDTA sensitivity assay ..... 41
3.9 Labeling of phage capsid for imaging ..... 41
3.10 Confocal microscopy for phage visualization in spheroids ..... 42
3.11 Internalization assay ..... 42
3.12 Phage λ and effects on spheroid growth ..... 44
3.13 MTT assay ..... 45
3.14 3D Toxicity assay ..... 46
3.15 Spheroid embedding in paraffin ..... 46
3.16 Statistical analysis ..... 47
Chapter 4: Results ..... 48
4.1 Characterization of spheroids with different seeding densities ..... 48
4.2 Generation of EGF-displaying λ phages and λ packaging tolerance of gpD::EGF fusion . 52
4.2.1 Assessment of phage viability in response to temperature ..... 54
4.2.3 EDTA resistance by λ wildtype and λ D::EGF phages ..... 55
4.3 Bacteriophage λ infiltration of multicellular spheroids ..... 56
4.3.1 Interaction of λ phages with NIH3T3 spheroids ..... 56
4.3.2 Interaction of λ D::EGF phages with HT29 spheroids ..... 59
4.4 Bacteriophage λ internalization by HT29 cells ..... 64
4.4.1 Quantitation of internalized bacteriophage λ particles ..... 65
4.5 Effects of EGF display on bacteriophage λ on spheroid growth ..... 70
4.5.1 Effects of EGF-displaying phages on initial cell aggregation ..... 73
4.5.2 Effects of phages on fully-formed HT29 spheroids ..... 76
4.6 Cytotoxicity of D::EGF λ phages to HT29 cells ..... 77
4.7 Spheroid embedding and sectioning ..... 80
Chapter 5: Discussion ..... 81

5.2 Bacteriophage λ accumulates in multicellular spheroids ..... 81
5.3 EGF display enhances bacteriophage uptake into HT29 cells ..... 86
5.4 EGF-displaying bacteriophage λ slows spheroid growth and HT29 cell aggregation ..... 88
5.5 Bacteriophage λ is not cytotoxic to HT29 cells ..... 91
Chapter 6: Conclusion ..... 93
Chapter 7: Future Research Objectives ..... 95
References ..... 98

# LIST OF TABLES

Table 1: Summary of bacteria, phage, plasmids and eukaryotic cells used in this study ..... 36

Table 2: HT29, NIH3T3 and HCT116 spheroid diameters are dependent on initial cell-seeding densities..... 51

Table 3: pD::EGF complements the *Dam15* mutation and increases viability of λF7 phages in the absence of suppressor host *E. coli* ..... 53

Table 4: Prolonged exposure of phages at 37°C decreases λ phage infectivity. ..... 54

Table 5: Susceptibility of Display Phage to EDTA ..... 55

Table 6: Effect of Trypsin-EDTA on phage viability. ..... 67

Table 7: EGF display increases the recovery of phage particles from HT29 spheroids..... 68

Table 8: HT29 spheroids treated with D::EGF phages are smaller on day 20 ..... 72

# LIST OF FIGURES

Figure 1: Schematic diagram of receptor tyrosine kinase (RTK). ..... 10

Figure 2: A schematic diagram of a multicellular spheroid. ..... 15

Figure 3: A schematic diagram of bacteriophage λ and one face of the capsid. ..... 27

Figure 4: Internalization assay. ..... 44

Figure 5: Growth of HT29 spheroids at various seeding concentrations. ..... 48

Figure 6: Growth of A549 spheroids at various seeding concentrations. ..... 49

Figure 7 Growth of MDA-MB-231 spheroids at various seeding concentrations. ..... 49

Figure 8: Growth of A2780 spheroids at various seeding concentrations ..... 50

Figure 9: HT29 cells seeded at various concentrations after 7 d. ..... 52

Figure 10: Optical cross-sections of NIH3T3 spheroids treated with fluorescent λ phages. ..... 57

Figure 11: NIH3T3 spheroid treated with polyethylene glycol. ..... 58

Figure 12: Optical cross-sections of HT29 spheroids treated with wildtype phages and EGF-displaying phages for 30 min (top) and 4 h (bottom). . ..... 60

Figure 13: Representative cross-sections of HT29 spheroids treated with wildtype phages and EGF-displaying phages for 8 h (top) and 24 h (bottom). ..... 61

Figure 14: Collective Z-stacks of HT29 spheroids treated with A. EGF-displaying phages and B. wildtype phages (bottom) for 24 h. ..... 63

Figure 15: Phage-associated fluorescence emitted inter- and intracellularly of HT29 cells. ..... 64

Figure 16: Testing the action of ammonium chloride as a lysosomotropic agent to improve phage recovery ..... 64

Figure 17: Percent internalization of phages determined from HT29 spheroids. ..... 64

Figure 18: Effects of D::EGF phages and wildtype phages on the growth of HT29 spheroids. . . 71

Figure 19: HT29 cells co-seeded with D::EGF phages or wildtype phages.. ..... 73

Figure 20: Growth of pre-chilled HT29 cells with phages. ..... 74

Figure 21: Effects of wildtype or Hi-D::EGF phages on HT29 spheroids grown for 5 d.. ..... 76

Figure 22: HT29 cell proliferation (MTT) assay in response to phage treatment relative to control. ..... 78

Figure 23: HT29 spheroid cell viabilities relative to control in response to phage treatment.. ... 79

# TABLE OF ABBREVIATIONS

| | |
|---|---|
| 5-FU | Fluorouracil |
| A2780 | Human ovarian cancer cell line |
| A549 | Adenocarcinomic human alveolar basal epithelial cells |
| AAVP | Adeno-associated virus/phage |
| ANOVA | Analysis of variation |
| ATCC | American Type Culture Collection |
| ATP | Adenosine triphosphate |
| B16 | Mouse melanoma cells |
| BB4 | Suppressor *E. coli* strain *(supE supF hdR)* that is a high efficiency plating natural host for bacteriophage λ and amber mutant derivatives |
| *BRAF* | Gene that encodes proto-oncogene *B-Raf*, involved in sending signals inside cells involved in directing cell growth |
| BSA | Bovine serum albumin |
| C6 | Rat glioma cells |
| CI | λ repressor gene product, allows phage to reside in lysogenic state |
| *cI857* | A common temperature-sensitive allele of the *λ cI* repressor |
| COS-1 | Fibroblast-like cells derived from monkey kidney tissue |
| *D* | Gene encoding gene product gpD |
| gpD::EGF | EGF peptide fused onto the gpD capsid protein expressed by a suppressor host carrying the *D::EGF* fusion plasmid. |
| DMEM | Dulbecco's Modified Eagle's Medium |
| DMSO | Dimethyl sulfoxide |
| ECM | Extracellular matrix |
| EDTA | Ethylenediaminetetraacetic acid, a chelating agent that possesses the ability to sequester divalent metal cations such as $Mg^{2+}$ |
| EGF | Epidermal growth factor |
| eGFP | Gene encoding enhanced green fluorescent protein |

| | |
|---|---|
| EGFR | Epidermal growth factor receptor |
| EOP | Efficiency of plating, the relative viability of phage sample in comparison to a positive control |
| EPR | Enhanced permeability and retention effect |
| ErbB | Family of proteins containing four receptor tyrosine kinases |
| Erk | Extracellular signal–regulated kinases |
| FACS | Fluorescence-activated cell sorter |
| FBS | Foetal bovine serum |
| FGF2 | Fibroblast growth factor |
| $G_1$ | Gap 1 phase, first of four phases in the cell cycle in eukaryotic cell division |
| GAGs | Glycosaminoglycans, long branched polysaccharides consisting of amino sugar with uronic sugar or galactose. |
| GI | Gastrointestinal |
| gp23 | Major capsid protein of T4 phage |
| gp24 | Bacteriophage T4 capsid vertex protein gp24 |
| gp41 | Glycoprotein 41 is a subunit of the envelope protein complex of retroviruses, including human immunodeficiency virus (HIV) |
| gpD | λ gene product D, a major structural protein in the λ phage capsid head |
| gpDQ68S | Allele conferred from growing λF7 on amber suppressor strain W3101 SupD (*serU132*) which inserts amino acid serine in place of the amber stop codon |
| gpDQ68Y | Allele conferred from growing λF7 on amber suppressor strain W3101 SupF (*tyrT5888*) which inserts amino acid tyrosine in place of the amber stop codon |
| gpE | λ gene *E* product – major structural protein in the λ phage capsid |
| gpV | Tail protein of phage λ |
| Grb2 | Growth factor receptor-bound protein 2 |
| HCT-116 | Human colon cancer cell line |
| HER-2/neu | Human epidermal growth factor receptor 2 |

| | |
|---|---|
| Hi-D::EGF phage | λF7 phage with maximal EGF surface decoration. Generated using SupD *E. coli* host at 37 ° C |
| HIF-1 | Hypoxia inducible factor-1 |
| HLA | Human leukocyte antigen |
| HPEV1 | Human parechovirus 1 |
| HT29 | Human colon adenocarcinoma cell line |
| IF γ | Interferon γ |
| IFP | Interstitial fluid pressure |
| IgG | Immunoglobulin G antibody isotype |
| IL | Interleukin |
| IL1RN | Anti-inflammatory IL1 receptor antagonist |
| KGD | Lysine-Glycine-Aspartic acid |
| *KRAS* | Gene that encodes K-Ras that is part of the RAS/MAPK pathway |
| LB | Luria Bertani broth, a widely used rich culture medium, for growth of bacteria and phage |
| Lo-D::EGF phage | λF7 phages with 40% less surface decoration than Hi-D::EGF phages. Generated using SupF *E. coli* host at 37 ° C |
| LOX | Lysyl oxidase |
| M13 | A filamentous ssDNA bacteriophage |
| mAbs | Monoclonal antibodies |
| MAPK | Mitogen-activated protein kinases |
| MCTS | Multicellular tumour spheroids |
| MDA-MB-231 | Highly aggressive, invasive human breast cancer cell line |
| MEK | Mitogen-activated protein kinase kinase |
| MPG | Cell penetrating peptide, short amphipathic peptides forming stable nanoparticles with nucleic acids |
| MTT | 3-(4,5-dimethylthiazol-2-yl)-2,5- diphenyltetrazolium bromide |
| NIH3T3 | Mouse fibroblast cells |
| OSF-2 | Osteoblast-specific factor 2 |

| | |
|---|---|
| PBMC | Peripheral blood mononuclear cells |
| PBS | Phosphate buffered saline |
| pD | Plasmid-borne D, resultant of the complementation of *Dam15* from a plasmid |
| PEG | Polyethylene glycol |
| PFU | Plaque forming unit—single immobilized phage that grows to form a plaque on an agar cell lawn. A means of calculating lysate titer |
| PI(3) | Phosphoinositide 3-kinase |
| PKC | Protein kinase C |
| p-PDGFR-β | Platelet-derived growth factor receptor beta protein encoded by the PDGFRB gene |
| pPL451 | High copy plasmid vector under the control of temperature sensitive repressor, CI857 |
| PTP1B | Protein tyrosine phosphatase |
| RES | Reticuloendothelial system |
| RGD | Arginine-glycine-aspartic acid |
| RTK | Receptor tyrosine kinase |
| SDS | Sodium dodecyl sulfate |
| serU132 | Mutation encoding amber suppressor strain W3101 SupD |
| Soc | Major coat protein of T4 phage, present in ~870 copies |
| SOCS3 | Suppressor of cytokine signaling 3 |
| Src | Proto-oncogene tyrosine-protein kinase |
| STAT | Signal transducer and activator of transcription |
| Sup-/sup | A wild type *E. coli* strain that does not confer any suppressor activity |
| Sup+ /sup+ | A mutant *E. coli* strain that confers suppressor activity to conditional mutations |
| SupD/*supD* | A tRNA mutation in *E. coli* that suppresses the amber stop codon conditional mutation (UAG) by reading this codon and inserting instead a serine amino acid |
| SupF/*supF* | A tRNA mutation of *E. coli* that suppresses the amber stop codon by inserting instead a tyrosine amino acid at this codon |

| | |
|---|---|
| SV40 | Simian virus 40, a polyomavirus that is found in both monkeys and humans |
| T4 | Member of the lytic T-even myoviridae bacteriophage of *E. coli* that is only capable of undergoing a lytic lifecycle |
| T7 | Member of the type T podoviridae bacteriophage family that infects *E. coli.* This phage is only capable of undergoing a lytic lifecycle |
| TAT | Gene product of the tat gene, the "trans-activator of transcription", from HIV-1 which acts as a regulatory protein by dramatically enhancing endocytosis and the efficiency of viral transcription |
| TGF- α | Transforming growth factor-α |
| TKI | Tyrosine kinase inhibitors |
| TNF- α | Tumour necrosis factor-α |
| tRNA | Transfer RNA, physical link between the nucleotide sequence of nucleic acids (DNA/RNA) and the amino acid sequence of proteins |
| tyrT5888 | Mutation encoding amber suppressor strain W3101 SupF |
| UAG | Amber stop codon |
| VEGF | Vascular endothelial growth factor |
| W3101 | *E. coli* strain (*F-, galT22, λ-, IN(rrnD-rrnE)1, rph-1*) that is a high efficiency plating natural host for bacteriophage λ |
| WT phages | λF7 phages without any surface decoration |
| λDam | λ phage that contains an amber mutation within the gene for protein gpD and thus can only produce wild-type length gpD alleles within specialized strains of *E. coli* |
| λF7 | Synonymous with λ*Dam15Dam15imm21cI*[Tts] that possesses a defective (suppressible) D gene and the immunity region (*imm*) of phage 21 |

# Chapter 1: Introduction

## 1.0 Perspective

Drug delivery technology has advanced in the recent years; however, the development of an efficient delivery system into solid tumours is still much needed. Ideally, this system would confer: i) specific targeting to minimize drug-associated systemic toxic effects; ii) effective extravasation into the tumour interstitium; iii) effective diffusion through the dense tumour extracellular matrix; and iv) internalization into desired cells to deliver drug payload. Various nanocarriers have been examined for their potential to improve the bioavailability and preferential accumulation in the tumour site. Oftentimes, these particles are found situated closest to the vessel from which they extravasated from in vivo and do not achieve effective infiltration into the tumour (Tannock et al., 2002).

Bacteriophages (phages), which are bacterial viruses, have a strong potential as a drug delivery vehicle and offer new avenues in anticancer therapy. Tumour-homing peptides and ligands of overexpressed receptors on tumour cell surfaces can be fused to phage capsid proteins for targeting. Phages are unlikely to undergo alterations in their tropism, which is a major concern with the exploitation of oncolytic viruses in anticancer therapy (Raja et al., 2018). Phages have demonstrated the ability to bypass the epithelium and endothelium and can accumulate in various mammalian tissues and organs following their administration (Dabrowska et al., 2005). Additionally, the production of phages is relatively low, and cost of phage purification appears to be declining with the advancements in technology (Mancuso, Shi, & Malik, 2018). Although transfection with phages for anticancer therapy has been explored, the interaction of phages with neoplastic cells in 3-dimensional cell culture has not yet been described to date.

This project was an exploratory study assessing the potential of bacteriophages as a tumour nanocarrier system. Multicellular spheroids were used to model the tightly-packed tumour interstitium and responses to the application of λ phages were described. Phages displaying ligands for overexpressed receptors were also examined in their accumulation in spheroids.

## 1.1 Solid tumours and the tumour microenvironment

The complex and dynamic processes of tumourigenesis highlight the need for the development of effective treatment. Different cellular and non-cellular elements of the tumour microenvironment have hindered the applications of emerging antineoplastic, low-weight molecules. Cellular resistance to anticancer drugs is caused by mechanisms such as drug export, changes in drug metabolism and mutations in drug targets that activate survival signaling pathways or inactivate death signaling pathways (Gottesman, 2002). Effective drug delivery adds another layer of complexity in treatment due to the pathophysiology of the tumour microenvironment. This includes irregular vasculature that generates considerable variations throughout the tumour microenvironment, creating regions that are hypoxic and poorly perfused (Mueller-Klieser, 1997). Different exposures to nutrients and oxygen cause variable proliferation rates in cells that then respond differently to drugs (Khawar, Kim, & Kuh, 2015). To achieve sufficient cytotoxicity in tumour cells, systemically administered anti-cancer drugs need to reach the tumour vasculature network, extravasate across the vessel into the interstitial space and reach each tumour cell at a pharmacologically-effective dose (Dreher et al., 2006b; Sriraman, Aryasomayajula, & Torchilin, 2014; Ying et al., 2010). For successful cancer treatment, all tumour cells must be accessible by the drug, otherwise survival of a few cells could lead to tumour recurrence for the patient. This is difficult for most conventional chemotherapeutic drugs to achieve. Hence, much attention has been directed to the development of novel drug delivery

methods for which optimal surface physio-chemical properties can be conferred to maximize tumour accumulation. Components of the tumour microenvironment that impede the therapeutic course of drug delivery are further discussed below.

### 1.1.1 Extracellular matrix (ECM)

A major component of the tumour stroma is the extracellular matrix (ECM), which is a network of collagen, elastin fibers, proteoglycans and hyaluronic acid present in the basement membrane and the looser matrix of the interstitial space (Yue, 2014). ECM provides structural integrity for tissues, modulates cell function, and serves as reservoirs for growth factors and signaling molecules (Yue, 2014). ECM components, however, will physically impede immune cells and therapeutic drugs from effectively penetrating into the tumour. Furthermore, ECM composition will be altered as proteins and growth modulators become overexpressed in the tumour microenvironment. Such molecules include osteoblast-specific factor 2 (OSF-2), which is involved in cell adhesion (Bao et al., 2004; Malanchi et al., 2012); versican, a large chondroitin sulfate proteoglycan (Ricciardelli et al., 1998); and hyaluronan, a glycosaminoglycan that is often deposited in solid tumour and has been implicated in epithelial-to-mesenchymal transition (EMT) and drug resistance (Kultti et al., 2014; Toole & Slomiany, 2008). Notably, collagen, a protein of the connective tissue that provides tensile strength, increases in its deposition over time with tumour progression and serves as a primary barrier against drug penetration (Cox et al., 2013; Provenzano et al., 2008). Collagen accumulation has been associated with ECM remodelling, which is caused by the aberrant expression of the enzyme lysyl oxidase (LOX). LOX mediates collagen cross-linking resulting in enhanced tumour cell survival, metastasis and overall tumour stiffness (Cox et al., 2013; Provenzano et al., 2008; Wang, Hsia, & Shieh, 2017). Netti et al. demonstrated the correlation between an extended collagen network and poor

penetration of model proteins, IgG and BSA, using xenografted tumours from four different tumour lines: human colon adenocarcinoma (LS174T), human glioblastoma (U87), human soft tissue sarcoma (HTS 26T) and murine mammary carcinoma (MCalV) (Netti, Berk, Swartz, Grodzinsky, & Jain, 2000). Accumulation of these proteins was poorer in U87 and HTS26T tumours. Histological staining showed that collagen and proteoglycan in these two tumours were well-defined and organized, likely contributing to resistance to macromolecular drug penetration. Enzymes such as collagenase have been used to digest these ECM proteins to improve penetration of nanoparticles (Netti et al., 2000; Svishchev & Goncharov, 1990).

### 1.1.2 Interstitial fluid pressure

The irregular vasculature in solid tumours consists of excessively-branched, dilated, leaky vessels with loosely-attached pericytes (Tredan, Galmarini, Patel, & Tannock, 2007). Vessels are highly heterogenous in tumours and can cause variable blood flow to tumour tissues – this limits oxygen and nutrient access for cells, ultimately influencing metastasis and sensitivity to drug treatment to poorly perfused cells (discussed below) (Aznavoorian et al., 1990; Vaupel, Kallinowski, & Okunieff, 1989). Drugs diffuse down their concentration or pressure gradients, but as the network of vessels have high resistance to blood flow, drugs may instead be pulled into tissues via osmotic forces (Sriraman et al., 2014). Moreover, these irregularities in tumour tissues can be exacerbated by the lack of a proper lymphatic drainage, resulting in the accumulation of fluids and increased interstitial fluid pressure (IFP) (Ferretti et al., 2015; Padera et al., 2002). IFP can vary between tumours of the same histological type, each then responding differently to chemotherapy or radiation (Curti et al., 1993). Normal interstitial pressure is close to atmospheric, the excess pressure ranging from 1-3 mm Hg. These incremental values can be elevated to up to 100 mm Hg in tumour tissues, which often correlates to poor survival and

treatment responses in patients (Kłosowska-Wardęga et al., 2009; Milosevic et al., 2004; Sen et al., 2011; Simonsen et al., 2012; Willett et al., 2004). IFP is also directly associated with tumour angiogenesis, whereby pro-angiogenic and anti-angiogenic factors are upregulated and downregulated in tumours, respectively (Huang & Bao, 2004). Blocking angiogenesis has shown to improve drug penetration against the pressure gradient (Kłosowska-Wardęga et al., 2009; Tong et al., 2004; Willett et al., 2004). Angiogenesis can be downregulated by inhibiting vascular endothelial growth factor (VEGF), which is a family of secreted polypeptides that regulates blood vessel formation, or by blocking platelet-derived growth factor receptor (PDGF-R), which is a tyrosine-protein kinase that promotes blood vessel development when bound by a growth factor (Kłosowska-Wardęga et al., 2009). PDGF-R is localized in the cells of mesenchymal origin, such as neurons and vascular smooth muscle cells, and is often overexpressed in tumour cells (Shen et al., 2012). Imatinib is a drug that binds to p-PDGFR-β and has been shown to downregulate VEGF, reduce IFP and increase tumour oxygenation (Vlahovic et al., 2006). Similarly, the VEGF-specific antibody bevacizumab has shown to decrease microvascular density in five of six patients with rectal tumours (Willett et al., 2004).

### 1.1.3 Hypoxic core

Gradients of nutrients and oxygen levels are established in tumour tissues, with rapidly proliferating cells situated closer to the vasculature where levels are highest (Tredan et al., 2007). In well-vascularized tissues, cells are localized within 50-100 μm of perfused blood vessels; this distance can increase up to 200 μm for tumour cells, severely impairing blood flow and poor oxygen delivery to cells in tumour tissues (Bilski, Daub, & Chignell, 2002). One study revealed that hypoxic (≤5 mmHg) and anoxic values were reached 70-80 μm and 150 μm away from the vessel, respectively (Helmlinger et al., 1997). Hypoxia is associated with the malignant

phenotypes of tumours, inducing genes that express angiogenic and metastatic factors (Harada, Kizaka-Kondoh, & Hiraoka, 2005). Extracellular acidity of pH 6.5 – 7.0 is also a common feature in areas distal from the vasculature in tumours and is a direct result of accumulated $CO_2$ and other metabolites produced from anaerobic glycolysis, such as lactic acid (Vaupel, 2004; Vukovic & Tannock, 1997). In tumours, pH was shown to have dropped by a factor of 0.32, 10 to 100 µm away from the vessel wall (Helmlinger et al., 1997). Conventional anticancer agents have limited access to these cells due to irregular blood flow, poor rate of diffusion and binding to other tissue components; thus they are often detected at the rim of the tumour, if any at all (Jain, 1990, 2012; Minchinton & Tannock, 2006; Seynhaeve et al., 2007; Tredan et al., 2007; Vukovic & Tannock, 1997). Furthermore, the cytotoxicity of chemotherapeutic drugs is reduced in hypoxic and acidic environments. Cytotoxicity of doxorubicin has been shown to be less substantial in low-pH-adapted cells than in normal cells, due to the transmembrane pH gradient that is established in these cells (Gerweck, Kozin, & Stocks, 1999; Yao et al., 2005). Additionally, low pH has been shown to direct cells into the $G_1$ phase, rendering them more resistant to the action of mioxantrone and topotecan (Vukovic & Tannock, 1997). Secondary metabolites produced by glycolysis have also been targeted as a therapeutic strategy; Sonveaux et al. showed that this can be achieved by targeting lactate transporters, such as MCT1, resulting in the effective inhibition of hypoxia-inducible factor-1 (HIF-1)-dependent angiogenesis in endothelial cells (Sonveaux et al., 2012).

## 1.2 Solid tumour therapy

Although surgical excision is the most widely used form of tumour therapy, it is most effective when the tumour is still considered small and confined to a limited area. This is, however, not an effective method for large, invasive and metastatic tumours, whereby resection of surrounding

normal tissues can lead to organ dysfunction (Gavhane et al., 2011). Radiation is another commonly employed method for inoperable solid tumours, such as lung cancer, but the potential co-injury of normal tissues must be considered. This can result in toxic effects such as bone marrow suppression and inflammation of the surrounding tissues for the patient (Barker et al., 2015; Ramnath et al., 2013). Conventional chemotherapeutic agents function mostly by targeting actively-replicating malignant cells and are often combined with radiation and surgery to increase the effectiveness of treatment. However, this mechanism is also non-specific and often harms normal cells of the bone marrow, gastrointestinal tract, hair follicles and gonads (Gavhane et al., 2011). Therefore, specific targeting remains the desired goal since it would ensure increased effectiveness of anticancer agents, driving the research into the development of alternative drug delivery systems and methods (Housman et al., 2014). New methods of payload delivery have been explored, such as nanoparticles (Rizvi & Saleh, 2018), liposomes (Alavi, Karimi, & Safaei, 2017; Kibria et al., 2013; Torchilin, 2005), and microspheres (Varde & Pack, 2004). These systems based on passive or active tumour targeting have been considered promising, but many are still limited by their larger size (Dreher et al., 2006a; Maeda, Sawa, & Konno, 2001; Yuan et al., 1994). Extravasation into the tumour interstitium remains a challenge, as liposomes of 100 nm have failed to extravasate into the SKOV-3 (human ovarian carcinoma) (Kong, Braun, & Dewhirst, 2001) and B16BL6 (melanoma) tumours in mice (Seynhaeve et al., 2007). A better strategy for targeting is therefore needed.

## 1.3 Cell receptors

Tumour cells are equipped with cell-surface receptors, including/and not limited to HLA antigens, cytokine receptors and growth factor receptors (Richter & Zhang, 2005). The overexpression of cellular receptors has long been exploited in targeting cancer therapeutics,

especially the inhibition of growth factor receptors (Richter & Zhang, 2005). A myriad of potential molecular targets have been identified in cancer therapeutics. A widely-known example is the HER-2/neu receptor, which can be inhibited by Herceptin® – an FDA-approved drug used for the treatment of patients with HER-2/neu-positive breast and gastric tumours (Yu & Hung, 2000). Currently marketed drugs include imatinib for myelogenous leukemia (Sacha, 2014), cetuximab for EGFR-overexpressing metastatic colorectal cancer (Wong, 2005) and bevacizumab for targeting VEGF of colorectal cancer (Ranieri et al., 2006). Gashaw et al. listed the key features of ideal drug targets: 1) they are critical in the perpetuation of cancer cells (not just implicated in the early stages of tumourigenesis); and 2) they are not critical in the function of normal cells (Gashaw et al., 2012). Moreover, they should be expressed at higher levels, if not exclusively, in the targeted tumour cells. Of the many growth factor receptors, receptor tyrosine kinases (RTKs) have been implicated in a wide range of cancers. ErbB family members are RTKs that are well-known targets in cancer therapy that have been implicated in the cancers of the breast, lung, colon, stomach, pancreatic, ovary, brain, prostate and kidney (Inchley, 1969). Small molecule tyrosine kinase inhibitors (TKIs) and monoclonal antibodies (mAbs) have been approved for use against ErbB family members (Richter & Zhang, 2005).

### 1.3.1 Epidermal growth factor receptor and other ErbB family members

Despite expression in normal cells, the epidermal growth factor receptor (EGFR, also known as ErbB1, HER1) is a transmembrane glycoprotein that has become an attractive target in cancer therapy, as it is often overexpressed in epithelial tumours and contribute to tumour progression. EGFR modulates growth, signaling, differentiation, adhesion and migration of cancer cells [68, 69]. Higher expression and ligand-independent signaling mutations of EGFR have been implicated in many cancer cells, including metastatic colorectal cancer cells, glioblastoma

(Emlet et al., 2014), pancreatic cancer (Oliveira-Cunha, Newman, & Siriwardena, 2011), and breast cancer (Yu & Hung, 2000). ErbB family members consist of not only EGFR, but also ErbB2 (HER2), ErbB3 (HER3) and ErbB4 (HER4), which are all structurally related. Each is composed of an extracellular ligand binding domain, transmembrane domain, tyrosine kinase domain, and a tyrosine-containing C-terminal tail (Fig. 1) (Wieduwilt & Moasser, 2008). EGFR and ErbB4 can each be bound by a ligand and autophosphorylated through intracellular tyrosine kinase domains. ErbB2, however, does not bind to ligands directly but is the preferred dimerization partner for EGFR (Graus-Porta et al., 1997). ErbB3 does not possess intrinsic tyrosine kinase activity but signal transduction can occur through dimerization with ErbB2 (Citri, Skaria, & Yarden, 2003; Shi et al., 2010; Telesco et al., 2011). There are various ligands that bind to the extracellular ligand-binding domain of EGFR that ultimately contribute to the signaling diversity of EGFR pathways: epidermal growth factor (EGF), transforming growth factor-α (TGF-α) and amphiregulin (Xu et al., 2005). Neuregulin-1 and neuregulin-2 can bind to ErbB3 and both ErbB3 and ErbB4, respectively (Peles et al., 1993).

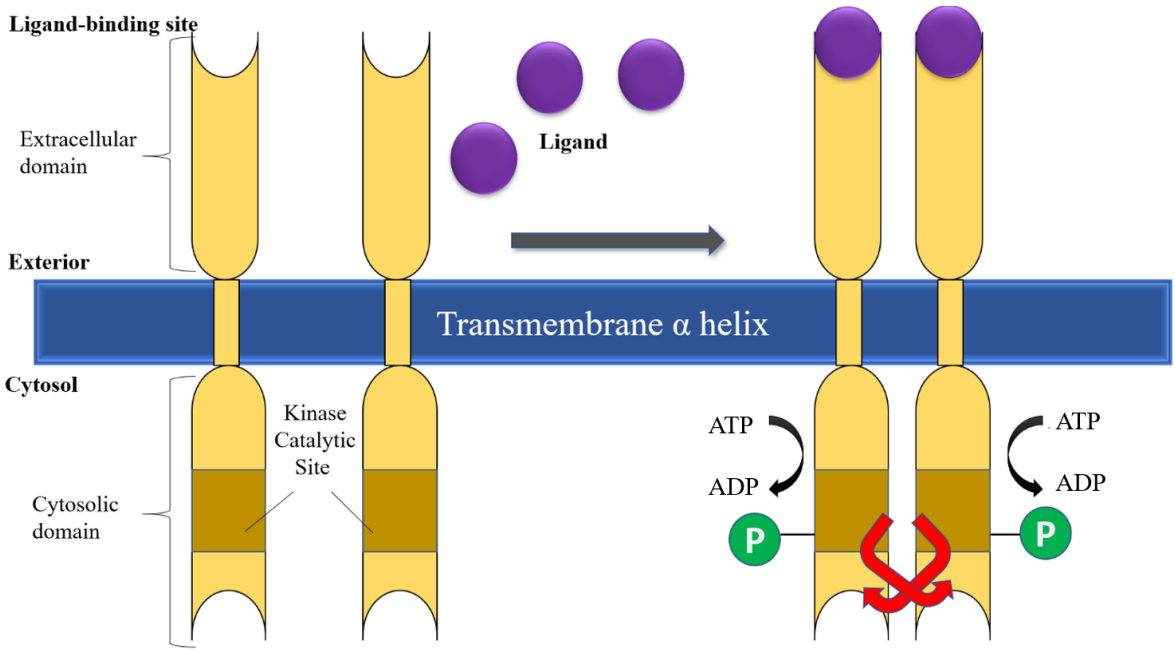


**Figure 1: Schematic diagram of receptor tyrosine kinase (RTK).** The extracellular binding domain of receptor tyrosine kinase binds to ligands, which can cause the receptor to dimerize with another RTK. This activates the kinase activity in the cytosolic domain of the RTK and induces auto-phosphorylation of the adjacent dimerization partner.

Upon binding of a ligand, EGFR dimerizes, which is an essential step for the activation of the protein-kinase in the cytosolic domain and the subsequent phosphorylation of the tyrosine residues on the adjacent dimer partner (Fig.1). The tyrosine phosphorylation of EGFR creates binding sites for Grb2 and Src homology 2 (Shc2), activating downstream signal-transduction events, such as the Ras/MAPK, PLCγ1/PKC, PI(3)kinase/Akt, and STAT pathways. This consequently alters cellular physiology and gene expression (Wieduwilt & Moasser, 2008). Gene expression may also be influenced by ErbB family members that escape the early endosomes and localize in the nucleus, although the mechanism is currently unclear (Ni et al., 2001; Xie & Hung, 1994). Activated receptors bound by ligands are most likely internalized via clathrin, whereby the receptors detach from the clathrin-coated pits and are directed to the lysosomes for degradation (Sorkin, 2001; Wang, Villeneuve, & Wang, 2005). Unbound EGFR is recycled more

rapidly to the surface. Ligand-bound EGFR may either be degraded in the lysosomes or de-ubiquintinated then recycled, depending on the specific receptor-ligand combination (French et al., 1995; Herbst et al., 1994). EGFR heterodimerization with ErbB2 can assist in the evasion of the lysosome; these receptors are recycled to the cell surface instead, increasing EGFR surface density and consequently the downstream signaling events due to prolonged EGFR autophosphorylation (Hendriks, Wiley, & Lauffenburger, 2003; Li et al., 2012; Waterman et al., 1998). Signal attenuation is initiated by dephosphorylation via phosphatases, such as density-enhanced phosphatase-1 (Berset, Hoier, & Hajnal, 2005) and protein tyrosine phosphatase PTP1B (Haj et al., 2003).

### 1.3.2 EGFR in cancer therapy

Clinical efficacy often depends on the density of EGFR expressed by cells and the effective blockage (Li et al., 2011). The extracellular domain of EGFR is accessible to monoclonal antibodies; the binding of these antibodies inhibits the intracellular signal transduction pathways that can then respond to angiogenic factors (Harding & Burtness, 2005; Laskin & Sandler, 2004; Wieduwilt & Moasser, 2008). Mechanisms of action of anti-EGFR therapeutics include physically blocking the ligand from binding (primarily antibodies) or inhibiting the tyrosine kinase enzymatic activity (small molecular weight tyrosine kinase inhibitors), which prevents autophosphorylation and downstream signaling events. Gefitinib (Iressa®) is a clinically-approved EGFR tyrosine kinase inhibitor, that has shown to suppress tumour growth at the end of a 4-week treatment period of 5 mg/dose in GEO cancer xenografts in immunodeficient mice (Ciardiello et al., 2000). Cetuximab (Erbitux®) and panitumumab (Vectibix®) are chimeric mouse/human monoclonal antibodies that target the extracellular domain of the EGFR. Cetuximab has demonstrated the ability to suppress xenograft tumour growth and has been

approved for clinical use against colorectal cancer (Matsuo et al., 2011a; Taniguchi et al., 2018). Upon binding of cetuximab, EGFR has been shown to dimerize, but is not accompanied by the phosphorylation of downstream proteins, such as Akt and Erk, which are essential in regulation of cell proliferation and survival (Matsuo et al., 2011a; Yoshida et al., 2007a). Binding of a ligand, such as EGF, will induce a rapid EGF-EGFR complex turnover. The occupation of EGFR will be reduced and consequently, interactions with signaling proteins that perpetuate the active state of the intracellular signaling pathways will also be reduced (Yoshida et al., 2007b). The enzymatic tyrosine kinase function can also be inhibited by low molecular weight molecules that compete for the intracellular Mg-ATP binding site to prevent further downstream intracellular signalling. Gefitinib (Iressa®) and Erlotinib (Tarceva®) are examples of EGFR tyrosine kinase inhibitors used as first-line treatments of advanced non-small cell lung cancer, that can achieve prolonged responses to treatment in chemotherapy-naïve patients (Burotto et al. 2015; Giaccone et al., 2006).

### 1.3.3 HT29 colon adenocarcinoma and EGFR expression

The colon adenocarcinoma cell line, HT29 (used in this study), expresses relatively high levels of EGFR and possesses wildtype *KRAS* and mutated *BRAF* (Lewandowska, Jóźwicki, & Żurawski, 2013; Van Cutsem et al., 2009). KRAS serves as an effector molecule for signal transduction from a ligand-bound EGFR to the nucleus for changes in gene expression; mutations in KRAS have displayed persistent downstream signaling without the influence of EGFR and high resistance to EGFR-targeted monoclonal antibody therapy (Malumbres & Barbacid, 2003). Clinical trial results have revealed that the addition of cetuximab to first-line chemotherapy is beneficial to patients with the wildtype *KRAS* gene (Venook et al., 2017). BRAF is a downstream effector of RAS in the EGFR pathway, promoting cell proliferation and

survival through the constitutive MAPK signaling pathway (BRAF GENE, 2015). The conventional criteria for cetuximab therapy is currently EGFR-positive and KRAS wildtype; colorectal cancer patients with the *BRAF* mutation may be considered to be a minor 'non-effective' group therapy as determined by clinical trials (Laurent-Puig et al., 2009; Van Cutsem et al., 2009). BRAF or KRAS mutations decrease the effectiveness of EGFR-targeting therapeutics, as the mutations enable constitutive cell proliferation and survival (Wan et al., 2004; Xu & Solomon, 1996). Therefore, KRAS mutations, and BRAF mutations to a lesser degree, typically serve as markers of resistance to anti-EGFR therapy, as patients have shown to express a lower response rate than those with wildtype tumours (De Roock et al., 2010; Zhao et al., 2017). Mouse HT29 cell xenografts displayed high sensitivity to cetuximab and mitogen-activated protein kinase (MEK) inhibitor, selumetinib (AZD2644) (Zhang et al., 2018). By inhibiting MEK, selumetinib further inhibited extracellular signal-related kinase (ERK) phosphorylation and tumour cell proliferation. The combination of cetuximab reactivated MAPK signaling, resulting in the significant inhibition of HT29 cell xenograft growth (Zhang et al., 2018).

One study revealed that EGFR signal transduction was altered by the cetuximab in HT29 cells. The level of phosphorylation by growth factors, TGF-α, IGF and EGF, decreased in the presence of cetuximab in HT29 cells and partially inhibited the MAPK pathway (Matsuo et al., 2011b). Another study by Solmi et al. showed by scanning electron microscopy, significant microvilli and filopodia reduction on HT29 cells in response to cetuximab (Solmi et al., 2008). These cells lost boundary contacts with other cells as a result, which were indicative of differentiation toward apoptosis. Downregulation in MAPK signaling, apoptosis and phosphatidylinositol signaling system of HT29 cells was also reported in the same study (Solmi et al., 2008).

## 1.4 3D Cultures

Clinically, targeting tumour cells without affecting normal cells is a major goal in cancer therapy as this would reduce side effects for patients. Low-weight molecules with passive and/or active tumour targeting have been investigated for potential clinical applications (Barua & Mitragotri, 2014; De Jong & Borm, 2008; Kibria et al., 2013; Torchilin, 2005). In vitro cell cultures provide a highly controlled environment; 3D tissue models, such as cells grown on structured scaffolds, multicellular layers and multicellular tumour spheroids, have been particularly useful in studying drug and nanoparticle penetration in vitro as they provide better representation of the complexity and state of cancer cells in their native environment (Mikhail, Eetezadi, & Allen, 2013). While conventional monolayer cultures may be a convenient and an effective way for predicting molecular targets and pathways, they are unable to completely recapitulate the complexity and heterogeneity of tumours (Mikhail et al., 2013). Previous studies have shown that while certain apoptosis-inducing drugs were effective against monolayer cell cultures, they failed to achieve the same level of cytotoxicity in 3D cultures, which may be analogous to the chemoresistance often observed in vivo (Barbone et al., 2008; Desoize & Jardillier, 2000; Vermeulen et al., 2008).

### 1.4.1 Multicellular spheroids

Multicellular tumor spheroids (MCTS) serve to bridge the gap between monolayer cultures and animal models by effectively mimicking the pathophysiological environment and morphology of in vivo solid tumours and demonstrating similar responses to therapy (Zanoni et al., 2016). They are preclinical models that re-establish the complex network of cells, ECM, gene expression, cell signals, gradients of pH, oxygen, metabolism and proliferation found in solid tumours (Däster et al., 2017). The cells in MCTS are concentrically-arranged whereby the outer region is comprised of proliferating cells that are abundantly exposed to nutrients and oxygen (Fig. 2). These cells

surround quiescent cells, closer to what is a necrotic core if the MCTS beyond a critical size of 500 um in diameter (Däster et al., 2017). These characteristics of spheroids ultimately influence protein expression, binding and penetration of drugs through the MCTS (Sriraman et al., 2014). Some molecular targets also become upregulated, which have previously been exploited for selective targeting (Barbone et al., 2008; Howes et al., 2007; Mueller-Klieser, 1997; Wolfgang Mueller-Klieser, 1987).

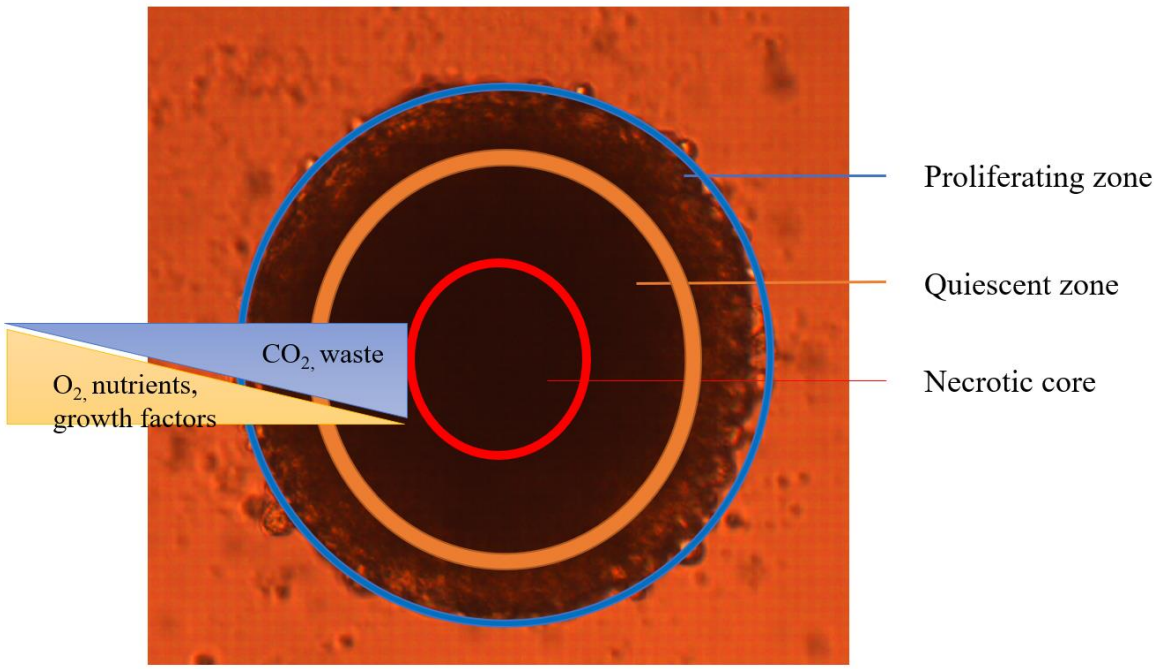


**Figure 2: A schematic diagram of a multicellular spheroid**. Cells in the outer region are rapidly proliferating due to an abundance of oxygen and nutrients. Inner cells are less metabolically-active due to decreases in oxygen and nutrients. This leads to the formation of a necrotic core in larger spheroids, whereby the lack of oxygen and nutrients leads to cell death.

One study showed that anticancer drugs, melphalan, irinotecan, oxaliplatin and fluorouracil (5-FU), were highly active in HCT116 monolayer cultures, but 6-day-old spheroids were almost completely resistant (Karlsson et al., 2012). These effects were suggested to have been caused by the suppression of genes implicated in DNA replication and cell cycle associated with the 3D culture (Karlsson et al., 2012).

A population of cells in spheroid culture will display stronger resistance to drugs even in the absence of intervening physical barriers (e.g. ECM components), as some cells will be required to be in proliferative state for the drug to induce toxicity (Kolonin et al., 2006; Mikhail et al., 2013). For example, one group treated A549 spheroids with paclitaxel, a microtubule-targeting drug that disrupts cell adhesion, to increase the interstitial spaces between cells to achieve equal access of cells by a chemotherapeutic drug. This was confirmed by observing the effective penetration of 10,000 Da dextrans through spheroids (Russell et al., 2017). Despite the increased accessibility of cells for the chemotherapeutic drug pemetrexed, a population of cells remained unperturbed and viable. 3D cultures reproduce the metabolic gradients and altered cell-cell contacts that are more representative of in vivo solid tumours; therefore, MCTS are considered to be more reliable in predicting a drug's therapeutic potential than conventional monolayer cultures in preclinical studies (Eriksson et al., 2009; Friedrich et al., 2009a).

Spheroids can be monitored for their change in size and morphology in response to a drug by standard phase-contrast microscopy, while the measurement of drug penetration can be accomplished by confocal microscopy (Bryce et al., 2009b; Mehta et al., 2012; Mittler et al., 2017; Svishchev & Goncharov, 1990; Vermeulen et al., 2008; Ying et al., 2010; Zanoni et al., 2016). Typically, spheroids with diameters of up to 300 μm are employed in drug testing, which exhibit well-developed cell-cell, cell-matrix interactions and reproducible results in drug screening (Enmon et al., 2003; Friedrich et al., 2009a; Moran et al., 2012; Rubin, Voronkov, & Zhivopistseva, 1975). Although the use of larger spheroids is tempting to model the behaviour and characteristics of solid tumours and their response to treatments, it is difficult to achieve reproducible results. Zanoni et al. demonstrated that the variability of parameters, such as

volume, shape and sphericity caused spheroids to display different responses to treatments – all of which were amplified by larger spheroid size (Zanoni et al., 2016).

### 1.4.2 Parameters affecting drug penetration into solid tumours

Physical properties of molecules such as particle size, shape, charge, and hydrophobicity can influence the passive transit through intercellular spaces of solid tumours (Aggarwal et al., 2009). Delivery agents are also affected by contact with the ECM and cell surface. Numerous drug delivery technologies have been developed as carrier systems for therapeutically active agents, including liposomes (Torchilin, 2005), micelles (Kataoka, Harada, & Nagasaki, 2012), antibodies (Walker et al., 1988), affinity targeting and macromolecular drug carriers (Dreher et al., 2006a). However, these particles were found to be restricted to the tumour vasculature with very little infiltration due to their sizes (Grill et al., 2002). Adenoviral gene transfer in spheroids has also been assessed but poor penetration was observed despite the application of high titers of $10^{10}$ PFU/spheroid; transfection was observed only occurring in the first two cell layers of the spheroid (Grill et al., 2002).

All nanoparticles move more slowly through the fluid than conventional therapeutic agents, as process of diffusion is much more efficient for smaller particles (Florence, 2012; Huang et al., 2017). However, larger particles can benefit from the enhanced permeability and retention effect (EPR). The rate of clearance in the tumour tissue is reduced due to the poor lymphatic system, which can facilitate the selective accumulation and retention of larger nanoparticles. Small molecules, however, can manage to escape the tumour vessels through the fenestrations (Khawar et al., 2015). Dreher et al. studied the depth of penetration of dextrans with sizes ranging from 3.3 kDa to 2 MDa. After 30 min, maximal accumulation in the tumour was observed for dextrans 40 – 70 kDa (diameters of 11.2 – 14.6 nm), approximately 15 μm from the vessel wall (Dreher et

al., 2006a). This was due to the increased accumulation of these molecules, whereas their lower molecular weight counterparts were subjected to a higher rate of clearance (Dreher et al., 2006a). Passive tumour targeting by nanoparticles relies primarily on EPR, which can enhance their accumulation in tumour tissues more than in healthy tissues (Maeda, Tsukigawa, & Fang, 2016).

Neutral and positive surface charges contribute to diffusion of nanoparticles into spheroids (Kostarelos et al., 2004). Negatively-charged quantum dots were able to penetrate deeply into HeLa spheroids, contrary to their positively-charged counterparts that were confined to the rim (Ma et al., 2012). The shallow depth of penetration by cationic liposomes was suggested to have been caused by the electrostatic binding between the positive liposomes and negatively-charged surface of cells, inhibiting further diffusion (Lee et al., 2002). Surface coating, such as by PEG, can reduce these electrostatic interactions of nanoparticles with cells and assist in evasion from the reticuloendothelial system (RES). However, depth of penetration can be compromised due to the increase in overall size (Kostarelos et al., 2004). Finally, the shape of the nanoparticle also determines its diffusivity. Although conventional carrier systems are spherical, rods or filamentous shapes may be more optimal. They have shown to diffuse more rapidly into spheroids with greater accumulation in vivo and in vitro (Chauhan et al., 2011; Decuzzi et al., 2010; Lee et al., 2013; Lee, Ferrari, & Decuzzi, 2009). Nanorods and nanospheres with the same hydrodynamic diameter of 33 nm were compared for transport across porous membranes in vitro. Nanorods were able to diffuse 5.3 times deeper than nanospheres through 100-400 nm collagen gel pores, which are approximate pore sizes of tumour vascular walls (Chauhan et al., 2011).

Fusion of molecules to enhance cellular uptake and penetration has been widely investigated. These molecules include tumour-homing and cell-penetrating peptides, such as arginine-glycine-aspartic acid (RGD) (Shi et al., 2015), TAT (Zong et al., 2014), and MPG (Sims et al., 2016).

The fusion of RGD to lipid coated nanoparticles significantly improved its biodistribution in spheroids of C6 glioblastoma cells that overexpress integrin α(v)β3 in vitro (Shi et al., 2015). iRGD is a 9-amino acid, cyclic tumour-penetrating peptide with greater binding affinity than the standard RGD motif (Sugahara et al., 2015). The co-administration of iRGD significantly improved the extravasation of nanoparticles from the tumour vessels into the glioma parenchyma, resulting in overall greater accumulation in nude mice (Gu et al., 2013). Another group designed liposomal systems modified with TAT and T7 to enhance penetration into the glioma the blood-brain barrier, respectively (Zong et al., 2014). TAT-liposomes showed deeper penetration into the C6 tumour spheroids in vitro than T7-liposomes, but the opposite was observed in vivo. This was probably caused by the nonselectivity of TAT, as well as interference of natural diffusivity by the liposomes (Zong et al., 2014). Having both molecules fused to liposomes resulted in the highest accumulation in the glioma due to synergistic effects (Zong et al., 2014). The ability of nanoparticles to diffuse through the spheroid does not always correlate to their total accumulation in the spheroid. The conjugation of MPG, synthetic peptide derived from HIV gp41 and SV40, increased uptake of nanoparticles in HeLa spheroids by almost three-fold. PEG-nanoparticles, however, were localized mainly in the spheroid periphery, but were able to penetrate tissue culture by almost two-folds further than the MPG-nanoparticles (Sims et al., 2016).

In vitro modeling of nanoparticle penetration into spheroids is also affected by external parameters such as temperature and cell type. The penetration efficiency is reduced at lower temperatures as modeled by the equation for Brownian motion. At higher temperatures, the viscosity of the liquid medium decreases, resulting in faster diffusion of nanoparticles (Florence, 2012). Cell type will affect in variations in packing density and intercellular channel sizes,

influencing the overall kinetics of the particle. Certain cells form larger interstitial spaces enabling nanoparticle movement, which does not necessarily reflect the penetrability of the nanoparticle itself. Stromal spheroids will appropriately model the structural barrier that restrict particle movement in vivo (Friedrich et al., 2009a; Priwitaningrum et al., 2016). Mikhail et al. reported that despite the treatment of HT29 and HeLa spheroids with the same concentration of docetaxel, different responses were observed; HT29 spheroids consist of more non-proliferating cells with higher packing density than HeLa spheroids (Mikhail et al., 2013). Therefore, it is crucial to screen therapeutic molecules in spheroids generated from various cell types to appropriately assess their kinetic properties.

## 1.5 Bacteriophages

Bacteriophages (phages) are viruses that exclusively infect bacteria, and like plant and animal viruses, phages are unable to propagate in the absence of a host. The bacterial host provides machinery and organic material for phage biosynthesis and packaging (Clokie et al., 2011). Phages are the most abundant biological entities on earth – an estimate of $10^{31}$ particles exist as free virions or within their bacterial hosts (Ashelford et al., 2000). All phages undergo the general process of adsorption to their bacterial host(s), DNA injection, replication, virion production, followed by release (Clokie et al., 2011).

The human body is extensively colonized by phages, and the ubiquitous nature of phages leads to constant exposure to a diverse spectrum of phages from birth. Phages colonize the skin (Oh et al., 2016), lungs (Dickson & Huffnagle, 2015), oral cavity (Pride et al., 2012), gut (Reyes et al., 2010), and urinary tract (Santiago-Rodriguez et al., 2015), contributing to an extensive genetic diversity to humans, and ultimately playing an essential role in maintaining our health (Abeles & Pride, 2014). The gut microbiota consists mainly of phages, with an estimate of $10^9$ virus-like

particles per gram of stool (Kim, 2011). In healthy humans, this includes double-stranded DNA viruses of the *Podoviridae*, *Siphoviridae* and *Myoviridae* family (Breitbart & Rohwer, 2005; Reyes et al., 2010). The diversity of phages contributes significantly to the gut microbiota structure and function. Phages may serve as reservoirs of genetic diversity by serving as vehicles for horizontal transfer of virulence and antibiotic resistance for their bacterial host (Nadeem & Lindi Wahl, 2016). Additionally, these entities may play a role in the defense of the mucosal barrier against bacteria. The Ig-like domains exposed on the surface of phages have been shown to interact with the mucin glycoproteins to decrease bacterial colonization of the mucosa, thereby reducing bacterial translocation and the potential for bacteremia (Barr et al., 2013a).

Phages have received enormous amount of attention in the last decade for its potential applications. This includes treatment of bacterial infections as well as its potential for genetic therapy (Bakhshinejad, Karimi, & Sadeghizadeh, 2014; Donnelly et al, 2015; Hosseinidoust, 2017). Phages have no natural tropism for mammalian cells as they would for bacterial hosts and have resided in our bodies throughout hominid evolution in a tripartite relationship with their bacterial and human hosts (Clokie et al., 2011). For decades, phages have extensively been used in Eastern Europe for treatment of bacterial infections, but have only recently garnered interest for their influence of cancer processes (Abedon et al., 2011; Kaur et al., 2012). Phages have demonstrated intrinsic antitumour activities such as slowing the tumour growth (Bloch, 1940; Dabrowska et al., 2007; Eriksson et al., 2009; Górski et al., 2015; Huh et al., 2019; Ivanenkov & Menon, 2000; Rangel et al., 2013). The most widely known example of this is perhaps the attachment of T4 phages to B16 melanoma cells mediated by the Lys-Gly-Asp (KGD) motifs present on the phage capsid with the integrin β1 and β3 integrin receptors on target cancer cells. This resulted in decreased tumour metastasis (discussed in Chapter 1.5.4) (Dabrowska et al.,

2004). Administered phages have also shown remarkable penetrative capabilities through various cell types, passing through relatively impermeable physiological barriers in our bodies. This includes the blood-brain-barrier, which often restricts the movement of molecules that are less than 500 Da, lipophilic, and share a structural homology to compounds that enter the brain through active transport (Abbott, Rönnbäck, & Hansson, 2006; Huh et al., 2019; Pardridge, 2003). Intraperitoneal (Dubos, Straus, & Pierce, 1943) and intranasal (Solomon, 2008) application of M13 phages in mice have resulted in their recovery in the brain as early as 1 h following administration. Phages can also cross the gut mucosal barrier as orally administered phages have been recovered in the blood of mice (Majewska et al., 2015; Międzybrodzki et al., 2017). Administered phages can bypass the gut flora, adhere to the glycoproteins in the mucosa and traverse the epithelium transcellularly or via M cells (Barr et al., 2013b; Huh et al., 2019). Recently, the mechanism for transcytosis across epithelial cells have been described by Nguyen et al. Transcytosis was observed for 0.1% of applied phages in the apical-to-basal direction. Phages applied topically to clear bacterial infections have shown to penetrate through the multiple layers of the skin, from the epidermis to the adipose tissues (Kumari, Harjai, & Chhibber, 2011). Soothill et al. excised and replaced skin grafts extending down to the subcutaneous fat, but the topical application of phages prevented the graft destruction by *Pseudomonas aeruginosa*, demonstrating the ability of phages to permeate the skin tissue (Soothill, 1994). This unique ability of phages to pass through minute intercellular spaces may lead to effective extravasation, infiltration and accumulation in the tumour microenvironment, possibly representing a huge potential for a drug delivery platform for phages in cancer therapy.

### 1.5.1 Phage internalization and cellular trafficking in eukaryotic cells

Despite the ubiquity of phages in the environment, our knowledge of phage interactions with mammalian cells is very limited. There is evidence that phages can bind to the surface and be internalized by eukaryotic cells, but the penetration of phage DNA into the nucleus, replication and release of progeny particles have not been directly observed. Over 40 years ago, lambda phage transduction in human fibroblasts was demonstrated by Merril et al. Cells infected with phages harboured about 0.2% of cellular RNA that was λ-specific (lambdoid phage-encoded β-galactosidase) (Geier & Merril, 1972). Since then, targeted phage transduction in mammalian cells have been extensively studied by measuring the expression of GFP, neomycin phosphotransferase or β-galactosidase (Kassner et al., 1999; Larocca et al., 2001; Larocca et al., 2008; Poul & Marks, 1999). Phage display (Chapter 1.5.2) can be used to fuse targeting ligands on the phage surface; this combined with a mammalian expression cassette can confer mammalian tropism for the phage (Baird, 2011). The interactions between targeting ligands and their cognate receptors increase the likelihood of phage-internalization in a concentration-dependent manner, and subsequently their transfection efficiency (Aalto et al., 2001; Dabrowska, et al., 2005; Kassner et al., 1999; Larocca & Baird, 2001; Lehti et al., 2017; Poul & Marks, 1999). Kassner et al. demonstrated that M13 filamentous phages displaying EGF peptides were able to transduce COS-1 cells by delivering a *GFP* gene. Transduction efficiency was shown to be greater by 100-fold than by control phages without any display (Kassner et al., 1999). Transduction was observed with concentrations as low as 250 phage particles/cell and increased in a dose-dependent manner. This ligand density-dependent increase in transduction efficiency has also been shown with the display of fibroblast growth factor (FGF2) (Kassner et al., 1999) and scFv antibody fragment (Poul & Marks, 1999), targeting the fibroblast growth factor

receptor and ErbB2 receptor, respectively. The display of RGD peptides by filamentous phages has also mediated cell internalization via multivalent binding to integrin receptors in vitro. Phages were internalized in less than 15 min, in a process resembling phagocytosis more than receptor-mediated endocytosis. Packaging into clathrin-coated vesicles require particles to be less than 100-150 nm in diameter, but filamentous phages are often between 800–2000 nm in length (Lamaze & Schmid, 1995).

Phage internalization is not contingent on phage surface modifications to display cell-targeting ligands. Recently, Lehti et al. demonstrated the ability of *E. coli* phage PK1A2 to bind specifically to polysialic acid receptors on eukaryotic neuroblastoma cells in vitro, without the mediation of phage surface modifications (Lehti et al., 2017). Furthermore, there was strong evidence that this induced internalization of the phage-polysialic acid complex; fluorescent phages appeared intracellularly as early as 30 min after incubation and increased up to 24 h. Polysialic acid bears structural similarity to a bacterial receptor that mediates phage entry (Petter & Vimr, 1993). It has been postulated by the authors that there are other undiscovered surface epitopes on eukaryotic cells that can be bound specifically by phages, due to an abundance of structurally-similar carbohydrates shared between pathogenic bacteria and host eukaryotic cells. Following cellular uptake, phages are likely directed to the endolysosomal pathway, losing infectivity in the lysosomes (Ivanenkov, Felici, & Menon, 1999; Lehti et al., 2017).

### 1.5.2 Phage display

Although wildtype T4 phages without any surface modifications have demonstrated antitumour activities (see 1.5.4) (Bloch, 1940; Dabrowska et al., 2007; Eriksson et al., 2009; Górski et al., 2015; Huh et al., 2019; Ivanenkov & Menon, 2000; Rangel et al., 2013), phages can be engineered to enhance their application and efficacy profile. Tropism for specific cells can be

conferred by fusing cell-targeting ligands to surface proteins (Beghetto & Gargano, 2011). This is known as phage display technology, whereby a peptide or protein coding gene is translationally fused to the capsid gene of the phage. As a result, the phage product will carry the gene for the protein/peptide of interest and will be capable of replication within the construct (Kaur et al., 2012). This approach has been extremely powerful in isolating ligands for drug discovery, identifying protein-protein interactions and antibody fragments, epitope mapping, as well as phage engineering for specific targeting of tissues and cells (Nicastro et al., 2016). Peptides with desired binding profiles can be selected for in a process called "biopanning," which has further progressed to live animal 'in vivo panning' (Pasqualini & Ruoslahti, 1996). This approach has since been extensively investigated in cancer therapy; tumour-specific ligands have been screened and isolated by their affinity and specificity to neoplastic cells and vascular endothelium (Pasqualini & Ruoslahti, 1996; Poul et al., 2000). While monoclonal antibodies can also achieve high affinity and specificity, their large size is a limiting factor for effective penetration into the tumour tissue (Scott, Wolchok, & Old, 2012).

Much success has been achieved by utilizing isolated peptides from screening phage display libraries for delivery of nanoparticles to tumours (Krumpe & Mori, 2006). Several peptides have been identified to bind to HER2 (Urbanelli et al., 2001), EGFR (Karasseva et al., 2002), IL-6 receptor (Su et al., 2005). Furthermore, peptides isolated from phage-display peptide libraries have progressed to phase III clinical trials, such as Amgen's AMG-386, an anti-angiogenic therapeutic for treatment of various cancers, and Romiplostim (AMG 531), drug approved by the FDA for the treatment of thrombocytopenia (Jamali et al., 2009; Shimamoto et al., 2012).

### 1.5.3 Tuneable λ phage display

Bacteriophage λ is a temperate phage in the family of *Siphoviridae* viruses, with icosahedral capsid (~50 nm in diameter), long fibrous tail (150 nm in length) and double-stranded genome (~48 kb) (Geier & Merril, 1972). The capsid consists of two major coat proteins, gpE and gpD, which are responsible for the structure of the prohead and stability during genome packaging, respectively (Fig. 3). gpD consists of 109 amino acids and cuts the concatemers at the cohesive end site (*cos*) during packaging of the DNA into the phage prohead while simultaneously stabilizing it. gpD-deficient mutants result in 82% of the DNA content of wildtype λ phage (Sternberg & Weisberg, 1977). Phage λ is able to carry large DNA fragments, has high infectivity and offers several advantages over filamentous phages (Lankes et al., 2007; Piersanti et al., 2004; Sternberg & Hoess, 1995). It is similar in size and shape to mammalian viruses, has double-stranded DNA genome, and despite its small size, the mature λ-head can package large amounts of DNA fragments of up to 50 kb (Beghetto & Gargano, 2011; Mikawa, Maruyama, & Brenner, 1996; Razazan et al., 2019; Sternberg & Hoess, 1995). It can also accommodate larger exogenous proteins with a high copy number, conferring high avidity for a target receptor (Piersanti et al., 2004). Phage λ can be employed for phage display via both gpD, and the tail protein, gpV (Mikawa et al., 1996; Santini et al., 1998; Sternberg & Hoess, 1995). There are 415 copies of gpE and 405 – 420 copies of gpD (Beghetto & Gargano, 2011). It was reported by Piersanti et al. that phage λ possessed a more efficient display system compared to filamentous phage, with greater gpD fusions of the same polypeptide by $10^4$-fold (Piersanti et al., 2004).

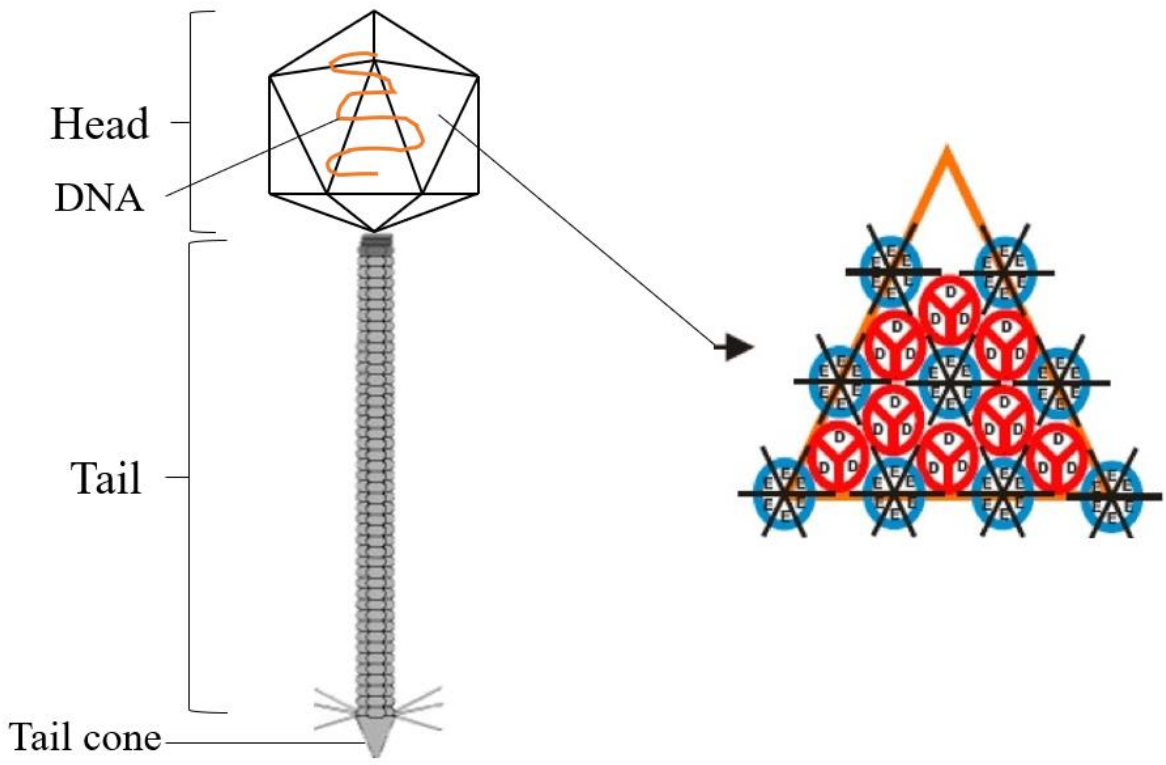


**Figure 3: A schematic diagram of bacteriophage λ and one face of the capsid.** The capsid head is composed of gpD and gpE proteins incorporated into trimers and hexamers, respectively. λ icosahedral head comprises a total of 20 faces and 405-420 of each gpD and gpE proteins (image adapted from Nicastro 2013).

### 1.5.4 Phages and cancer

Anticancer properties of T4 phages have been reported, demonstrated by the inhibition of lung metastasis of B16 melanoma cells by the binding of T4 and its sub-strain HAP1, mediated through the KGD motif on the gp24 phage capsid protein and to the cell surface β3 integrins (Dabrowska et al., 2004; Dabrowska et al., 2004, 2007). Certain animal viruses, such as adenovirus, HIV, HPEV1 virus and hantavirus, use integrins for cell entry, which are present on platelets, monocytes and some neoplastic cells (Gavrilovskaya et al., 1999; Lafrenie et al., 2002). The blockade of integrins downregulates its functions, which has been postulated to be the cause of anti-metastatic activity imparted by these phages (Gorski et al., 2003). Phages in the context of cancer immunotherapy has also been of interest, as Eriksson et al. described the phage-

induced tumour regression in mice (Eriksson et al., 2009). Administration of tumour-specific phages secreted proinflammatory cytokines IL-12 and interferon γ, resulting in the migration of mouse neutrophils to the site of tumour and potentiating tumour destruction (Eriksson et al., 2009). Arab et al. also studied the immunogenicity of λ phage particles displaying E75 peptide derived from HER2/neu in a TUBO cell xenograft model of BALB/c mice (Arab et al., 2018). This resulted in the induction of CD8+T cells for mice that were vaccinated with the phages with significantly reduced the size of the tumour.

### 1.5.5 Immune response to phage therapy

Immune response to phage administration can be influenced by: i) the size and number of surface epitopes; ii) route of administration; iii) dose and frequency of phage administration and iv) patient history of exposure (Kaur et al., 2012). Antibodies against naturally-occurring phages, such as T4, are detected in the sera of humans. In one study, 50 healthy humans were tested for phage antibodies, of whom 81% were found to possess IgG antibodies against the T4 capsid proteins – gp23, gp24 and Soc. This was most likely a result of natural contact with phages in the environment (Dąbrowska et al., 2014).

Oral phage administration has typically shown weak immune responses in humans, with only marginal changes in serum anti-phage antibodies (Bruttin & Brüssow, 2005). Intravenous injection of phages, however, result in the rapid phage clearance from the reticuloendothelial system (RES) (Clark, 2015; Merril, Scholl, & Adhya, 2003). The RES is comprised of phagocytic cells that reside in the lymph nodes and the spleen, including Kupffer cells (specialized mononuclear phagocytes) of the liver. These cells remove foreign phage particles, posing a significant challenge to the maintenance of applied phage titers in vivo (Hodyra-Stefaniak et al., 2015). As a result, significant titers of phages have been recovered from the

spleen in mice, regardless of the route of administration (Gieir, Trigg & Merril, 1973). The half-life of phages in circulation often depend on phage surface protein sequences; Merril et al. showed the ability to select for mutant λ phages that were able to persist in circulation for several hours by effectively evading Kupffer cells in mice (Geier et al., 1973; Merril et al., 1996) 61].

There have been reports of both pro- and anti-inflammatory cytokine release in response to phages. Weber-Dabrowska et al. studied the effects of phages on the tumour necrosis factor-α (TNF- α) and interleukin 6 (IL-6) levels in the sera of 51 patients with suppurative infections (Weber-Dabrowska, Zimecki, & Mulczyk, 2000). Long-term treatment with phages led to elevated levels of these cytokines; however, like many other similar studies testing cytokine levels in response to phage therapy, it is unclear whether the short-term normalization or reduction in the proinflammatory cytokine levels were influenced by the reduced burden of pathogenic bacteria in the body. A different study monitored changes of 12 proinflammatory cytokines including IL1, IL2, IL10, IL17, IFN-γ and TNF- α in response to orally fed T7 phage in mice, and only IL17A was slightly elevated (less than 10%) compared to the control group that was fed SM buffer (Park, Cha, & Myung, 2014). Histopathological analysis of the same study showed no noticeable differences in the tissue samples of the gastrointestinal tract. Anti-inflammatory action of phages has also been reported; a study used highly purified *Staphylococcus aureus* and *Pseudomonas aeruginosa* phages to stimulate peripheral blood mononuclear cells (PBMCs) derived from healthy human donors. The genes for IL1RN (an anti-inflammatory IL1 receptor antagonist) and SOCS3 (suppressor of cytokine signaling 3) were upregulated, while proinflammatory cytokines such as IL1A and IL1B, were also elevated. Therefore, phages appear to activate several immunological pathways following administration (Van Belleghem et al., 2019).

### 1.5.6 Phage penetration of solid tumours

The ability of phages to penetrate through the various regions of solid tumours may depend on several factors including the size and morphology of the phage, surface charge of the phage, interactions with the ECM, and the potential binding and internalization to the eukaryotic cells. Diffusing particles often interact with molecules during their transit through intercellular spaces, although outcomes will vary significantly depending on whether the interaction is specific or non-specific (Florence, 2012). Specific interactions, such as those of monoclonal antibodies and tumour antigens, can impair tumour penetration by binding to external cells, resulting in poor biodistribution in the solid tumour in what is known as the "binding site barrier" (Adams et al., 2001; Juweid et al., 1992). This effect is often dependent on the binding affinity and antigen density, and is often the cause of poor nanoparticle diffusion and unintended internalization by stroma cells near the blood vessels (Juweid et al., 1992; Miao et al., 2016).

Recently, *E. coli* phage lysate enriched from sewage has been reported to bind to three major macromolecules of the ECM– gelatin (denatured collagen), fibronectin, and heparin by column-based assays (Porayath et al., 2018). ECM biochemically impedes vector access to tumour cells (Netti et al., 2000). The same phage lysate was used to test their ability to protect HT29 cells against infection by pathogenic host bacteria. Phage adherence to HT29 cells was evidenced, as phages were able to reduce the bacterial load by 48%, even after washing of the cells to discard unbound phages. These phages did not show signs of cytotoxic effects on HT29 cells by the Resazurin assay.

Adeno-associated virus/phage (AAVP) is a hybrid phage vector with a mammalian transgene cassette harbouring inverted terminal repeats from adeno-associated virus 2 as well as a peptide display vector from fd phage genome. The AAVP displays iRGD that enables homing and entry

to αv integrin receptors and has been used widely for gene delivery into cancer cells (Hajitou et al., 2007; Przystal et al., 2013; Smith et al., 2017). A study by Yata et al. showed that despite the narrow shape (6.5 nm x 1400 nm) of AAVP, diffusion through the ECM-gel matrix was still very poor. Infiltration, internalization and gene expression were significantly improved after the depletion of ECM constituents with collagenase and hyaluronidase (Yata et al., 2015). Bacteriophage penetration through a MCTS has not been clearly characterized but remains to be a parameter that needs to be clearly defined in the development of a drug delivery platform for phages.

# Chapter 2: Rationale, Objectives and Hypothesis

## 2.1 Rationale

A prominent problem with cancer gene therapy is the incomplete eradication of tumors, which frequently results in the recurrence of cancer. Bacteriophages have naturally demonstrated the ability to bind to the surface of mammalian cells as well as the capacity to penetrate different cell type layers and various physiological barriers in the human body. Phages may be able to overcome physical barriers commonly presented in solid tumour drug delivery, including high packing density of constituent cells and the high interstitial fluid pressure. Therefore, we sought to understand whether unmodified bacteriophage λ can passively target and diffuse within multicellular spheroids generated from NIH3T3 mouse fibroblasts. Fibroblasts are stromal cells that secrete connective tissue components, hindering drug penetration into solid tumours. Phage λ was selected for its ability to tolerate larger and higher density of protein fusions without compromising phage assembly. Additionally, the dual-control display system to variably decorate the surface of phage λ has previously been investigated in our lab.

The display of peptides to the surface of phages can enhance specific targeting of phages to cells and tissues. We chose EGF for peptide of display for phage λ, as it has been successfully used for targeting of other types of vectors in several gene therapy applications to date (Kassner et al., 1999; Larocca, Burg, & Baird, 2005). EGFR blockade has also been implicated in slowing of tumorigenesis and cancer progression (Harding & Burtness, 2005; Matsuo et al., 2011a; Scaltriti & Baselga, 2006). HT29 colon adenocarcinoma cells were selected for spheroid culture, which expresses high EGFR levels. The multivalent EGFR display on phages would likely enhance their accumulation in HT29 spheroids. Through this exploratory research, a greater understanding of bacteriophages and mammalian cells may be gained for future applications.

## 2.2 Hypothesis

Bacteriophage Lambda (λ) can interact with multicellular spheroids generated from colorectal adenocarcinoma HT29 cells and mouse fibroblast NIH3T3 cells. The display of EGF on lambda phage will further enhance binding, uptake and accumulation into spheroids. The specific binding to EGF receptors on cells can thereby slow spheroid formation and growth.

## 2.3 Objectives

The main objective of this research was to assess the phage-mammalian cell interactions in the context of 3D multicellular spheroid cell culture. Specific objectives were:

1. To visualize the intrinsic capacity of fluorescent phage λ to adhere and accumulate in HT29 and NIH3T3 multicellular spheroids.
2. To assess the impact of phage λ on HT29 spheroid formation and growth.
3. To measure the internalization of phage λ into HT29 cells in spheroids.
4. To assess cytotoxicity induced by phage λ in HT29 monolayer cells and spheroids.
5. To compare objectives 1-4 between wildtype and EGF-displaying λ phages.

# Chapter 3: Materials and Methods

## 3.1 Buffers and solutions

Ampicillin Stock (Sigma Aldrich, Oakville, Canada)

This was used as a selective marker for the pPL451 plasmids in the *E. coli* hosts and was added to broth at 100 μg/ml from a stock prepared at a concentration of 50 mg/ml into filter-sterile water. This stock powder was stored at -20 °C.

Luria Bertani Broth

LB broth is a nutritionally-rich medium used for the rapid propagation of bacteria in culture. It consists of 10 g tryptone, 5 g yeast abstract and 5 g NaCl dissolved in 1 L MilliQ $H_2O$, sterilized (autoclave) and stored at room temperature.

LB Agar

LB agar was used as a solid support for the growth of bacterial cultures. It consists of 10 g tryptone, 5 g yeast abstract, 5 g NaCl and 13g Grade A Bacto™ agar (Difco Laboratories) dissolved in 1 L MilliQ $H_2O$. It was sterilized, poured onto sterile plates and stored at 4 °C.

LB Top Agar

LB top agar was used as an overlay on top of regular nutrient agar plates. The semi-solid consistency permits progeny phages to diffuse through the media to infect the evenly-dispersed, "lawn" of bacterial culture. It consists of 10 g tryptone, 5 g yeast abstract, 5 g NaCl and 7 g Grade A Bacto™ agar, dissolved in 1 L MilliQ $H_2O$, sterilized and stored in 52 °C water bath to maintain the molten state.

PEG (Polyethylene Glycol)

PEG was used to precipitate phage particles and purification. It was prepared by dissolving 0.2 M PEG 8000, 0.15 M NaCl in 1 L MilliQ $H_2O$ (pH 7.8), filter-sterilized and stored at room temperature.

TN Buffer

Phages were stored in TN buffer at 4 °C. It was prepared by dissolving 0.1 M NaCl, 0.01 M Tris-HCl (pH 7.8) and autoclaving afterwards. This was stored at room temperature.

TN/EDTA Buffer

This buffer was used to test for phage sensitivity. 0.1 M NaCl, 0.01 M Tris-HCl, 0.1 M EDTA was dissolved in 1L MilliQ $H_2O$ (pH 7.8). This was sterilized and stored at room temperature.

PBS

PBS was used to perform washes of spheroids to rid of unbound phages and dyes. It was prepared by dissolving 1370 mM NaCl, 27mM KCl,100mM of $Na_2HPO_4$, 18mM of $KH_2PO_4$ in MilliQ $H_2O$ (pH 7.4) and was filter-sterilized.

## 3.2 Bacterial and bacteriophage strains, plasmids and eukaryotic cells

**Table 1: Summary of bacteria, phage, plasmids and eukaryotic cells used in this study**

| Cell | Genotype | Source/Reference | Additional Information |
|---|---|---|---|
| **BB4** | *supF58 supE44 hdR514 galK2 galT22 trpR55 metB1 tonA* DE*(lac) U169* | Agilent Technologies, Inc. | This strain encodes a double suppression action (SupE and SupF) and serves as the positive control for the efficiency of plating (EOP) of λF7 samples. |
| **W3101** | *F-, galT22, λ-, IN(rrnD-rrnE)1, rph-1,* | CGSC #4467 Bachmann (1972) | This strain does not exert any amber suppression action and serves as the negative control for λF7 samples as λF7 is not viable on this host. |
| **W3101 SupD** | *F-, galT22, λ-, IN(rrnD-rrnE)1, rph-1, uvrC279::Tn10, serU132(AS),* | Nicastro et al. (2013) | Amber isogenic suppressor SupD strain of W3101. W3101 SupD (*serU132*) |
| **W3101 SupF** | *F-, galT22, λ-, IN(rrnD-rrnE)1, rph-1, oppC506::Tn10, tyrT5888(AS)* | Nicastro et a. (2013) | Amber isogenic suppressor SupF strains of W3101. W3101 SupF (*tyrT5888*) |
| **Phage Strains** | | | |
| **λF7** | *λDam15imm21cI ts* | Mikawa et al. (1996) Maruyama et al. (1994) | λ phage harbouring an amber mutation in the gene encoding gpD, and is able to form viable particles in the presence of the amber (UAG) stop codon at the position 68 of the 110 amino acid protein. |
| **Plasmids** | | | |
| **pPL451 gpD::EGF (pD::EGF)** | *pM-cI857-pL-cI857-pL-D::EGF-tL* | Sokolenko et al. (2012), Nicastro et al. (2013) | Multicopy plasmid pPL451 that is under the control of a temperature-sensitive allele of the λ CI857 repressor. The EGF sequence is fused to the C-terminal of the gpD capsid gene that is separated by an in-frame linked sequence p(TSGSGSGSGSGT) and a *KpnI* cut site. |
| **Eukaryotic Cell Line obtained from the American Type Culture Collection (ATCC®)** | | | |
| **NIH3T3** | Mouse fibroblast cells | | |
| **HT29** | Human colorectal adenocarcinoma | | |

## 3.2 Cell culture

Cell lines were obtained from the American Type Culture Collection (ATCC®) and were maintained in T25 flasks at 37 $^{o}$C in a humidified atmosphere of 95% air and 10% $CO_{2.}$ Cells were cultured in Dulbecco's Modified Eagle's Medium (DMEM, Thermo Scientific) supplemented with 5% heat-inactivated foetal bovine serum (FBS). The culture medium was replaced every 3 d.

## 3.3 Spheroid culture

The characteristics and growth of multicellular spheroids with various seeding densities and cell lines were observed and recorded. At 90% confluency, NIH3T3 or HT29 monolayer cells were trypsinized (0.25% trypsin-EDTA) into single cell suspensions and were counted with a hematocytometer (Fisher Scientific). NIH3T3 fibroblast spheroids were generated at 30,000 cells for initial seeding density and were cultured for 10 d. HT29 colon adenocarcinoma spheroids were generated by seeding 5, 000 cells and were cultured for 7 d. To examine the spheroid growth over time, various seeding densities were imaged every 2 d using a bright-field microscope (Nikon® TE200). The spheroid diameters were measured using the QCapture Pro™ 7 software and Micropublisher 5.0 RTV camera by projecting a bright-field image of the spheroid onto the screen and using the calibration wizard for the select objective lens and obtaining a measurement by extending the bar over the spheroid.

Spheroids were generated using 1.5% agarose (weight/volume) in serum-free DMEM and cast in a 96-well cell-culture plates. Cells were seeded in 200 µl of DMEM supplemented by 5% FBS and incubated at 37 $^{o}$C and 10% $CO_2$. The growth of each spheroid was recorded for up to 14 d. Each spheroid was harvested using a glass pipette and treated with $10^8$ PFU of phage, unless otherwise stated.

## 3.4 Phage display

Phage display of EGF molecules on λ phage particles was achieved by the dual-control expression system that using amber mutant *D* capsid phage, λF7, that imparts a truncated gpD protein in a wildtype *E. coli* host. Through this system, viable progeny particles can be produced via amber suppression from suppressor strains of *E. coli* that possess mutated tRNA that reads the UAG stop codon and insert a different residue, allowing the full translation of *Dam15* for a full length gpD capsid protein. W3101 SupD (*serU132*) and SupF (*tyrT5888*) are amber suppressor strains of *E. coli* that form alleles of gpD that is less optimal due to the insertion of amino acid serine and tyrosine, respectively, in the place of the UAG stop codon. In contrast, the SupE (*glnV44*) suppressor strain counterpart can fully restore gpD by the replacement of glutamine in place of the amber stop codon, fully suppressing the amber mutation. Functional gpD alleles can also be provided *in trans* via complementation using a plasmid [pPL451 gpD::EGF] encoding a D allele translationally fused to the EGF or other gene of interest, resulting in the EGF peptides fused to gpD capsid proteins.

### 3.4.1 Transformation

[pPL451-gpD::EGF] is a multicopy plasmid that expresses *gpD:EGF* and is under the control of a temperature-sensitive allele of the λ CI857 repressor that induces the gene at temperatures above 37 $^{o}$C, conferring ampicillin resistance to the host (Sokolenko et al., 2012). A C-terminal EGF fusion to the capsid protein gpD was designed and constructed. Competent W3101 SupD and SupF – amber suppressor *E. coli* cells – were transformed with [pPL451-gpD::EGF] via heat shock and transformed colonies were selected on Luria Bertani (LB) ampicillin agar plates.

BB4 (supE, supF) *E.coli* is the double amber suppressor that results in functional λF7 phage particles without the presence of the fusion plasmid; this strain served as a positive control for efficiency of plating, and a negative control for EGF decoration (Nicastro et al., 2013).

Nicastro et al. demonstrated that maximal decoration of λF7 is conferred by generating phages at higher temperatures (37 $^{o}$C), using SupD *E.coli* amber suppressor host for propagation (denoted as 'Hi-D::EGF phage') (Nicastro et al., 2013). Phages generated from the SupF *E. coli* strain resulted in reduced complementation from the plasmid expressing the gpD fusion than the SupE *E. coli* strain, therefore phages generated from SupF was used in this experiment to represent minimal surface decoration (denoted as 'Lo-D::EGF phage'). Fluorimetric analysis of gpD::eGFP decorated phages in the same study estimated about 147 molecules per phage for the maximal fusion (SupD, 37 $^{o}$C), and 89 molecules per phage generated from SupF at 37 $^{o}$C. From these values, we can infer that the Lo-D::EGF phages will be approximately 40% less decorated than Hi-D::EGF phages. These values are not absolute and have been provided as a point of reference to infer the relative degree of surface decoration.

### 3.4.2 Phage lysate preparation

Transformed SupD and SupF *E. coli* cells were grown in LB broth over night at 37 $^{o}$C. 10-fold dilutions of primary lysates were prepared in 1 ml of TN buffer and were added to 0.3 ml of the transformed cells (grown to $OD_{600}$ = 0.4 at 37 $^{o}$C), then incubated overnight at 37 $^{o}$C. 10 ml of TN buffer were added the next day on to each plate and incubated for 24 h at 4 $^{o}$C. The top agar was scraped and transferred to a conical tube, which was centrifuged at 23183 x g (Avanti J-E Centrifuge, Beckman Coulter, Mississauga Canada) at 4 $^{o}$C for 20 min. Negative control λF7 generated with a double suppressor BB4 *E. coli* host (that will not confer phage display, denoted as wildtype λ phage herein) was prepared in parallel for future experiments.

## 3.5 Phage purification

All phage lysates were filtered through a sterile 0.2 µm syringe filter to remove cellular debris, followed by polyethylene glycol (PEG) -precipitation (Sigma-Aldrich). Precipitated phages were resuspended in DMEM supplemented with 5% FBS and were further purified through a gel chromatography. This is comparable to that purification via CsCl centrifugation in dissociating unincorporated fusion and other smaller cellular debris (Zakharova et al., 2005). Phage samples were resuspended in DMEM and 5% FBS and standardized to a concentration of $10^9$ PFU/ml. 100 µl of each sample was added to each spheroid for a total of $10^8$ PFU.

## 3.6 Phage titration and standard plaque forming unit assays

Plaque assays were used to determine concentration of phages following the purification process. It was also used to assess change in phage infectivity over time under various conditions. Soft-agar overlay technique was used on fresh BB4 *E. coli* cells, as this strain generates the highest titers of λF7 (it possesses double suppressor activity, SupE, SupF). A liquid culture of BB4 (300 µl) was added to 3 ml of molten top agar (Bacto Tryptone and Bacto Agar from Difco Laboratories, Sparks, MD), as well as a 100 µl volume of phage dilution in suspension. Each phage particle produced a visible clearing zone on the lawn of bacteria; greater dilution of phages in the supernatant resulted in fewer plaques. Solutions containing purified phage were generally standardized to $10^9$ PFU/ml and 100 µl ($10^8$ PFU) was added to each spheroid, unless otherwise stated.

## 3.7 Assessing phage viability

To test the infectivity of phages under the experimental conditions outlined, changes in phage titers were measured over time using the plaque assay. Wildtype and gpD::EGF expressing

phages were incubated at both 4 and 37 °C, suspended either in DMEM supplemented by 5% FBS or TN buffer, and were then measured at 4, 8, 24, and 48 h, post-application. Phages were quantified on *E. coli* BB4 cells and were plated on LB agar, diluted in TN buffer by a standard factor to generate countable plaques within the ranges of 20-200 PFU/plate. Efficiency of plating (EOP) was expressed relative to the initial phage titer determined at t = 0 h as the 100% plating control.

## 3.8 EDTA sensitivity assay

Structural stability of phages displaying EGF molecules were tested using the EDTA sensitivity assay. Phages were diluted in TN buffer (0.01 M Tris-HCl and 0.1 M NaCl, pH 7.8; Fisher Scientific, USA) to a standardized concentration of $10^8$ PFU/ml, then were diluted 100-fold into TN/EDTA buffer (0.01 M Tris-HC; (pH 7.8), 0.1 M NaCl, and 0.01 M EDTA) and incubated for 30 min at 25 °C. The EDTA-phage reaction was stopped by diluting experimental reactions 100-fold into TN buffer. Phages were then plated on an overlay of BB4 cells and incubated overnight at 37 °C. EOP was determined for each sample, using the formula below:

$$\frac{\text{plaque counts by the original phage concentration}}{\text{100\% positive plating control (using plaque counts on BB4 cells)}}$$

## 3.9 Labeling of phage capsid for imaging

The primary amines of wildtype λ phage or EGF-displaying phage capsids were conjugated with Alexa Fluor® 488 (Thermo Fisher) according to manufacturer's instructions. Briefly, $10^{12}$ PFU of PEG-precipitated phages were resuspended in 95 µl of 0.1-M $NaHCO_3$ buffer (pH 8.3) and were incubated with 5 µl of dye (10 mg/ml in dimethyl sulfoxide, (DMSO) at room temperature for 1 h with brief vortexing every 10 min. The volume was then brought up to 1 ml and was centrifuged for 30 min at 23183 x g at 4 °C, then for 10 min at the same speed. The unbound dye

in the supernatant was replaced with DMEM and 5% FBS to resuspend the Alexa Fluor® 488-conjugated phages.

## 3.10 Confocal microscopy for phage visualization in spheroids

HT29 spheroids were grown for 7 d (seeding density of ~5,000 cells). Spheroids were transferred into 1.5 ml microcentrifuge tubes and treated with $10^8$ PFU of phage for either 30 min, 4 h, 8 h and 24 h and incubated at 37 $^{o}$C, 10% $CO_2$. Each spheroid was stained with 10 µM of CellTracker Red CMPTX dye™ (Molecular Probes, Invitrogen) for 1 h at 37 °C prior to visualization. CellTracker is mildly thiol-reactive and can diffuse through the live cell membranes. It is retained in the cell for at least 24 h as it becomes membrane-impermeable by reacting with other intracellular proteins (Gonzalez et al., 2013). Cell medium was discarded, and spheroids were washed 3X with PBS and transferred with a glass pipette onto a glass bottomed 24-well plate (MatTek P-24G-0-13_F). Treated spheroids were visualized with laser scanning confocal microscope, 20X objective (Zeiss LSM 710). Z-stack images from the bottom to the center were obtained for each spheroid. Confocal microscopy was done with the assistance of Drs. M. Foldvari and R. Chen and J. Fux.

## 3.11 Internalization assay

HT29 spheroids were grown for 7 d (seeding density of ~5,000 cells). Prior to the application, spheroids were treated with 5 mM of $NH_4Cl$ for 45 min at 23 °C to prevent internalized phages from entering the lysosomes. Ammonium chloride and chloroquine are considered to be lysosomotropic weak bases that selectively accumulate in lysosomes to reduce endosome-lysosome acidification (Misinzo, Delputte, & Nauwynck, 2008). Spheroids were washed with PBS and treated with $10^8$ PFU of phages for 30 min, 4 h, 8 h and 24 h at 37 °C. Following the incubation periods, spheroids were washed 5 times with PBS to remove unbound phages. Cold

0.2 M glycine (pH 2) was added to spheroids for 10 min, followed by 2 washes with PBS to inactivate unassociated phages suspended in the media. 100 µl of 0.25% EDTA-trypsin was added to spheroids and incubated at 37 °C for 20 min, then cells were vigorously pipetted and gently vortexed for complete disaggregation. The suspended cells in trypsin were centrifuged at 7,000 x g for 10 min to separate the phages recovered from the intercellular spaces of the spheroids. The supernatant was removed and set aside as "*inter*cellular" phages for each sample (Fig. 4). The pelleted cells were resuspended and washed in PBS, and the centrifugation step was repeated. The wash media was collected in the same "intercellular" fraction. The pelleted cells were resuspended in 100 µl MilliQ $H_2O$, subjected to 3 freeze/thaw cycles to release internalized phage particles. This mixture was centrifuged and the supernatant was set aside as the "*intra*cellular" fraction of the phage mixture. The collected fractions were serially-diluted by $10^{-2}$ – $10^{-8}$ in PBS, and 10 µl of each dilution of phages were "spotted" onto a lawn of BB4 cells to determine the optimal dilution factor for well-separated, countable plaques. These plates were incubated overnight at 37 °C and whole plates were prepared the next day to determine the EOP of each fraction.

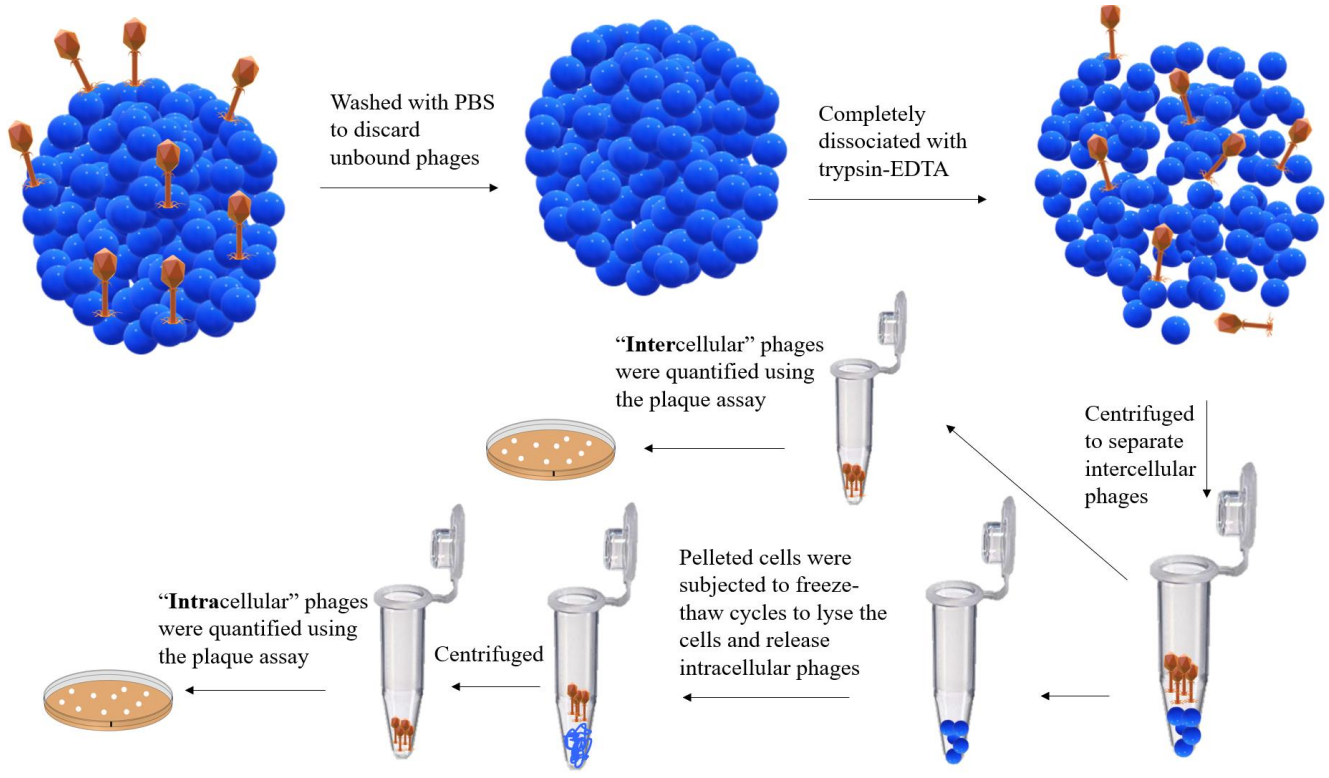


**Figure 4: Internalization assay.** Spheroids were pre-treated with ammonium chloride prior to the addition of phages for 0.5, 4, 8 and 24 hours. Spheroids were washed with PBS to discard unbound phages on the surface of spheroids. Spheroids were then completely dissociated with trypsin-EDTA to release intercellular phages within the spheroid. Cells were lysed by freeze-thawing, which released intracellular phages. All recovered phages were quantified using the plaque assay.

## 3.12 Phage λ and effects on spheroid growth

5,000 HT29 cells were seeded on agarose to form spheroids previously described (see 3.2). Phages were added to partially-formed and fully-formed HT29 cells; cells were also co-seeded with phages to observe the effects of phages on initial cell-aggregation (detailed below). The following conditions were imaged with brightfield illumination on a Leica DM2000 microscope, 10X objective and a QImaging Micropublisher 5.0 RTV camera using the QCapture Pro™ 7 Software (QImaging). No phages were added to the "control spheroid". All images were qualitatively representative of three replicates of two independent experiments:

i. Cells were grown for 48 h on agarose for initial aggregation for partially-formed spheroids prior to the addition of $10^8$ or $10^4$ PFU of resuspended D::EGF or wildtype λ phages. Pictures were obtained every 2 d over a duration of 20 d.

ii. Cells were co-seeded with $10^8$ or $10^4$ PFU of D::EGF or wildtype phages and were grown for 7 d. Pictures were obtained every 2 d over a duration of 7 d.

iii. Cells were pre-chilled with $10^8$ or $10^4$ PFU of D::EGF or wildtype phages for 1 h on ice, then co-seeded on to agarose. Pictures were obtained over a duration of 10 d.

iv. Fully-formed HT29 spheroids, cultured for 5 d (seeded at 3,000 cells), were treated with $10^8$ or $10^4$ PFU of D::EGF or wildtype phages. Pictures were obtained over a duration of 5 d.

## 3.13 MTT assay

The size of the viable cell population with the treatment of phages was measured by the 3-(4,5-dimethylthiazol-2-yl)-2,5- diphenyltetrazolium bromide (MTT) assay and its conversion to formazan by viable cells. Cells were seeded in DMEM supplemented with 5% FBS in 96-well plates and incubated at 37 °C, 10% $CO_2$ for 48 h to allow for initial adherence. Cells were then treated with either $10^8$ or $10^4$ PFU of D::EGF or wildtype phages for 24 h at 37 °C, 10 % $CO_2$. The medium was aspirated and 20 µl of 0.5 mg/ml MTT in PBS was applied and the plate was swirled and incubated at 37 °C for 1 h to allow for the conversion of MTT into formazan. The MTT reagent was then removed and replaced with 100 µl of DMSO per well for 30 min at room temperature for the dissolution of formazan dye. At the end of this incubation period, the absorbance of the plate was measured at $A_{492}$ nm on a SpectraMax M5 Plate Reader. The results were normalized by subtracting $A_{492}$ of blank wells.

## 3.14 3D Toxicity assay

Phage-treated HT29 spheroids were assessed for cytotoxicity using CellTiter-Glo® 3D (Promega) – a viability assay for 3D cell cultures. It determines the number of viable cells in multicellular spheroids based on the quantitation of ATP, a marker for metabolically-active cells. This assay was used to visually determine whether cells within spheroids remained viable in response to phage treatment. This was conducted according to the manufacturer's directions, as follows. 5,000 HT29 cells were seeded to produce robust spheroids, as previously described, and grown for 7 d. Spheroids were transferred with glass pipettes and placed into opaque multiwell plates. A volume of acid solution (4 mM diaminocyclohexane triacetic acid in water) was added, equivalent in volume to the cell culture medium containing the spheroid. The contents were mixed vigorously for 5 min on an orbital shaker and incubated at room temperature for additional 15 min. Half of the sample was transferred to a separate container and diluted by 10-fold in MilliQ $H_2O$ with repeated mixing to ensure homogeneity. The diluted sample was then transferred to a fresh assay well. An equal volume of CellTiter-Glo® 3D Reagent was added, and the contents were mixed for an additional 2 min on an orbital shaker. The plates were incubated at room temperature for 10 min to stabilize the luminescent signal, which was then recorded on the SpectraMax M5 spectrophotometer using the luminescence mode at the wavelength range of 250–850 nm.

## 3.15 Spheroid embedding in paraffin

HT29 spheroids grown for 7 d (seeding density of 5,000 cells) were treated with fluorescently-tagged wildtype or D::EGF phages (see 3.8). The spheroids were placed in 20X volume of 10% formalin at room temperature and dehydrated by passing through successive changes of 70% ethanol (in Millipore water), two changes in 100% ethanol and two changes in 100% xylene. The

spheroids were embedded into paraffin wax by passing through two changes of 100% wax at 56 – 58 ℃. The sections were mounted onto slides and air dried. The sections were deparaffinized the following day in 2-3 changes of xylene, 5 min each. Sections were then hydrated in 2 changes of 100% ethanol for 3 min each, 70% ethanol for 1 min each. Samples were fully hydrated with 2 changes of MilliQ $H_2O$ and mounted with aqueous mountant (Biomeda©).

## 3.16 Statistical analysis

GraphPad Prism 5 software was used for the analysis of data and a threshold of $p<0.05$ was deemed to be significant for all statistical tests. Changes in phage viability in response to temperature was analyzed by two-way analysis of variation (ANOVA) by comparing values between incubations at 4 ℃ and 37 ℃. HT29 spheroids treated with ammonium chloride was compared with the untreated by the Mann-Whitney test. Percent internalization of D::EGF phages were compared to that of wildtype for each treatment durations by the Mann-Whitney test. Percent viability of HT29 cells in response to phage treatment was compared to the untreated cells by the Mann-Whitney test. Experiments were performed with a minimum of three independent biological replicates.

*p< 0.05

**p≤0.005

****p<0.005

# Chapter 4: Results

## 4.1 Characterization of spheroids with different seeding densities

Cells were seeded on agarose, which resists cell adhesion and causes the cells to preferentially stick to each other and form spheroids. The growth of spheroids and morphological changes were monitored for the following cell lines: HT29, MDA-MB-231, A549 and A2780. Growth of spheroids were visualized with a bright-field microscope for up to 10 d to choose optimal cell lines for downstream applications.

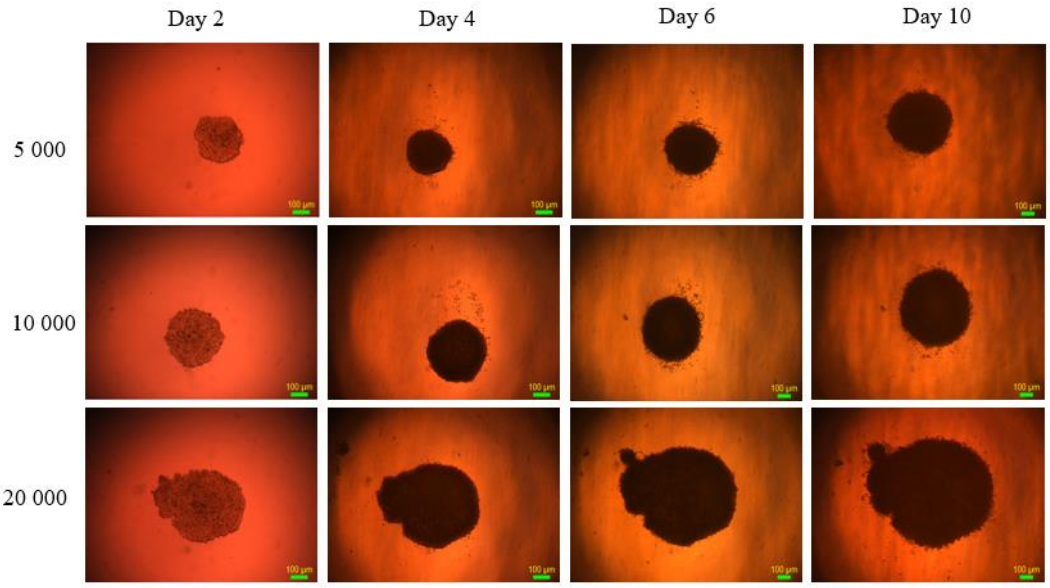


**Figure 5: Growth of HT29 spheroids at various seeding concentrations, imaged for 10 d.** Spheroids seeded with more than 10,000 cells were generally flatter in morphology. These cells dispersed laterally onto agarose, which could not be used to assess phage penetration. 6-10 day-old spheroids generated from 5,000 cells were used in all experiments, unless otherwise stated.

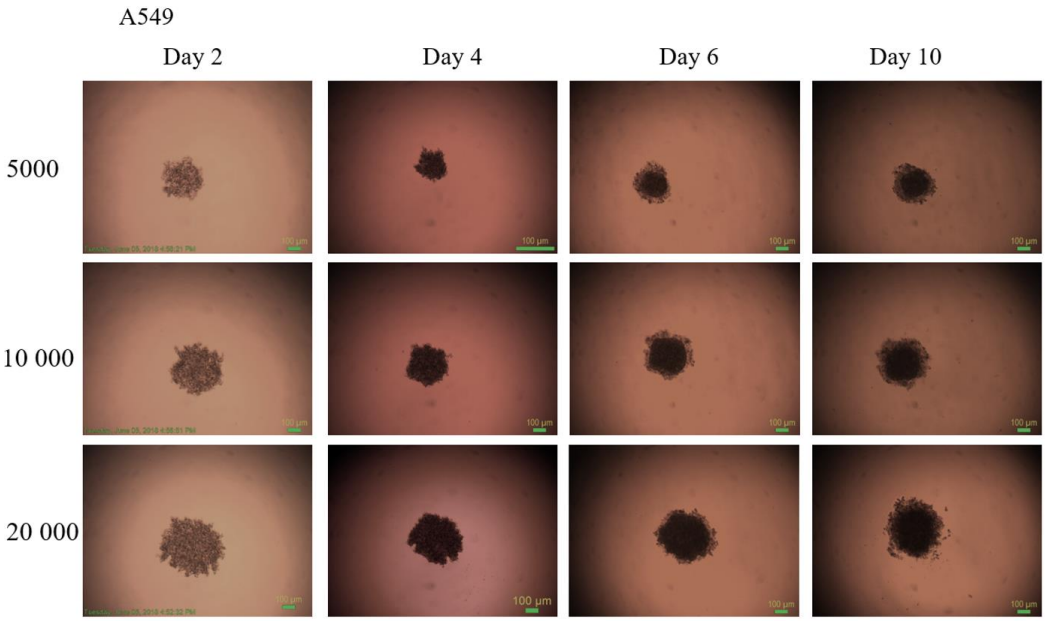


**Figure 6: Growth of A549 spheroids at various seeding concentrations, imaged for 10 d.** Spheroids demonstrated poor reproducibility and were also generally flatter in morphology.

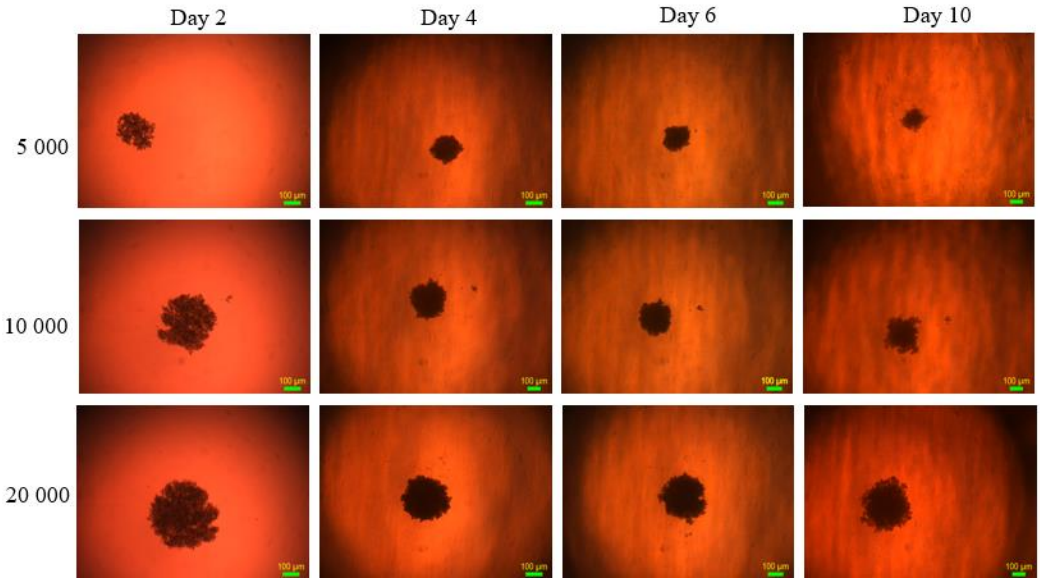


**Figure 7 Growth of MDA-MB-231 spheroids at various seeding concentrations, imaged for 10 d.** Spheroid morphology was inconsistent among replicates and demonstrated poor reproducibility.

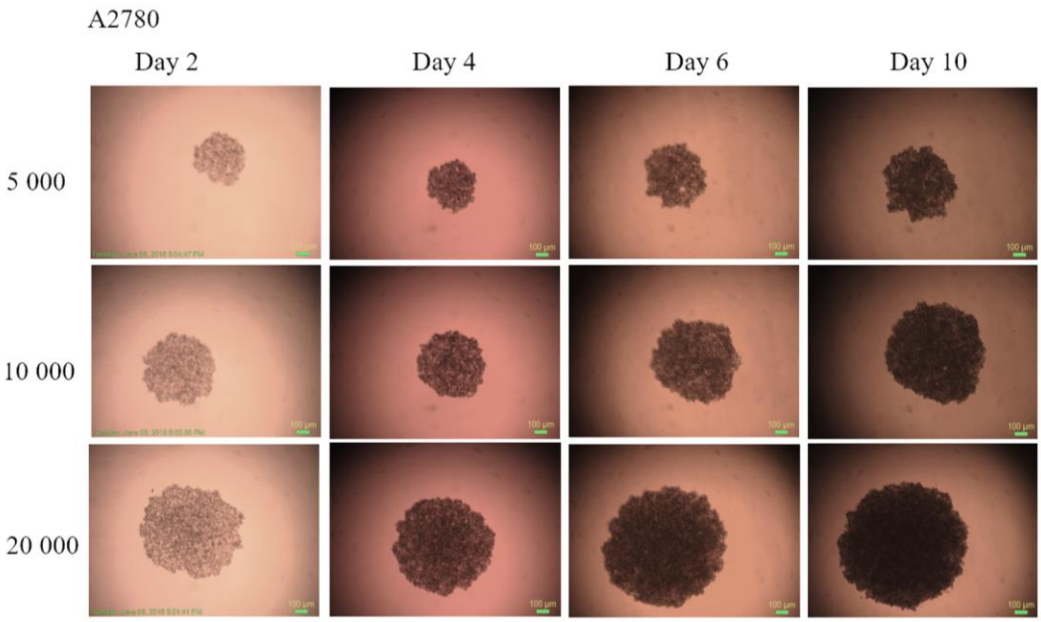


**Figure 8: Growth of A2780 spheroids at various seeding concentrations, imaged for 10 d**. Cell-cell connections appeared to be loose and gaps were visible between cells. Spheroids did not form fully and appeared to be disc-like in morphology.

Fig. 5-8 shows representative optical images of spheroids with different cell seeding densities. Several stages were uniformly observed in spheroid formation across most cell lines; within the initial 24 h after seeding, cells spontaneously aggregated and appeared to form of intercellular connections. However, MDA-MB-231, A549 and A2780 spheroids were not robust and disintegrated upon handling. A2780 spheroids in particular, showed dispersed cells with visible intercellular gaps after 10 d, likely having failed in forming effective cell-cell connections (Fig. 8). Conversely, robustness was achieved within 6-10 d of growth for HT29 cells seeded at a concentration of 5,000 to 30,000 cells (Fig. 5). Definite intercellular connections appeared to have established by days 3-5, as the surfaces of spheroids were smoother and diameters decreased slightly. This was likely a result of cells adhering more tightly to each other. Diameters increased again by day 6, and cell proliferation was visible on days 4-6. Spheroids exhibited rougher edges and cells scattered in the surrounding media. Cells visibly dissociated from spheroids on day 10, as cells lost their circular morphology. The relationship between cell

seeding concentrations and spheroid diameters for cell lines HT29, NIH3T3 and HCT116 after 5 d of growth are shown in Table 2.

**Table 2: HT29, NIH3T3 and HCT116 spheroid diameters are dependent on initial cell-seeding densities.**

| Seeding Densities | Diameter of NIH3T3 spheroids (μm)[1] | Diameter of HT29 spheroids (μm) [1] | Diameter of HCT116 spheroids (μm) [1] |
|---|---|---|---|
| **100** | N/A[2] | 70 ± 8.2 | N/A |
| **500** | N/A | 175 ± 19.2 | 150 ± 18.2 |
| **1,000** | N/A | 205 ± 20.4 | 175 ± 19.7 |
| **5,000** | 70 ± 10.5 | 320 ± 35.1 | 225 ± 28.3 |
| **10 000** | 130 ± 15.9 | 580 ± 50.3 | 530 ± 41.2 |
| **20 000** | 190 ± 16.2 | 700 ± 66.4 | 615 ± 50.8 |

[1]Diameters are represented as a mean ± SEM of 3 separate spheroids.
[2]N/A denotes the insufficient cell density for effective aggregation and ability to form a defined spheroid. Diameters of each group were highly uniform (SD <15%).

HT29 cells were selected for downstream applications because diameters were uniform and reproducible – 90% of wells formed spheroids and diameters varied by less than 15% (Table 2). Reproducibility of spheroid sizes was crucial to ensure consistency in parameters that could ultimately influence the pharmacokinetics of phage penetration. However, it is important to note that individual spheroids can still be highly heterogeneous despite exhibiting similar diameters. HT29 cells can also be useful in modeling epithelial cells forming tight junctions between cells (Martínez-Maqueda, Miralles, & Recio, 2015). In this project, ~350 μm diameter HT29 spheroids, initially seeded with 5,000 cells and grown for 6-10 d were often used for treatment. Larger spheroids may exhibit hypoxic and necrotic cores, which may potentially complicate the characterization of phage penetration because of accumulated fluid and cellular debris (Zanoni et al., 2016).

The complete aggregation of cells to form robust spheroids was also contingent on the initial seeding densities. For example, the initial concentration of < 1,000 cells was not sufficient for aggregation after 7 d and failed to form defined spheroids (Fig. 9). HT29 spheroids seeded with ≥10,000 cells were compact and usable for downstream applications

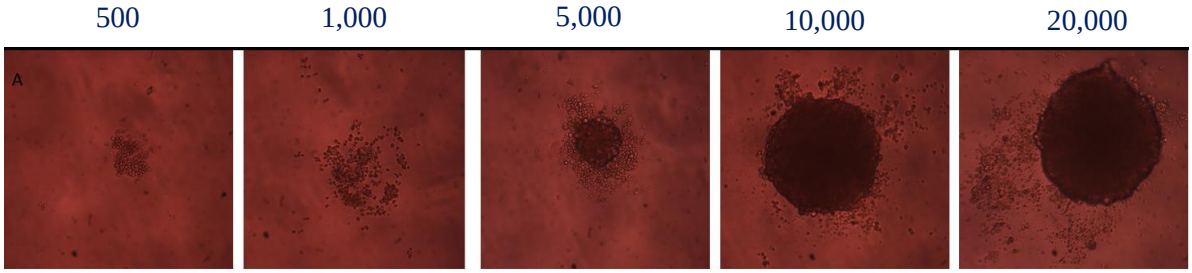


**Figure 9: HT29 cells seeded at various concentrations after 7 d.** Cell proliferation was evident by the scattered cells surrounding the spheroids. Seeding fewer than 1,000 cells resulted in aggregation of cells, but they failed to form defined spheroids.

## 4.2 Generation of EGF-displaying λ phages and λ packaging tolerance of gpD::EGF fusion

The ability of the pD::EGF plasmids to complement the *Dam15* mutation of λF7 to generate phages displaying EGF was dependent on the tolerance of the gpD allele conferred from the SupD and SupF isogenic suppressor strains. Theoretically, poor suppression of the amber mutation by the Sup+ hosts would lead to the greater reliance on the pD::EGF plasmids for complementation of *gpD*. This was determined by assessing the restoration of viability of λ *Dam15* phages generated from the different Sup+ hosts as compared to the Sup− wild type *E. coli* host.

**Table 3: pD::EGF complements the *Dam15* mutation and increases viability of λF7 phages in the absence of suppressor host *E. coli***

| Strain [+/- Plasmid][1] | Relative efficiency of plating (EOP)[2] | Increase in plating (compared to Sup-) |
|---|---|---|
| Sup− | $2.8 \times 10^{-5}$ | 1.0 |
| Sup− [pD::EGF] | 0.05 | $1.79 \times 10^{3}$ |
| SupD | $1.6 \times 10^{-5}$ | 0.57 |
| SupD [pD::EGF] | 0.12 | $4.29 \times 10^{3}$ |
| SupF | 0.23 | $8.21 \times 10^{3}$ |
| SupF [pD::EGF] | 0.10 | $3.57 \times 10^{3}$ |

[1]The *E. coli* suppressors are W3101 derivatives, and the plasmid pPL451 is under the temperature-regulated repressor CI857.

[2]All EOPs have been expressed as a mean of three assays with 3 replicates, determined using BB4 (SupE, SupF double suppressor *E. coli*) as the 100% plating control, plated at 37°C.

Table 3 shows the ability of the *gpD::EGF* expression plasmid to complement for the *Dam15* mutation of λF7 by restoring plating by more than a 1000-fold in the absence of suppressor activity (Sup−). The EOP (determined by BB4, SupE, SupF double suppressor, as the 100% plating control) increased by over a 4000-fold in SupD with the *gpD::EGF* complementation despite the poor suppressor activity and low viability on the SupD derivative. SupF strain possesses effective suppressor activity and there were no significant differences with the complementation for the *Dam15* mutation on the viability of phage. These results were in agreement with those of Nicastro et al. 2013, whereby the SupD host was the least effective at reversing the *Dam15* mutation, while SupF suppressed the mutation with near perfect efficiency (Nicastro et al., 2013). Plasmid pPL451 is under the control of a temperature-sensitive repressor, CI857, but all phages were generated at 37 °C, rendering the repressor ineffective and allowing the expression of downstream gene sequences. This resulted in maximal fusion of EGF to gpD on the λ*Dam15* phage capsid at 37 °C, specifically in the suppressor host with the poorest functionality, SupD *E. coli*.

### 4.2.1 Assessment of phage viability in response to temperature

Phages are typically stored at 4 °C, which generally provides long-term stability (Lech, Reddy, & Sherman, 2004). The effects of long-term incubation at 37 °C and in cell media on the ability of wildtype and EGF-displaying phages were assessed. Phages were exposed to these conditions for defined intervals up to 48 h and plaque assays were used to quantify changes in the concentration of infective phage particles over time.

**Table 4: Prolonged exposure of phages at 37°C decreases λ phage infectivity.**

| | EOP of λF7 incubated at 4°C[1] | EOP of λF7 incubated at 37°C[1] | EOP of D::EGF phages incubated at 4°C[1] | EOP of D::EGF phages incubated at 37°C[1] |
|---|---|---|---|---|
| **0 h** | 1.00 ± 0.02 | 1.00 ± 0.05 | 1.00 ± 0.05 | 1.00 ± 0.02 |
| **4 h** | 0.98 ± 0.01 | 0.91 ± 0.01* | 0.95 ± 0.04 | 0.57 ± 0.02**** |
| **8 h** | 0.86 ± 0.05 | 0.73 ± 0.02*** | 0.82 ± 0.05 | 0.43 ± 0.04**** |
| **24 h** | 1.12 ± 0.02 | 0.46 ± 0.02**** | 0.86 ± 0.03 | 0.19 ± 0.08**** |
| **48 h** | 0.94 ± 0.03 | 0.35 ± 0.03**** | 0.86 ± 0.02 | 0.28 ± 0.04**** |

[1]All EOPs have been expressed as a mean ± standard deviation of three independent assays, n=3, determined using BB4 (SupE, SupF double suppressor) as the 100% plating control and plated at 37 °C.
Comparisons of each phage types at two temperatures were made for each treatment period using the 2-way ANOVA test. Viability decreases of both phage types at 37 °C were statistically significant for all treatment periods.

This viability assay provides a relative change in phage titers; it is not an accurate representation of total phage particle counts in the media. Re-suspension and dilution of phage incubations in cell media supplemented at 4 °C slightly reduced phage infectivity, but this effect on phage viability increased dramatically at 37 °C. Changes in phage viability for both phage types with higher temperatures were statistically significant at all treatment durations, but D::EGF phages were impacted more by these external conditions than the wildtype λF7 phages. To minimize the effects of external variables on experimental outcomes, all titer assays were expressed as EOPs to the PFU/ml of the phage concentrations at each set of conditions in Table 4 to accommodate

for these confounding variables. All experiments were conducted with maximum incubation periods extending up to 24 h at 37 °C, as phage titers were decreased dramatically by this time point.

### 4.2.3 EDTA resistance by λ wildtype and λ D::EGF phages

Phages expressing EGF decoration were assessed for structural integrity with incubation in EDTA. EDTA is a chelating agent and will sequester cations such as $Mg^{2+}$ and $Ca^{2+}$, which are necessary co-factors to destabilize the λ capsid (Gilcrease et al., 2005).

**Table 5: Susceptibility of Display Phage to EDTA**

| Strain [+Plasmid] | Relative efficiency of plating (EOP)[1] |
|---|---|
| SupD [pD] | 0.41 ± 0.03 |
| SupD [pD::EGF] | 0.62 ± 0.02 |
| SupF [pD] | 0.46 ± 0.06 |
| SupF [pD::EGF] | 0.61 ± 0.04 |
| Sup− [pD::EGF] | 0.21 ± 0.05 |
| Sup−[pD] | 0.89 ± 0.03 |

[1]All EOPs have been expressed as a mean of three assays determined using BB4 (SupE, SupF double suppressor) as the 100% plating control and plated at 37 °C.

Phages grown on SupD *E. coli* had a lower survival rate (41%) than lysates grown on SupF (46%), which may be attributed to the higher stability in packaging. Decoration of the gpD protein resulted in consistent survival rates of 62% and 61% for the maximal decoration and minimal decoration, respectively. Phages developed on Sup− [pD::EGF] exhibited low survival rates of 21%, which may indicate low tolerance for the incorporation of the D::EGF into the phage capsid. Combination of complementation with pD::EGF and gpD alleles was found to be more stable than either one alone. Sup−[pD] conferring the wildtype gpD allele had the greatest resistance to EDTA at 89%, as expected.

## 4.3 Bacteriophage λ infiltration of multicellular spheroids

To demonstrate λ association and infiltration into the spheroids, 3 μm cross-sectional Z-stack images of spheroids were obtained with an inverted confocal microscope. The inner, densely-packed regions of the spheroid could not be observed, where the scattering of light obscured the detection of fluorescent phages in these regions. General observations were made on the spheroid surface-phage interactions as well as the overall accumulation of phages in the visible regions of the spheroid.

### 4.3.1 Interaction of λ phages with NIH3T3 spheroids

First, in order to observe the native interaction between unmodified, wildtype phages and fibroblast spheroids, $10^8$ PFU of wildtype λF7 phages tagged with Alexa Fluor® 488 were added to each 6- d old NIH3T3 spheroid for 0.5, 6 and 24 h. Spheroids were washed to discard unbound phages and were stained with CellTracker (red) (Fig. 10). After 6 h of treatment, the phage-associated fluorescence (green) was concentrated primarily at the periphery of the spheroid and were visible in the spheroid depths of 25 μm. After 24-h of phage treatment, phage-associated fluorescence completely dominated all cross-sections of the spheroid, likely indicating that phages have successfully accumulated in the spheroid (Fig. 10).

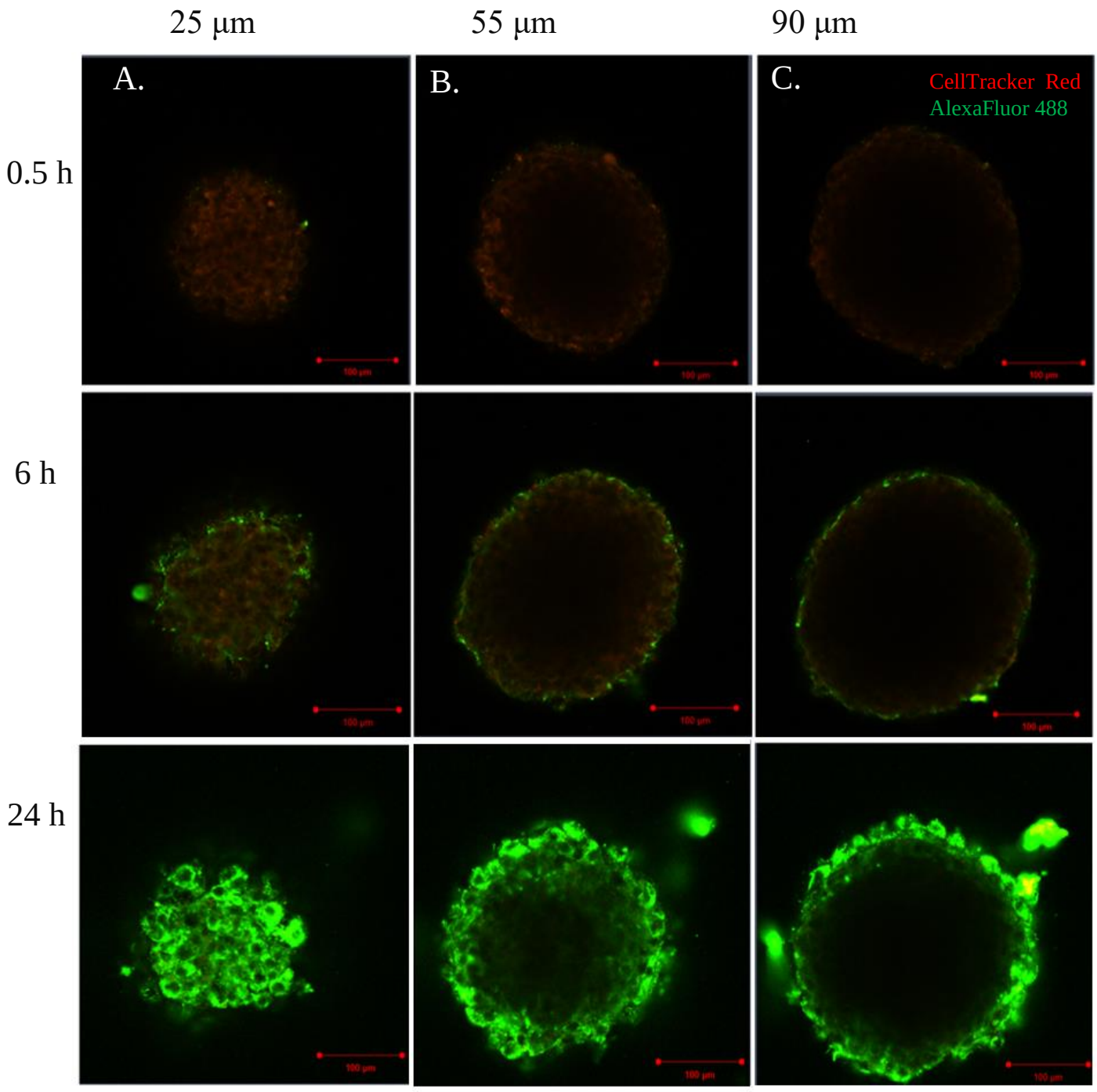


**Figure 10: Optical cross-sections of NIH3T3 spheroids treated with fluorescent λ phages**. Representative images of spheroids treated for A. 30 min, B. 6 h, and C. 24 h at optical sections 25, 55 and 90 µm from the bottom-most surface (n=3). All the spheroids were counterstained with CellTracker™ Red prior to imaging. Green fluorescence is associated with the presence of Alexa Fluor 488- phages.

The purification process of phages involved precipitation of phages by polyethylene glycol (PEG). This raised the possibility of PEG being bound by Alexa Fluor 488 and providing false positive signals in Fig. 10. Therefore, PEG was processed with Alexa Fluor 488 as a control, without the addition of phages, in Fig. 11.

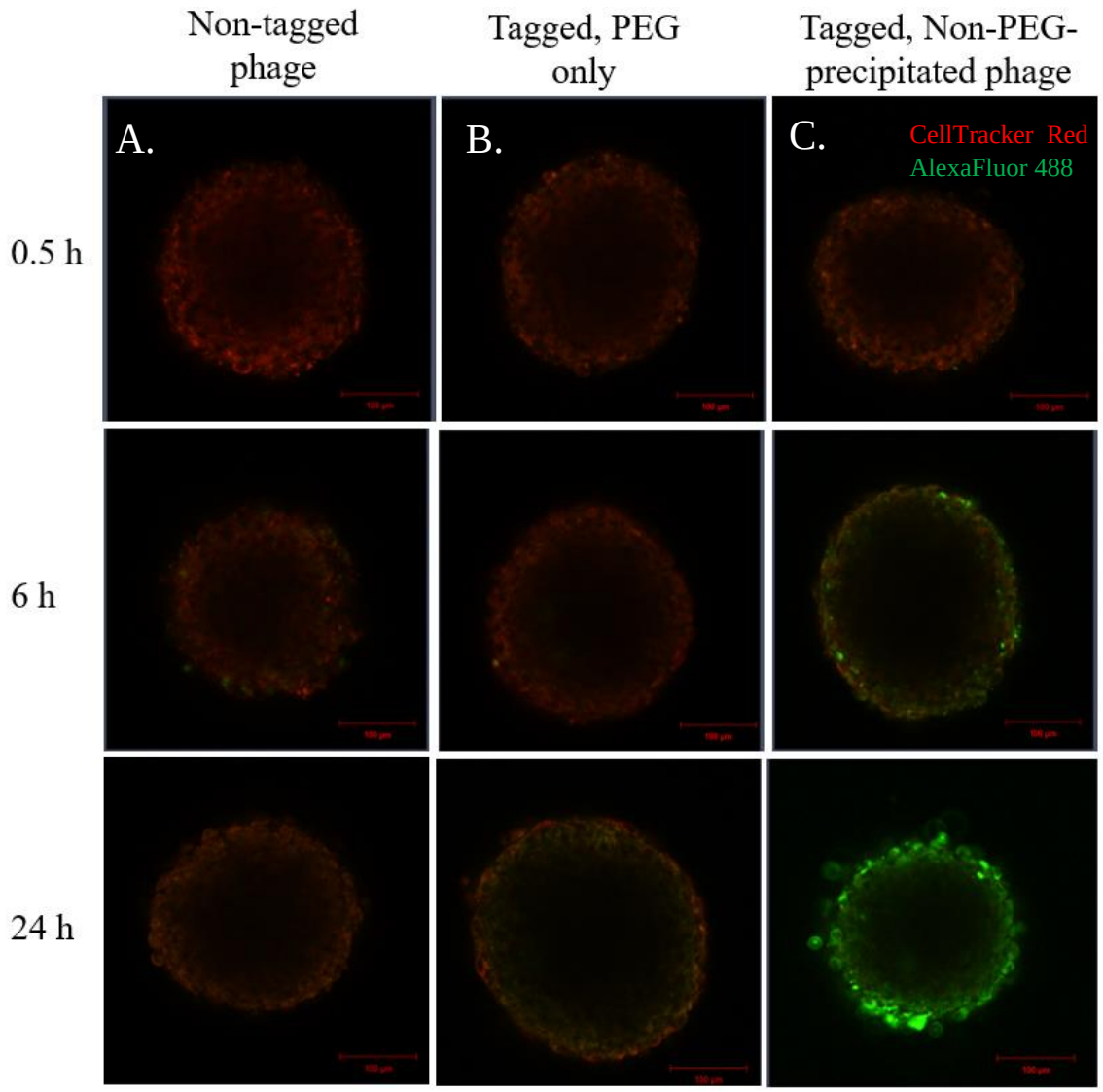


**Figure 11: NIH3T3 spheroid treated with polyethylene glycol.** Representative images of NIH3T3 spheroids treated with A: unlabeled λ phages, B: polyethylene glycol (PEG) without the addition of phages subjected to Alexa Fluor 488 reaction; and C: Alexa Fluor 488- λ phages. Spheroids were treated for 0.5, 6 and 24 h. Optical sections 55 μm from the bottom of spheroids are shown. All the spheroids were counterstained with CellTracker™ Red prior to imaging. Green fluorescence is associated with the presence of Alexa Fluor 488- phages. All images are representative of three replicates of spheroids.

The very low signal in the PEG-only control in Fig. 11 suggests the view that the strong green fluorescence observed in Fig. 10 was very likely emitted by tagged phages. We can infer that phages began to adhere to the surface of the spheroid as early as 0.5 h and diffused through the intercellular spaces, freeing up the external surface of cells at 6 h. More phages bound to the external surface of spheroids and accumulated in a time-dependent manner up to 24 h (Fig. 10). Based on these results, there appears to be a great level of natural interaction between unmodified, wildtype λ phages and NIH3T3 fibroblasts, and infiltration into NIH3T3 spheroids likely occurs as early as 6 h after $10^8$ PFU of phage application.

### 4.3.2 Interaction of λ D::EGF phages with HT29 spheroids

Spheroids were generated from HT29 cells to study phage accumulation in the context of rapidly proliferating neoplastic cells that form tight cell-cell contacts (Riffle & Hegde, 2017). Additionally, we wished to observe potential changes in phage-spheroid interactions with the display of EGF on the same phage (λ). EGFR is overexpressed in HT29 cells and has been associated with aggressive biological behaviour (Grandis et al., 1998; Yang et al., 2004). D::EGF phages (EGF fused to gpD capsid proteins) were generated for maximal fusion of molecules (grow on the SupD host at 37 ℃). $10^8$ PFU of either the wildtype and D::EGF phages were added to HT29 spheroids (~300 μm diameter) for up to 24 h, and Z-stack images were obtained at 12 and 24 μm depth from the bottom surfaces (Fig. 12, 13).

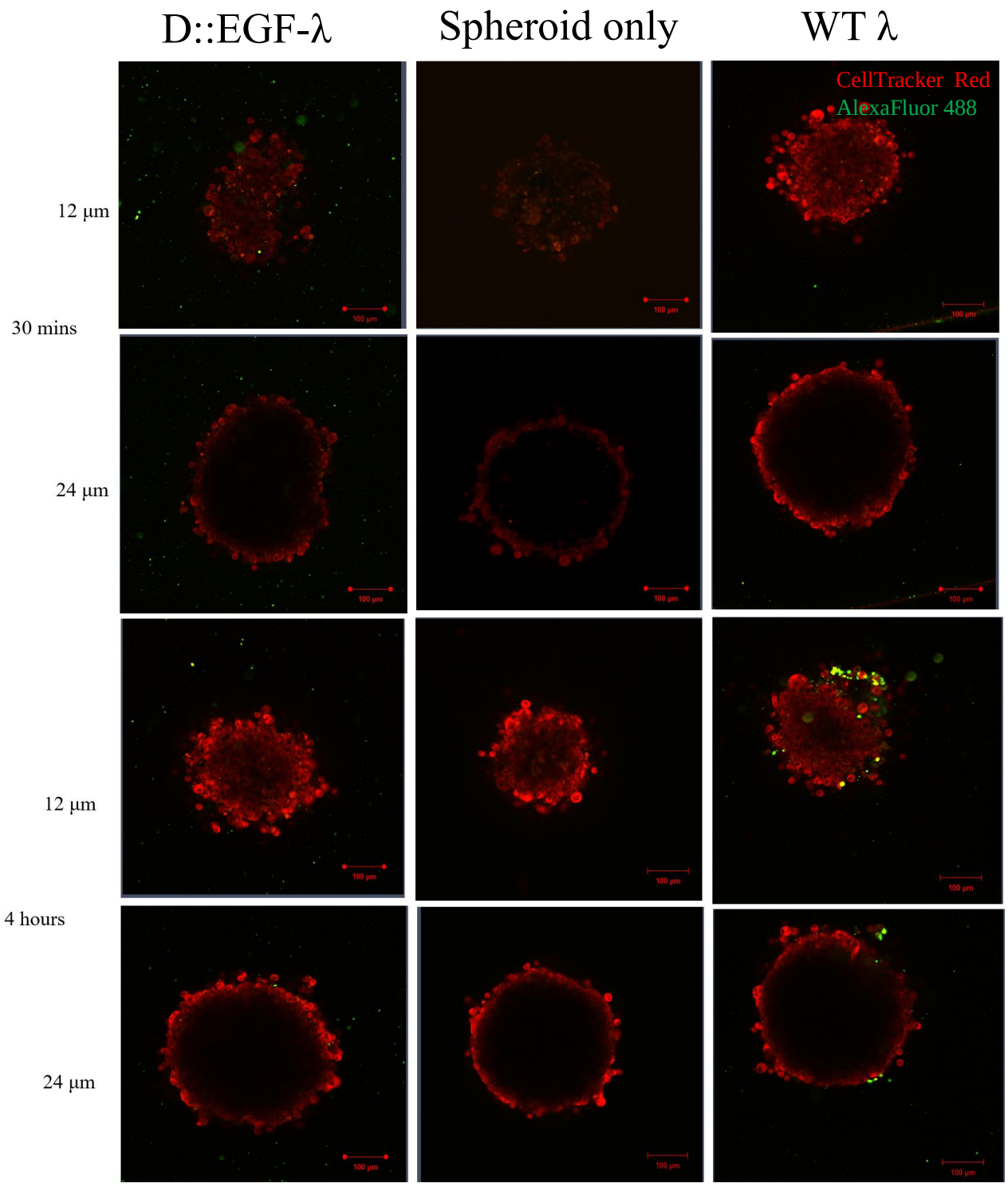


**Figure 12: Optical cross-sections of HT29 spheroids treated with wildtype phages and EGF-displaying phages for 30 min (top) and 4 h (bottom).** 6-d old HT29 spheroids (~300 µm diameter, seeded with 5,000 cells) treated with Alexa Fluor 488 tagged phages (green) for given durations. Z-stacks were obtained at 12 and 24 µm from the bottom-most surface of the spheroids. All images are qualitatively representative of three replicates of spheroids.

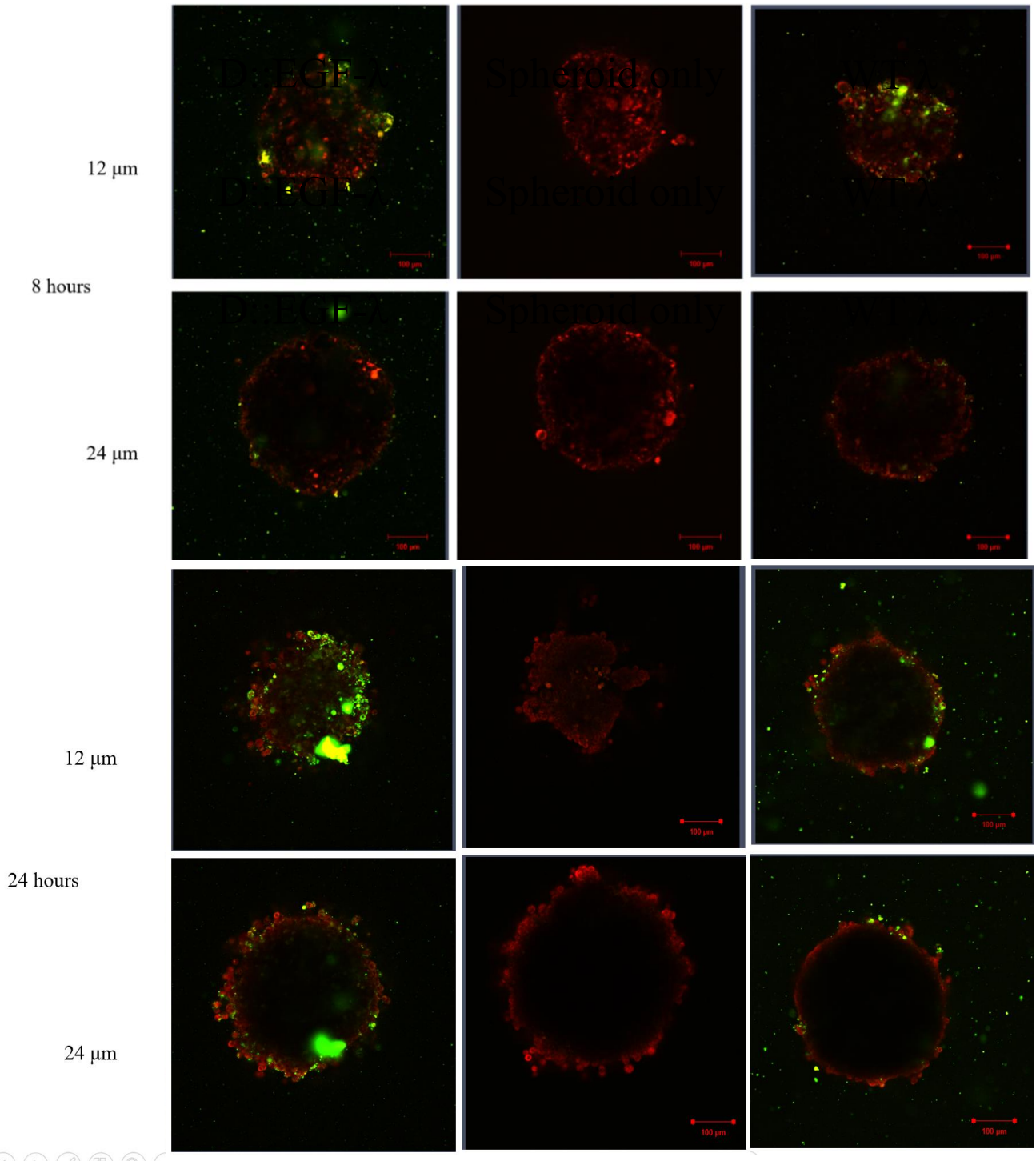


**Figure 13: Representative cross-sections of HT29 spheroids treated with wildtype phages and EGF-displaying phages for 8 h (top) and 24 h (bottom).** Continued from Fig. 9

Fluorescent wildtype (EGF$^{-}$) phages were visible on the outer edges of the surface of HT29 spheroid as early as 4 h. Spheroids treated with D::EGF phages were relatively free of fluorescence until after 8 h of treatment. After 24 h, positive fluorescence was visible in the spheroids treated with both types of phages at 12 and 24 μm depths. Positive fluorescent spots were observed throughout all optical sections.

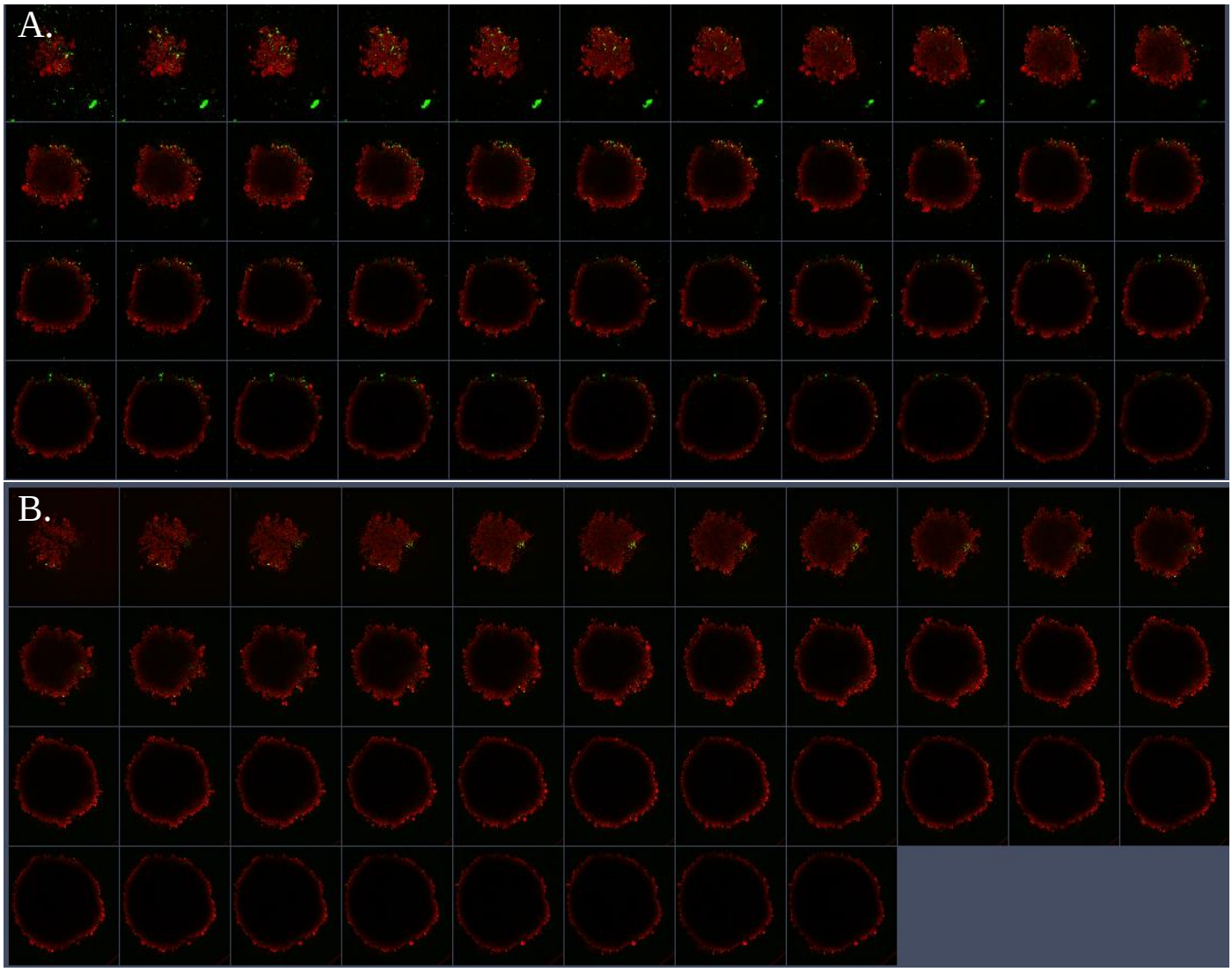


**Figure 14: Collective Z-stacks of HT29 spheroids treated with A. EGF-displaying phages and B. wildtype phages (bottom) for 24 h.** Each square represents 3 μm slices of spheroids from the bottom-most surface (top left) to the centre (bottom right). 6-day old HT29 spheroids (~300 μm diameter, seeding concentration of 5,000 cells) were washed to discard unassociated phages (green) after incubation periods.

Fig. 14 shows the collective Z-stacks of HT29 spheroids treated with D::EGF phages (Fig. 14A) and wildtype phages (Fig. 14B) after 24 h. There were noticeably more green fluorescent spots embedded in the spheroid treated with λ D::EGF phages than with wildtype phages, in all optical sections. There also appeared to be more fluorescent particles floating in the medium of the spheroid treated with D::EGF phages than the WT phages (14A & B, respectively, top left squares).

This may have been a result of more loosely-bound phage particles on the spheroid coming unbound and settling to the surface, after spheroids were transferred.

## 4.4 Bacteriophage λ internalization by HT29 cells

Certain spots of positive green fluorescence exhibited diffuse edges, appearing to be confined by the boundaries of the cell membranes (yellow arrows, Fig. 15). This suggested the possibility that they were emitted from within cells, rather than from the surface of the cells. Intracellular fluorescence suggest that the phage-associated particles have been internalized by HT29 cells. We queried other studies involving the use of confocal imaging to visualize cells stained with CellTracker to use as a point of reference for the appearance of these internalized, fluorescent particles. A study by Bhagawat et al. (2018) showed α3 integrin antibodies labeled with Alexa

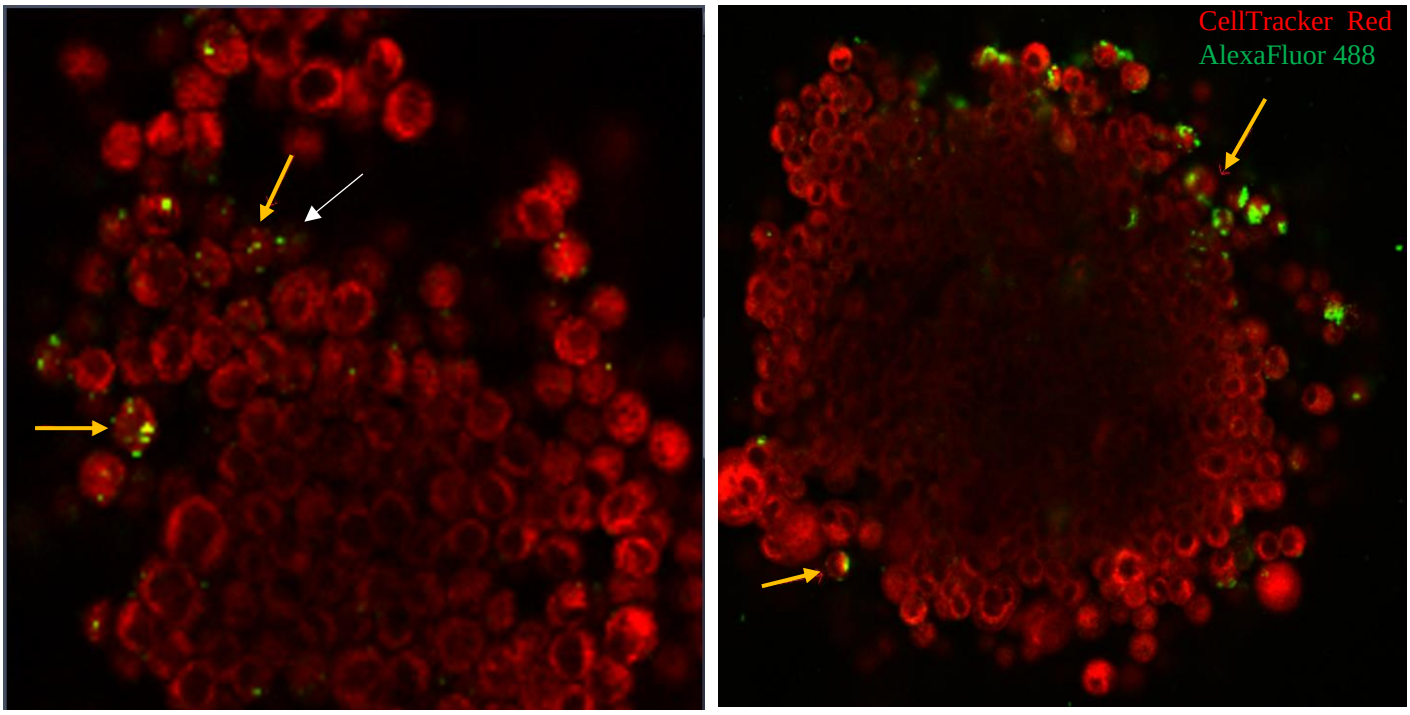


**Figure 15: Phage-associated fluorescence emitted inter- and intracellularly of HT29 cells.** Diffused pattern of green fluorescence signal suggests a possible internalization of phages by the HT29 cells (yellow arrows); discrete fluorescent dots suggest the surface localization of phages (white arrow). HT29 spheroids were treated with wildtype phages (left) and EGF-displaying phages (right) for 4 h

Fluor 488 internalized by cells stained with CellTracker Red (Subramanian, Moissoglu, & Parent, 2018). Once internalized, these antibodies also appeared yellow with diffuse edges. We determined that the extracellular fluorescence would appear more discrete with distinct edges, such as those indicated by white arrows in Fig. 15.

### 4.4.1 Quantitation of internalized bacteriophage λ particles

To further investigate the potential cellular uptake of phages by HT29 cells, cells comprising the spheroids were lysed to release internal contents and the PFU was quantified by a conventional plaque assay. Previous studies have shown that recovered intracellular phages can retain their infectivity after 24 h (Kim et al., 2012). However, as phages are not stable at 37 $^{o}$C outside of a bacterial host, this temperature was expected to reduce overall viability counts (Table 4). Additionally, to investigate the potential D::EGF-EGFR association, λ D::EGF phage decorated with fewer molecules, approximately 40% fewer per phage (Lo-D::EGF phage) than the achievable maximal decoration (Hi-D::EGF phage), was generated using the SupF *E. coli* host (see 4.3.1) (Nicastro et al., 2013) . The purpose of generating a less-decorated phages was to determine whether the phage-cell association would be reduced in response to the decreased avidity of the presumed D::EGF-EGFR interaction. These phages were also fluorescently tagged and added to HT29 spheroids similarly as above, alongside the Hi-D::EGF phages and wildtype phages.

In order to minimize intracellular trafficking of phage particles into lysosomes, spheroids were pre-treated with a lysosomotropic agent (ammonium chloride) prior to the addition of phages. This was expected to minimize the degradation of phage particles that would underestimate the overall quantitation of internalized phage particles, First, the effects of ammonium chloride in improving phage viability was assessed by comparing the enumeration of wildtype phage

recovered from pre-treated spheroids to untreated spheroids (Fig. 16). Cells were lysed using the freeze-thaw method, and in order to fully recover internalized phages by cells situated closer to the core, spheroids were completely dissociated by trypsinization at 37 ºC.

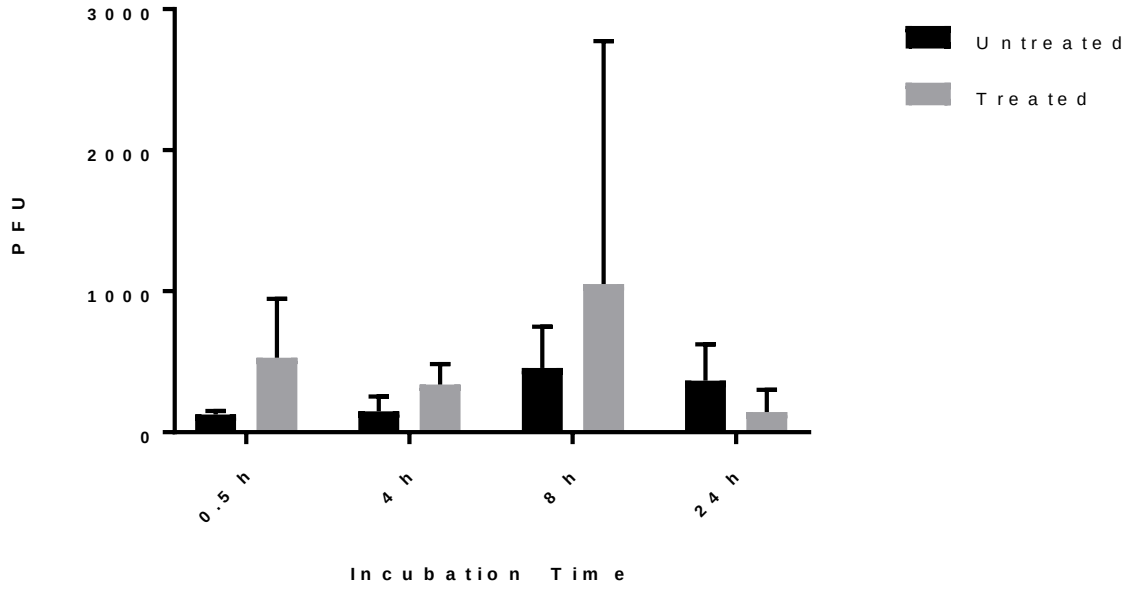


**Figure 16: Testing the action of ammonium chloride as a lysosomotropic agent to improve phage recovery.** 6-d old HT29 cells (seeding density of 5,000 cells) were treated with 5mM of ammonium chloride for 45 min at room temperature. Following treatment, remaining ammonium chloride was removed and $10^8$ PFU of wildtype phages were added to spheroids for up to 24 h. Spheroids were completely dissociated with 0.25% trypsin-EDTA and washed to discard extracellular phages. Cells were subjected to freeze-thaw cycles for lysis and release of phage particles. Phages recovered from lysed cells were plated on BB4 *E. coli* cells for quantification of plaques. Data is presented as the mean + SEM of three independent experiments, carried out in triplicates. Differences in PFU between treated and untreated were not determined to be statistically significant by the Mann-Whitney test, $p>0.05$

Furthermore, to ensure that exposure to trypsin-EDTA was not going to deactivate phages, viability assays were also conducted on phage particles resuspended in different concentrations of trypsin-EDTA at 37 °C for 1 h (Table 6).

**Table 6: Effect of Trypsin-EDTA on phage viability.**

| EDTA-Trypsin concentration | EOP of λF7 incubated at 37°C[1] | EOP of D::EGF phages incubated at 37°C[1] |
|---|---|---|
| **0 %** | 1.00 ± 0.01 | 1.00 ± 0.02 |
| **0.10 %** | 0.89 ± 0.03 | 0.87 ± 0.03 |
| **0.25 %** | 0.89 ± 0.07 | 0.89 ± 0.09 |
| **0.50 %** | 0.84 ± 0.07* | 0.79 ± 0.07** |
| **1.00 %** | 0.72 ± 0.10** | 0.76 ± 0.12* |

[1]All EOPs have been expressed as a mean of three independent assays and determined using BB4 (SupE, SupF double suppressor) as the 100% plating control and plated at 37 °C.
Reductions in viability of D::EGF and wildtype phages were not statistically significant using the 2-way ANOVA for 0 – 0.25% trypsin EDTA.

The pre-treatment of spheroids with ammonium chloride on the yield of internalized phages was not determined to be significant. However, treatment enhanced the recovery of phages for up to 8 h, but appeared to be slightly detrimental in recovering phages after 24 h (Fig. 16). Pre-treatment of spheroids with ammonium chloride was carried out for the internalization assays (Table 7).

Phages were recovered from intercellular spaces of spheroids and intracellularly from lysed cells. Differences in phage recovery were compared between the wildtype and Hi-D::EGF phages after 0.5, 4, 8 and 24 h of treatment, to determine whether D::EGF-EGFR interactions would increase the percentage of internalized cells (Fig. 17). To minimize possibly scoring extracellular phages that were bound to the surface of cells as intracellular, we incubated the cells with an acidic wash (pH 2) to inactivate the phages. However, this technique does not inactive 100% of phages, as

such a background of extracellular bound phages is inevitable (Lehti et al., 2017). Counts in Table 7 should be considered as relative.

EOP's in Table 6 were corrected by taking account of the viability decrease at 37 °C (Table 3) as the 100% control using the formula:

$$adjusted\ EOP\ = \frac{PFU\ of\ inter-\ or\ intracellular\ phages}{10^8 PFU \times percent\ viability}$$

PFU of recovered inter and intracellular phages were expressed as 'percent internalization' in Fig. 17 by using formula:

$$\frac{adj.\ EOP\ of\ intracellular\ phages}{adj.\ EOP\ of\ intracellular\ phages + adj.\ EOP\ of\ intercellular\ phages} \times 100\%$$

**Table 7: EGF display increases the recovery of phage particles from HT29 spheroids**

| Duration of Treatment | | EOP of WT phage[1] | EOP of Lo-D::EGF-phage[1] | P[4] | EOP of Hi- D::EGF-phage[1] | p |
|---|---|---|---|---|---|---|
| **30 min** | **Intercellular[2]** | 6.59E-04 | 1.27E-03 | 0.541 | 1.56E-03 | 0.296 |
| | **Intracellular[3]** | 5.17E-05 | 1.20E-04 | 0.779 | 1.30E-04 | 0.722 |
| **4 h** | **Intercellular** | 1.66E-02 | 4.10E-02 | 0.966 | 5.72E-02 | 0.438 |
| | **Intracellular** | 7.62E-05 | 7.35E-05 | 1.000 | 3.92E-03 | 0.483 |
| **8 h** | **Intercellular** | 1.03E-03 | 1.71E-02 | 0.102 | 1.83E-02 | 0.081 |
| | **Intracellular** | 6.36E-05 | 1.24E-03 | 0.273 | 1.47E-03 | 0.177 |
| **24 h** | **Intercellular** | 1.01E-03 | 7.15E-03 | 0.794 | 1.13E-02 | 0.475 |
| | **Intracellular** | 7.77E-06 | 4.16E-04 | 0.477 | 3.12E-04 | 0.653 |

[1]All EOPs were adjusted to take account of decrease in cell viability with prolonged incubation at 37 °C and are expressed as a mean of three independent assays + SEM, n=3, and determined using BB4 (SupE, SupF double suppressor) as the 100% plating control.

[2]Phages recovered from the interstitial spaces of HT29 spheroids

[3] Phages recovered from lysed HT29 cells.

[4]Statistically significant differences in expression were determined by two-way ANOVA Tukey's multiple comparisons test, p - values were compared to the WT phage as a control.

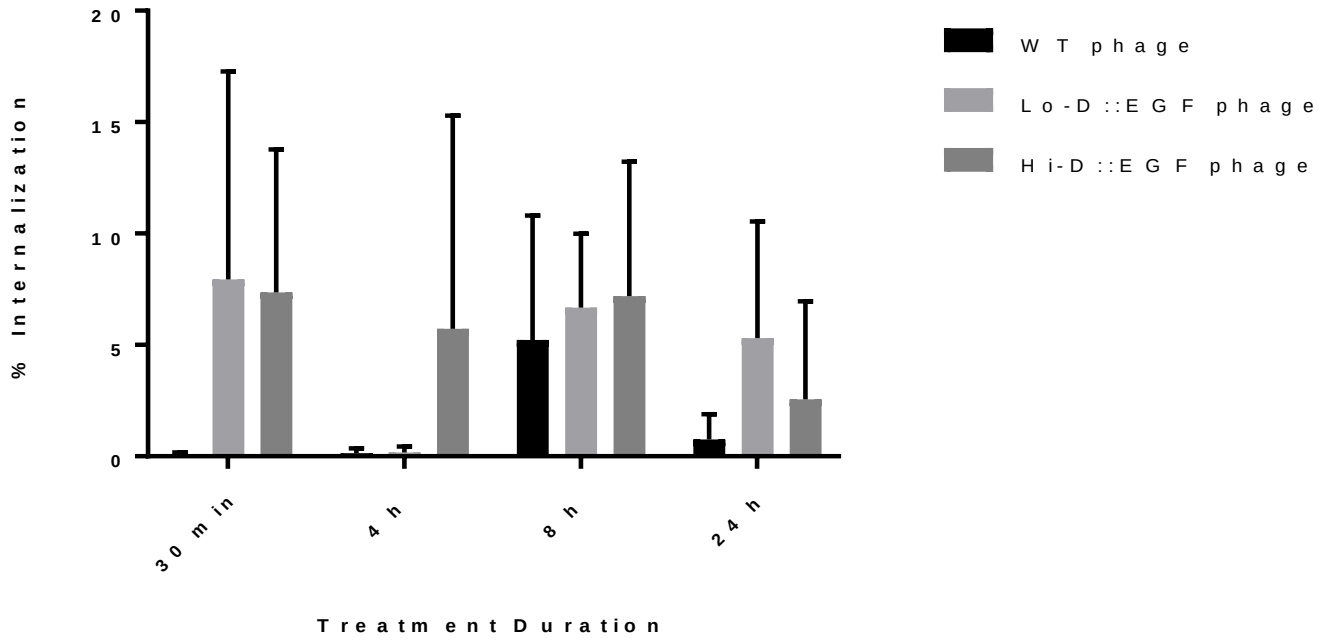


**Figure 17: Percent internalization of phages determined from HT29 spheroids.** The percentage of internalized phages that were associated with the spheroid was calculated from the data shown in Table 6 using the formula above. The display of EGF correlated with the mean percentage of intracellular phages particle intracellularly at all treatment periods. Percent internalization did not appear to be dependent on the density of EGF molecules displayed on the surface of phage. 2-way ANOVA multiple comparisons test indicated no statistically significant differences in the % internalization difference between WT phages and both D::EGF-phages $p>0.05$.

The mean of recovered phages indicates that the uptake of phages by HT29 cells was enhanced by the display of EGF molecules; however, this was not determined to be statistically significant (Fig. 17). Large variances in the recovery of phages were expected as large titer of phages were initially added, and spheroids were manually washed to discard unassociated phages. Therefore, relative trends in the association must be considered instead. Substantial differences in phage uptake between the D::EGF phages and wildtype phages was observed at 30 min. Recovery of both types of EGF-displaying phage particles from the interstitial spaces and within cells were greater by over 150-fold than wildtype phages (Table 7). This suggests that EGF may assist in the initial attachment of phages to the cells, resulting to a greater percentage of internalization.

At 4 h, the number of phage particles associated with the spheroids extracellularly were similar for both Lo- and Hi-D::EGF phages (Table 7). However, the percentage of internalization was much higher for the Hi-D::EGF phages, suggesting a ligand density-dependent mechanism. After 8 h, average uptake of phage particles was at peak for both D::EGF and wildtype phages, although there were fewer phages associated with the spheroids than at 4 h. After 24 h of treatment, internalized phage particles were likely degraded in the cells even with the assistance of ammonium chloride (Fig. 16), and it is unclear whether the quantitation provided accurate representation of internalized phage particles.

## 4.5 Effects of EGF display on bacteriophage λ on spheroid growth

To determine whether phages would interfere with spheroid growth, 5,000 HT29 cells were seeded on agarose and low ($10^4$ PFU) or high ($10^8$ PFU) concentrations of Lo-D::EGF, Hi-D::EGF and wildtype phages were added after 48 h to the partially-formed spheroids. EGF displayed on phages were expected to bind to the EGFR on the surface of HT29, blocking cells from receiving EGF and other growth signals, and consequently slowing the growth of HT29 spheroids.

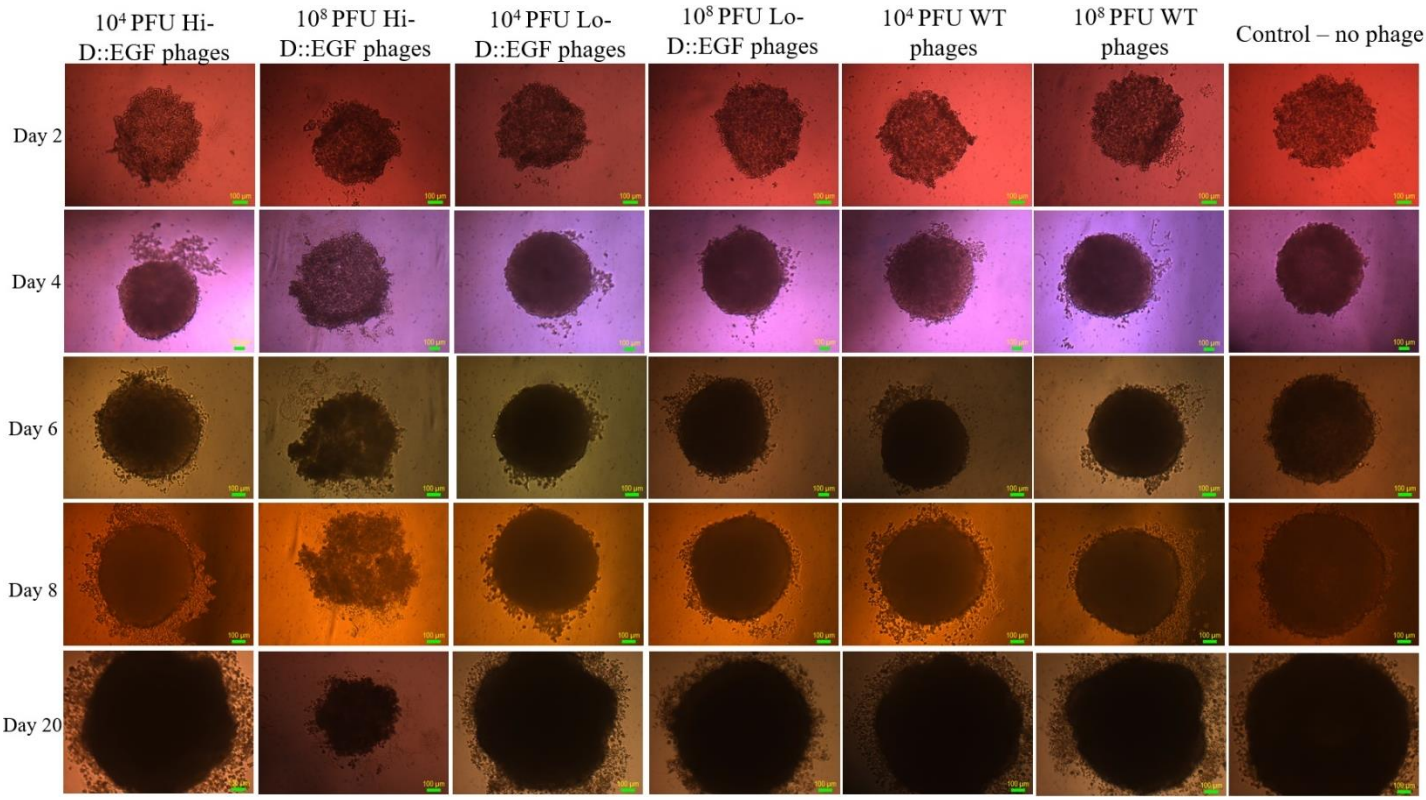


**Figure 18: Effects of D::EGF phages and wildtype phages on the growth of HT29 spheroids.** HT29 cells were seeded for 48 h to form partially-formed spheroids. $10^4$ or $10^8$ PFU of phages were added to each spheroid. The formation and growth of spheroids were monitored for 20 d with a bright-field microscope. Each picture is representative of 3 replicates of spheroids for each condition.

**Table 8: HT29 spheroids treated with D::EGF phages are smaller on day 20**

| Spheroid treated with: | Diameter (µm) |
|---|---|
| Control (no phage added)[2] | 1533 ± 47 |
| $10^8$ PFU Hi-D::EGF phages[3] | 422 ± 28 |
| $10^4$ PFU Hi-D::EGF phages[4] | 1329 ± 54 |
| $10^8$ PFU Lo-D::EGF phages[5] | 1198 ± 19 |
| $10^4$ PFU Lo-D::EGF phages[6] | 1509 ± 52 |
| $10^8$ PFU Wildtype phages[7] | 1410 ± 35 |
| $10^4$ PFU Wildtype phages[8] | 1473 ± 202 |

[1]n=3 ± SD and diameters were measured with the QCapture Pro software
[2]max = 1598, min = 1516
[3]max = 459, min = 389
[4]max = 1406, min = 1280
[5]max =1218, min = 1172
[6]max =1580, min = 1455
[7]max =1459, min = 1377
[8]max =1754, min = 1283

Figure 18 shows the growth of partially-formed spheroids affected by the presence of phages. There were no visible differences in the morphology of spheroids until about 2 d after the application of phages (4 d after seeding). Adding high concentration of Hi-D::EGF phages appeared to have interfered in the complete aggregation of cells, which was more apparent after 6 d of phage application (‘day 8’). By day 20, these spheroids treated with Hi-D::EGF phages appeared to be more dense and compact than they had been previously; they were approximately three-fold smaller in size than the control spheroids (Table 8). Adding a low concentration of Hi-D::EGF phages, however, did not result in the same pattern of growth inhibition in spheroids; these spheroids developed similarly in shape and size to those treated with wildtype phages. Spheroids treated with wildtype and Lo-D::EGF phages of both high and low concentrations

exhibited similar sizes and density. These spheroids were slightly smaller than the control spheroids.

### 4.5.1 Effects of EGF-displaying phages on initial cell aggregation

Next, in order to determine whether Hi-D::EGF phages would interact with cell-surface receptors to disrupt initial cell aggregation, phages were co-seeded with 3,000 HT29 cells and were imaged with a bright-field microscope every 2 d.

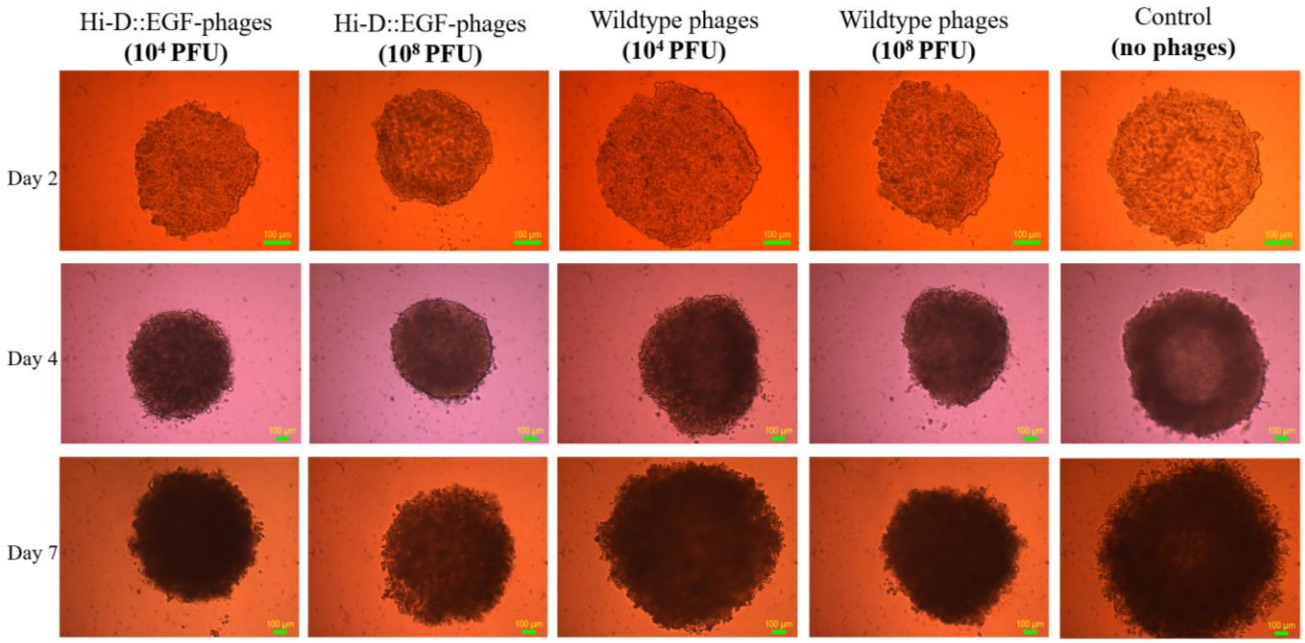


**Figure 19: HT29 cells co-seeded with D::EGF phages or wildtype phages**. Effects of phage presence on initial cell aggregation to form spheroids were monitored. Representative spheroids are shown above of three replicates of spheroids. All images were taken on a Leica DM2000 microscope and QImaging Micropublisher 5.0 RTV camera using the QCapture Pro 7 Software.

As shown in Fig.19, HT29 cells co-seeded with D::EGF phages and high concentration of λ wildtype were smaller and more compact than the control spheroids. Low concentration of wildtype phages did not appear to have imparted any visible effects in initial spheroid formation and was similar in morphology and size to the control spheroid on day 2. By day 4, cells treated with phages had formed smaller, compact, three-dimensional spheroids. The control spheroid

without phages was greater in size, but cells appeared to be sparser and loosely-associated at the centre.

Phages may have settled to the agarose surface in Fig. 19, which would diminish the amount of phages interacting with HT29 cells. Therefore, phages were incubated with HT29 cells on ice for 3 h to allow initial cell-phage connections to form. Pre-chilling on ice for at least 1 h is a common approach for blocking cellular receptors with antibodies (Vainshtein et al., 2015) and ligands (Schwartz, Fridovich, & Lodish, 1982). Following this adsorption phase, the cell-phage mixture was seeded normally onto the agarose surface (Fig.20).

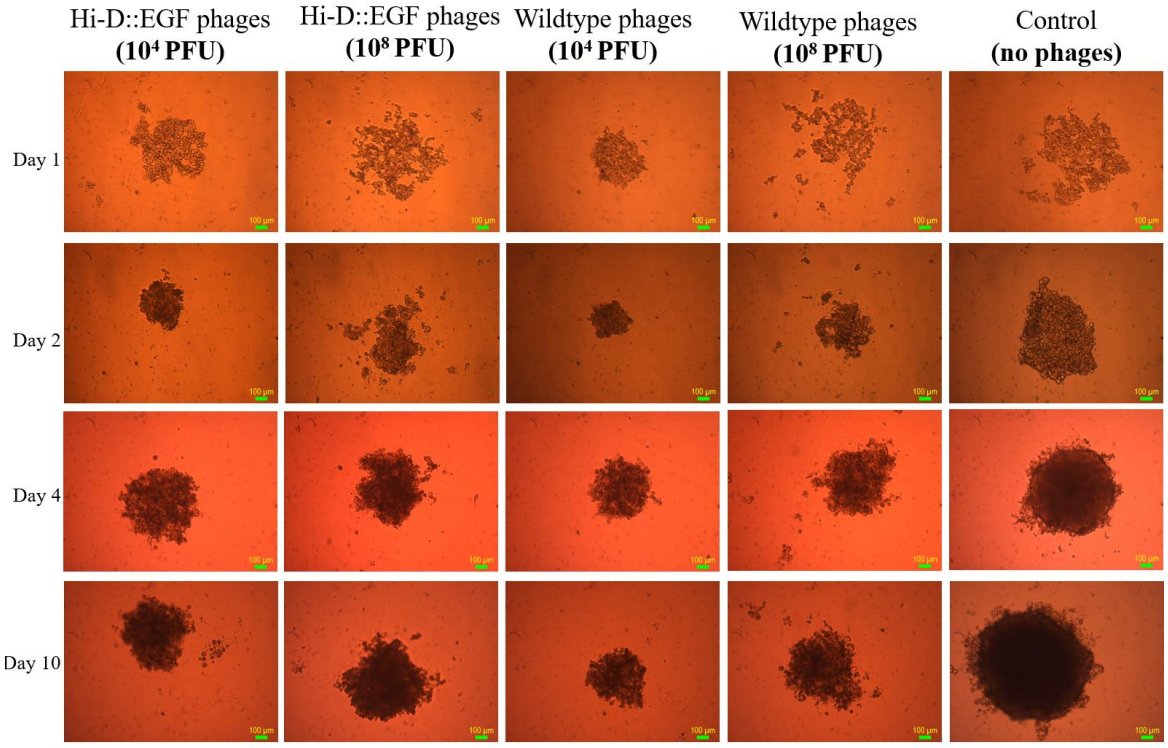


**Figure 20: Growth of pre-chilled HT29 cells with phages.** 3,000 HT29 cells were incubated for 3 h on ice with$10^4$ or $10^8$ PFU of wildtype or D::EGF phages. Phages and cells were then co-seeded onto an agarose surface and grown for 10 d. Images are representative of 3 replicates of spheroids. All images were taken on a Leica DM2000 microscope and QImaging Micropublisher 5.0 RTV camera using the QCapture Pro 7 Software.

Unexpectedly, lower concentrations of both wildtype and D::EGF phages appeared to assist in the compact packing of the cells by day 2 compared to the control. Cells co-seeded with higher concentrations did not fully aggregate after the first 24 h, but fully assembled by day 4. At this stage, spheroids treated with phages did not adopt well-defined shapes. The high concentration of phages adhered to the surface of cells may have obstructed the cells from fully forming cell-cell connections. Additionally, this may have prevented cell-signaling molecules from binding to their surface-receptors, inhibiting growth and proliferation. There were no discernible differences between cells treated with wildtype phages and D::EGF phages during the initial process of cell aggregation in Fig. 20. Cell proliferation appeared to be much more accelerated in the control spheroid after 10 d.

### 4.5.2 Effects of phages on fully-formed HT29 spheroids

In order to determine whether phages can infiltrate HT29 spheroids and induce visible changes in spheroid morphology, 5-d old HT29 spheroids were treated with high and low concentrations of wildtype and D::EGF phages.

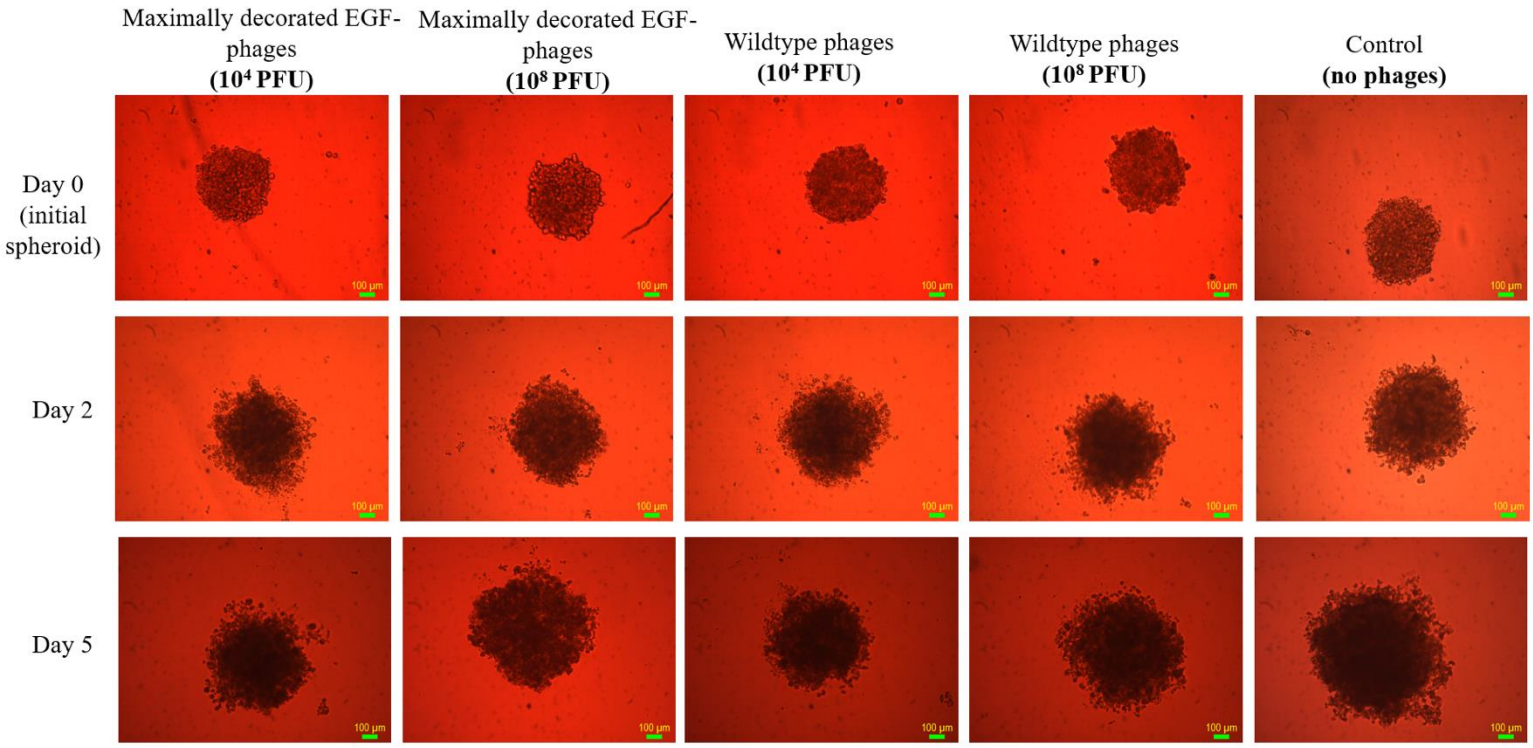


**Figure 21: Effects of wildtype or Hi-D::EGF phages on HT29 spheroids grown for 5 d.** Images are representative of 3 replicates of spheroids. All images were taken on a Leica DM2000 microscope and QImaging Micropublisher 5.0 RTV camera using the QCapture Pro 7 Software.

Cell proliferation continued to occur despite the presence of phages (Fig. 21). 2 d after adding phages to the spheroids, there were no visible differences to the control spheroid. 5 d after adding both types of phages, the lag in cell proliferation was noticeable when compared to the control. The spheroid treated with a high concentration of Hi-D::EGF phages exhibited sparse areas between cells. These cells appeared to have dissociated from neighbouring cells, contributing to

a larger diameter overall. D::EGF phages may have bound to EGFR on the surface of the cells, reducing the overall cell-cell contacts holding the spheroid together.

## 4.6 Cytotoxicity of D::EGF λ phages to HT29 cells

We sought to test the level of EGF-phages and wildtype phages on cell viability and performed an MTT assay. Cells were exposed to low ($10^4$) or high ($10^8$) PFU of phages for 24 h and HT29 cells cultured in serum-containing medium were used as the 100% viable control (Fig. 22). The percentages of viability for all conditions were expressed relative to the 100% viable control. At the end of the 24 h exposure to phages, cell viabilities were only marginally reduced; there was approximately 15% reduction in HT29 cell viability in response to Hi-D::EGF phages, of both concentrations. The differences in viability in response to both D::EGF phages and wildtype phages were not determined to be significant.

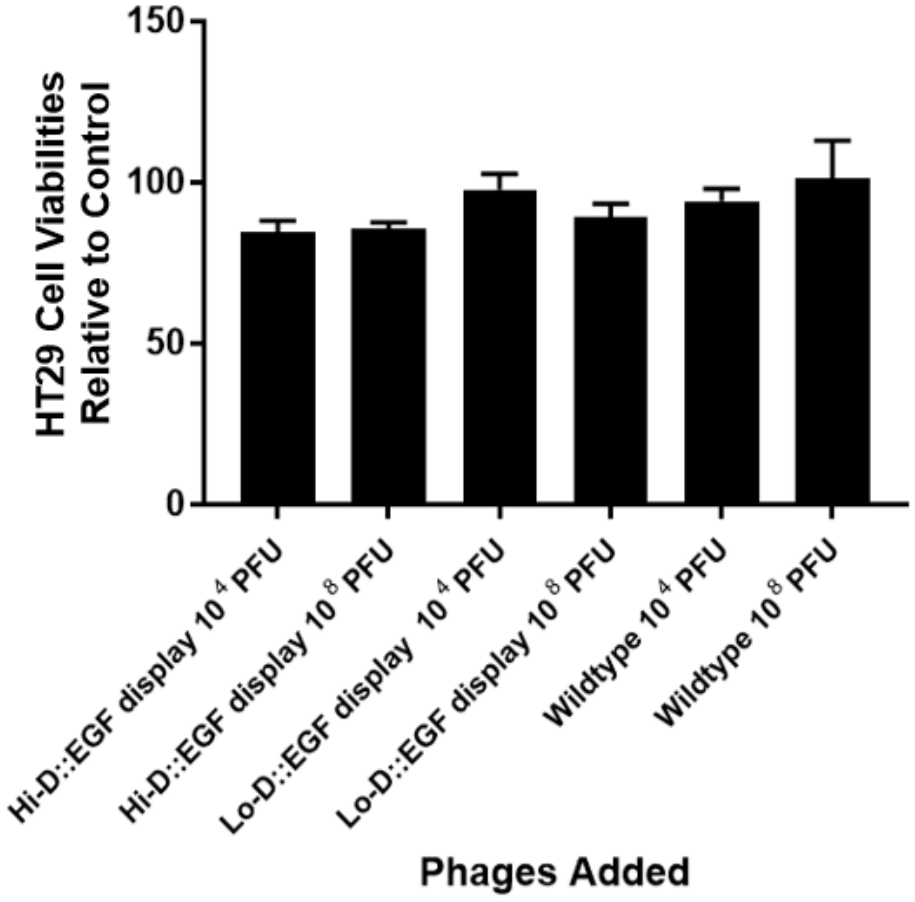


**Figure 22: HT29 cell proliferation (MTT) assay in response to phage treatment relative to control.** Cells were seeded into the wells of a 96-well plate in 9 replicates for each treatment group. Cells were cultured normally for 72 h before the addition of phages. Cells were then exposed to phages for 24 h. At the end of this period, an MTT assay was performed to assess cellular viability. Cells cultured normally with serum were considered 100% viable and all percentage of cell viabilities above are expressed relative to the 100% control. The results shown represent three independent experiments. The relative viabilities of monolayer untreated HT29 versus HT29 treated by phages were not statistically different by a Mann-Whitney test.

Cytotoxicity induced by phages after a 24 h exposure was also measured in spheroids using the CellTiter-Glo® 3D cell viability assay (Fig. 23). This assay tested the amount of ATP, which is proportional to the number of viable cells in 3D culture. HT29 spheroids were grown, treated with $10^8$ PFU of wildtype and D::EGF phages for 24 h, and were assayed for cell viability.

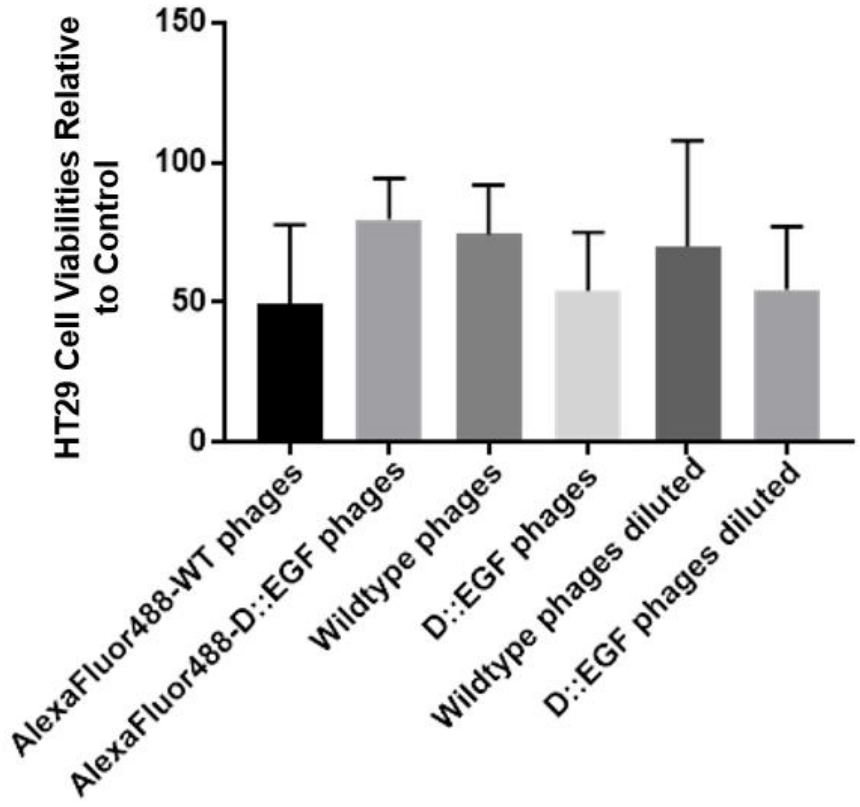


**Figure 23: HT29 spheroid cell viabilities relative to control in response to phage treatment.** 7-day old HT29 spheroids (seeding density: 5,000 cells) were treated with wildtype phages, Hi-D::EGF phages or AlexaFluor488 tagged phages for 24 h. Cell viability of HT29 spheroids treated with phages were assessed by measuring ATP content and the luminescence output via the luciferase enzyme supplied in the ultra-Glo™ reagent. All viabilities are expressed as relative values to spheroids cultured normally with serum, which were considered to be 100% viable. The results shown represent four replicates. The relative viabilities of spheroids untreated HT29 versus HT29 treated by phages were not statistically different by multiple comparisons one-way ANOVA test. This assay was kindly conducted by Julia Fux.

The mean cell viability was higher for HT29 spheroids exposed to wildtype phages than D::EGF phages (74% versus 54%). This result correlates to the brightfield images of HT29 spheroids that were smaller in size in response to D::EGF phages than wildtype phages (Fig. 18-21). The mean cell viabilities were similar between spheroids treated with diluted and undiluted wildtype and D::EGF phages. However, the results were reversed for phages following AlexaFluor488 tagging – spheroids applied with D::EGF phages had 79% viability, versus 49% for wildtype phages. Percentage of cell viability was analyzed by the multiple comparisons one-way ANOVA test, however, these results were not deemed statistically significant ($p<0.05$).

## 4.7 Spheroid embedding and sectioning

Spheroids grown for 7 d (seeding density of 5,000 cells) were treated for 24 h with AlexaFluor 488 tagged phages, D::EGF and wildtype phages and were processed to visualize phage activity in the inner regions of the spheroid that were obscured in the confocal optical sections. Spheroids were sectioned, embedded onto glass slides and imaged with a fluorescent microscope. Fluorescent particles that may have been phage-related were found dispersed throughout the slides, unassociated with the spheroid sections (not shown). It was unclear whether these particles were background fluorescence or intra-tumoral fluorescent phages that have become unbound during the process of de-waxing. Therefore, our attempt to assess the depth of phage infiltration into spheroids using paraffin embedding was unsuccessful.

# Chapter 5: Discussion

Bacteriophages have emerged as potent and efficient tools in medicine, specifically with the advent of phage display technology. This technology has created new avenues for phages in cancer treatment as a means for targeted delivery into malignant cells and tissues in recent years. Their genetic flexibility to undergo surface modifications to target specific cells and tissue types have made them an attractive target in therapeutics.

This was an exploratory study with the purpose of characterization of λ phages and their interaction with mammalian cells. Here, we discovered that λ phages naturally adhere to the surface of mammalian (mouse and human) cells and can accumulate in three-dimensional multicellular spheroids, in which both stromal and neoplastic cells of a tumour could be modeled.

We chose HT29, which expresses the highest level of EGFR in relation to other colorectal cancer cell lines, to determine whether tumour growth was altered by the signal intervention with D::EGF phages (Matsuo et al., 2011b). They are also representative of wildtype-*KRAS* and *BRAF*-mutated tumours, which have been reported in approximately 5-15% of patients with colorectal cancers (Xu & Solomon, 1996; Yuen et al., 2002). EGF was the peptide of choice for display, as it retains its function when displayed on phage, and has been well-documented in targeting of other types of vectors in gene therapy applications (Roth & Cristiano, 1997; Souriau et al., 1997).

## 5.2 Bacteriophage λ accumulates in multicellular spheroids

The NIH3T3 spheroids employed in this project were relatively small, approximately 300 μm in diameter, and lacking the hypoxic regions exhibited by large, solid tumours. Despite the small

size, NIH3T3 spheroids provided a proof-of-concept for native interactions between λ phages and mammalian cells in the context of 3D culture, specifically for assessing the ability for adherence and penetration of the intercellular spaces. Fibroblasts are the most common type of cells of the connective tissue and synthesize the ECM, forming a structural network that is difficult to infiltrate in tissues. Confocal images showed the propensity of λ phages to adhere and accumulate between the fibroblasts. This implicates that phages may be able to penetrate through the network of connective tissues interposed between malignant cells and normal host tissues, which often structurally prevents the effective infiltration of nanoparticles.

As all spheroids were thoroughly washed to discard unbound/weakly-bound phages, the phage-associated fluorescence emitted on the surface of the spheroids evidences surface interaction between phages and fibroblasts. This is in accord with other findings arguing for inherent phage adherence to cancer cells in vivo and in vitro (Dabrowska et al., 2004, 2005). Green fluorescence associated with wildtype λ phages was observed throughout various cross-sections of NIH3T3 spheroids. Phage adherence appeared to be time dependent; this was observed as early as 30 min, whereby small fluorescent green dots could be visualized at the rim of spheroids (Fig. 10). A major limitation of the confocal microscope was the inability to visualize dense inner regions of the spheroids. Fig. 10 shows evenly-distributed phage-associated fluorescence throughout visible regions in the optical sections at 24 h, rather than simply at peripheral cells of spheroids as seen at 6 h. At 24 h, phages have likely localized both inter- and intracellularly; while the exact nature of this interaction is unknown, this increase in positive signal over time, both in intensity and the areas covered, suggests a deeper infiltration and internalization of phages into the spheroids. More phages were likely able to accumulate on the surface of cells, as bound phages diffused

inwards into the spheroid, freeing up the surfaces of the cells for binding by phages. This would result in prevailing green fluorescence throughout the cross-sections as seen in Fig. 10.

Next, we were interested in the interaction of phages and HT29 colon adenocarcinoma cells, which overexpress EGFR (Matsuo et al., 2011a). Using the dual control phage display system, maximally and minimally decorated D::EGF λ phages were generated and applied to HT29 spheroids. These spheroids were consistently robust, possessing diameters of ~350 μm. As expected, D::EGF phages demonstrated greater accumulation within spheroids at 8 - 24 h than wildtype phages, which suggests that λ-EGF-EGFR association mediated this interaction (Fig. 12-14). However, wildtype phages appeared to have interacted with the spheroids at an earlier time point of 4 h (Fig. 12, 13). This could be attributed to the overall bulkiness of the D::EGF phages; phages suspended in solution must rely on Brownian motion to come into contact with spheroids. Wildtype phages, which do not carry an additional load, may be able to diffuse more rapidly to interact with the cells. Prior study by Nicastro et al. compared sizes of λF7 phages displaying eGFP molecules under the permutations of various *E. coli* suppressor hosts and temperature by dynamic light scattering; phages grown on SupD at 37 °C (maximal display) was about 3 times greater in diameter than wildtype phages, which are approximately 62 nm in diameter and 150 nm in length (Hendrix & Duda, 1992). Phages grown on SupF at 37°C (minimal display) was about 1.6 times greater than the wildtype phages (Nicastro et al., 2013).

Interestingly, wildtype phages appeared to have a better accumulation within NIH3T3 spheroids than HT29 spheroids, specifically at 24 h (Fig.10–13). This may be caused by differences in cell-cell contacts found in different cell types. Epithelial cells are characterized by tight and adherence junctions that hinder the passage of molecules through the paracellular spaces between adjacent cells (Choi et al., 2013). For example, one study showed 400-500 um human cervical

carcinoma (SiHa) spheroids consisted of tight junctions connecting neighbouring cells that restricted movement of materials, which was not observed with spheroids of other cell lines. Furthermore, ECM creates a physical barrier to prevent intratumoral drug penetration, and its composition can vary among different cell lines (Fechner et al., 1999; Görlach et al., 1994; Jain, 1990; Kuh et al., 1999; Li et al.,2004; Pluen et al., 2001). Spheroids required collagenase treatment for effective penetration of nanoparticles greater than 100 nm (Svishchev & Goncharov, 1990). Hence, HT29 spheroids may consist of greater percentage of collagen or other ECM components than NIH3T3 spheroids, obstructing the penetration and accumulation of phages.

Lastly, a raised concern in the analysis of fluorescent images was the possible dissociation of EGF molecules from the phage surface, which may lead us to mistake fragmented EGF molecules as infiltrated phage particles in the spheroids. Although this was not directly tested, the images of the fluorescently-tagged wildtype phages without EGF molecules fused to the surface provides a visual reference for the appearance of a positive signal. The pattern and appearance of fluorescence exhibited by D::EGF phages in Fig 12 & 13 were similar to those of wildtype phages. Additionally, EGF molecules are covalently linked to the capsid and therefore should form a stable product that is unlikely to dissociate from gpD (Aldred 2009; Sevier & Kaiser, 2002). EGF molecules are not likely proteolytically degraded in cell media, until phages are internalized and digested by the proteases in the lysosomes. The effect of pH, buffer and temperature on EGF stability were investigated by Yang et al. Maximum stability of recombinant human EGF (rhEGF) was from pH 6.0 to 8.0. rhEGF was shown to unfold at extreme pH conditions (pH < 4 and pH > 8) and thermal denaturation occurred at 40 – 76 °C (Yang et al., 2004). Therefore, it is unlikely that EGF would have been cleaved or structurally modified in cell

media. Disassembly of λ phages was highly unlikely as well. Disassembly is characterized by the disruption of the λ capsid, which deactivates phages and inhibit infectivity (Qiu, 2012) Higher temperatures are detrimental for phage infectivity, affecting attachment, penetration and division in their bacterial hosts. However, it is unclear whether physical degradation of λ phages would occur over 24 h of incubation at 37 °C, as half-lives of λ phages are 3.4 d at 37 °C (Jepson & March, 2004). Qiu measured the melting transitions of λ particles and showed that λ head and DNA disassembly occurred at 87 °C and 91 °C, respectively, with no noticeable effects at room temperature (Qiu, 2012). The long tail of λ is more susceptible to mechanical shearing than the capsid, but this was also shown to occur above 68 °C (Qiu, 2012). Furthermore, Ivanovska et al. demonstrated that wildtype λ capsids were relatively stiff when measured with atomic force microscopy (AFM) indentation technique, with the maximum deformation force equal to ~0.8 nN (Ivanovska et al., 2007). pH levels can also greatly affect the physical stability of phages, as hydrogen ion concentrations can cause phages to coagulate; however, λ phages can tolerate a wide range of pH and have not shown significant decreases in titers at pH's of 3 -11 at room temperature (Jepson & March, 2004). Other external conditions that can render phages physically unstable include incubation in ultrapure water, which can also cause head degradation and tail fragmentation of phages (Governal & Gerba, 1997); and low salt concentrations, which can increase the pressure of the packaged DNA, causing the capsid to burst open (Cordova et al., 2003). SDS and phenol can chemically disrupt the λ capsid protein (Rau et al., 1984). Phages were not exposed to any of these conditions in this study. Therefore, incubations in cell media supplemented by 5% FBS at 37 °C are unlikely to disrupt the λ capsid for EGF molecules to completely disengage from phages. While Table 4 demonstrates higher loss of infectivity of D::EGF phages at 37°C in DMEM and 5% FBS to 19% of initial titers, it is not representative of

the loss of structural integrity of phages. This is not likely to prevent their visualization after 24 h of incubation, as D::EGF phages may still exist as EGF-expressing particles.

## 5.3 EGF display enhances bacteriophage uptake into HT29 cells

Monoclonal antibodies that target the extracellular domain of EGFR, such as cetuximab, are internalized with EGFR as antibody-receptor complexes. During this process, the receptor dimerizes, but downstream signaling events are not triggered (Berger, Madshus, & Stang, 2012). Similar cellular events were expected upon binding of D::EGF phages to EGFR.

Certain green fluorescent particles appeared more yellow and diffuse in the confocal images. This suggested intracellular fluorescence from λ phages internalized by the HT29 cells (Fig. 15). CellTracker-cytosolic labeling does not obscure the green fluorescence emitted by internalized phages. Another study demonstrated that fluorescently-labeled organelles were visible via confocal microscopy, even though cells were co-stained with CellTracker Red (Gonzalez et al., 2013).

The recovery of D::EGF phages both intercellularly and intracellularly were greater than wildtype phages by almost two-folds at 30 minutes. This is in agreement with the confocal images showing phage localization (Table 7, Fig. 12-14). This was expected, as the EGF display would enhance the phage adherence to the HT29 cells. Ivanenkov et al. (1999) also showed that 15-60 min is sufficient for cellular uptake of phages displaying ligands, which is also the length of incubation employed by Kim et al. (Kim et al., 2012). 30 min incubation in Fig. 17 may be the most representative time point to compare the differential rate of cellular uptake between D::EGF phages and wildtype λ phages, without the influence of intracellular phage degradation. Percentage of phage internalization was significantly greater for D::EGF phages at all time

points, but did not appear to correlate to the density of displayed EGF molecules. This does not agree with the study by Ivanenkov et al.; the uptake of filamentous phages with differential expression of integrin-binding peptides containing the RGD motif was dependent on the density of displayed peptides (Ivanenkov & Menon, 2000). Kassner et al. (1999) also stated similar findings, whereby transduction efficiency of multivalent EGF on the phage surface was much higher than no display of molecules (Kassner et al., 1999). A limitation in the technique we used to quantify internalized phages was the inability to completely remove or degrade extracellular phages. Despite the extensive washing of spheroids prior to the dissociation step, intracellular and extracellular phages were unable to be completely separated. Therefore, residual extracellular phages were most likely still included in the values in Fig. 17. Furthermore, it is important to note that the plaque assay does not precisely quantify total phages in stock solution and instead, general trends must be observed. While significant differences in titers such as those between EGF-displaying phages and wildtype phages (over 10-fold) can be noted, this assay may not be the most suitable to determine differences in recovered Lo-D::EGF and Hi-D::EGF phages.

Wildtype λ phages and D::EGF phages are also likely to be internalized via caveosomes and/or clathrin-coated vesicles, as these vesicles can package particles of  500 and 200 nm, respectively. EGF is believed to primarily be internalized by pathways involving clathrin (Chem et al., 1990; Wiley, 1988). Internalization of M13 phages displaying cell-penetrating-peptide 3D8 VL transbody and TAT has been evidenced to be internalized through clathrin- and caveolae-mediated endocytosis (Kim et al., 2012). Clathrin-mediated endocytosis has been shown to be involved in the uptake of larger M13 phages (900 nm length) packed very compactly; therefore, larger maximally-decorated D::EGF λ phages can be still packaged via vesicles. Although the

mechanism cannot be specified, wildtype λ phages may also bind to surface receptors of HT29 cells for internalization. Non-specific electrostatic interactions with negatively-charged GAGs have been evidenced to serve as major cellular receptors for internalization of phages displaying TAT and 3D8 VL transbody (Kim et al., 2012). In this similar manner, the cationic amino acids (Lys and Arg) of gpD and gpE capsid proteins may be interacting biochemically with the negatively-charged carboxyl and sulfate groups present on GAGs. This may mediate phage-cell interaction and enable cellular uptake without the assistance of a displayed ligand. Moreover, there may be specific cell surface receptors that bind to unmodified, native phages. As previously mentioned, polysialic acid has been uncovered as a receptor for *E. coli* phage PK1A2. These phages were bound and internalized via the endolysosomal route and remained infective up to 24 h (Lehti et al., 2017). Internalized phages have been shown to localize in the late endosomal/lysosomal compartments after 2 h, but some phages internalized via caveolae-mediate endocytosis has been found to be released directly into the cytosol and remained infective without degradation (Ivanenkov & Menon, 2000; Lehti et al., 2017). Although the fate of internalized λ phages are unclear, the lysosomal route appears to be common, as the treatment of cells with lysosomotropic agent enhanced phage recovery for up to 8 h. This study requires follow-up experiments in order to determine the intracellular route and eventual fate of the internalized phages.

## 5.4 EGF-displaying bacteriophage λ slows spheroid growth and HT29 cell aggregation

EGF molecules displayed on λ phages likely bound to the EGFR on HT29 cells, preventing the downstream signaling events that promote spheroid growth. Monoclonal antibodies that bind to EGFR have been shown to successfully inhibit growth and induce apoptosis of HT29 by competitively inhibiting the binding of endogenous ligands and EGF-induced tyrosine kinase-dependent EGFR phosphorylation (Gill et al., 1984; Harding & Burtness, 2005). Similarly, high concentration of maximally-decorated D::EGF phages appeared to slow cell proliferation and prevent complete cell-cell connections from forming, as shown in Fig. 18. Interestingly, this did not appear to be ligand density-dependent, as minimally-decorated D::EGF phages (Lo-D::EGF phages) did not influence spheroid growth and formation. Avidity of the receptor-ligand interaction between phages and cells may be a possible explanation. To conceptualize this, the larger size of each maximally-decorated D::EGF phage particle may enable the interaction with many cells simultaneously through greater density of EGF molecules. This would entrap phage particles between each cell, forming lattice-like structures composed of phages interposed between HT29 cells via EGF-EGFR connections. This would effectively and simultaneously block EGFRs on multiple cells, impeding any growth factors from reaching the receptors. Eventually, the rate of cell proliferation would overcome the EGFR block, as observed from later days.

All spheroids treated with phages, including wildtype phages, exhibited smaller spheroids by day 20 compared to the control (Fig. 18), most likely due to surface-bound phages blocking the potentiation of cell-cell interactions. This effect was also apparent when phages were co-seeded with cells (Figs 19 & 20). Lehti et al. posited that phage internalization via polysialic acid will induce biological changes in the cell because the turnover of cell surface polysialic acid will reduce the numbers of available on the surface, reducing its role in regulating cell interactions.

Similarly, we can expect that application of phages, which are subject to internalization, will induce changes in cell activities and ultimately affect spheroid formation.

The signaling kinetics and the alteration of downstream effects to the treatment with D::EGF phages and their subsequent binding to EGFR on HT29 cells can only be speculated. It is likely that multiple cellular mechanisms are altered in response to the D:EGF-EGFR reaction. Cell proliferation appears to have slowed, which may be a result of the inactivation or reduced signaling of the Ras/MAPK pathway. This pathway is normally induced upon EGFR phosphorylation and the binding of Grb2 and Src homology 2 (Chattopadhyay et al,. 1999). Reduced cell survival is also implicated with the cells treated with D::EGF phages in Fig. 18, which suggests the involvement of EGFR in the PI(3)K/Akt pathway through adaptor protein Gab-1 (Mattoon et al., 2004). HT29 cell adhesion appears to also be lost in response to D::EGF phages as shown in Fig. 19 & 22, which may be a result of the loss in the ability of STAT3 from binding to the activated EGFR. Consequently, this would prevent STAT3 dimerization and translocation into the nucleus to regulate gene transcription to maintain epithelial cell polarity and adhesion (Bromberg, 2008). These results were not anticipated, as HT29 colon adenocarcinoma cells harbour the *V600E* BRAF heterozygotic mutation, which is often responsible for resistance (8.3%) to anti-EGFR therapy (Benlloch et al., 2006; De Roock et al., 2010; Xu & Solomon, 1996). Mutations in *BRAF V600E* can allow for downstream signaling events to persist in the absence of signaling molecules, leading to constitutive cell survival and proliferation. However, this study has demonstrated that phages with a maximal display of EGF molecules will slow spheroid growth, most likely through the reduced cell proliferation and survival. The same effects were not exhibited when spheroids were treated with wildtype phages.

Follow-up studies on the cellular and molecular mechanisms altered in response to D::EGF phages are warranted.

## 5.5 Bacteriophage λ is not cytotoxic to HT29 cells

MTT assay (Fig. 22) did not show significant differences in the viability of monolayer HT29 cells in response to phage application. Porayath et al. also reported that unmodified *E. coli* phages were not cytotoxic to HT29 cells in monolayer culture after 24 h by Resazurin assay. In this assay, the morphology of treated cells was similar to untreated cells (Porayath et al., 2018). D::EGF phages did not induce cytoxicity in the monolayer culture. This agrees with the findings of Solmi et al., which also revealed no statistically significant differences in HT29 cell viabilities in response to 24 h exposure to cetuximab (Solmi et al., 2008). In the 3D culture, cell viability was expected to be different as gene expression profiles are often different from monolayer cultures (Fig. 23). It was also expected to be more representative of in vivo HT29 tumour response to phages (Barbone et al., 2016). Wildtype phages did not significantly reduce the viability of HT29 spheroids after 24 h. D::EGF phages, however, reduced the mean of number of viable cells to 54% (Fig. 23). These results are in agreement with the brightfield images (Fig. 18 - 21); spheroids demonstrated loose cell-cell connections and were smaller when treated with D::EGF phages. These spheroids consisted of fewer cells compared to the control in later stages, suggesting a slower cell proliferation and/or cell death (Fig. 18). 100-fold diluted mixtures of both D::EGF and wildtype phages resulted in similar levels of toxicity for the cells as the undiluted mixtures. The dilution of phages used in this experiment may not have been high enough to see correlating reduction in cytotoxicity as toxicity levels could plateau at certain concentrations of phages. Serial dilutions of phages must be added to the spheroids to see correlating reduction of viable cells, which will be confirmed in future studies.

Unexpectedly, results were reversed with phages that were labeled with AlexaFluor 488, with reduced viability in spheroids applied with wildtype phages. It is unclear what caused this – phage surface biochemistry may have been altered, changing the overall surface interactions with the HT29 cells. These toxicity assays confirm that wildtype phages are relatively inert in mammalian cells. However, the fusion of ligands may confer advantages such as specific targeting and reduction in viable cancer cells, enhancing their therapeutic potentials.

The therapeutic potential of phages against solid tumours are promising as λ phages are able to interact with mammalian cells and accumulate in both spheroids and in cells. Phages can be genetically modified to display a targeting moiety on the surface for specificity; this can also slow growth by binding to plasma membrane receptors to induce/inhibit signalling events that result in changes in gene expression and cell growth regulation. The heterogeneity of tumours and the response to phages will be variable between cancer cell lines.

# Chapter 6: Conclusion

The intention of this work was to characterize bacteriophage λ and its interaction with cells in the context of three-dimensional culture. The number of applications for phages is growing in the field of cancer biology as well as the interest in developing a phage-based drug delivery system; however, the ability of phages to penetrate tightly packed cells in the tumour microenvironment has not been investigated to date. In this work, wildtype λ phages without any surface modifications and EGF-displaying λ phages have been compared for the adherence and penetration into HT29 colon adenocarcinoma spheroids, cellular uptake and impacts on spheroid growth. λ phages did not require ligand mediation to adhere to the surface of spheroids, although the display of EGF peptides on λ phages increased the level of phage-associated fluorescence on the surface of HT29 spheroids. Visualization of phages localized in the inner regions of spheroids was limited by confocal microscopy; however, phage-associated fluorescence was diffuse in all regions that were visible after 24 h in fibroblast spheroids. The significance of effective phage penetration and accumulation into spheroids is its potential to successfully traverse the dense tumour microenvironment composed of fibroblasts, immune cells and ECM, and potentially resulting in better biodistribution than other nanoparticles.

EGF-displaying phages showed higher propensity to be internalized by the HT29 cells than wildtype λ phages. The implications for lambda phage internalization into mammalian cells is the potential for successful targeting of phages for gene delivery. However, one of the limiting steps of phages for gene delivery is nuclear localization, as phages are most likely routed to the lysosomes upon internalization. Lastly, the application of EGF-displaying phages in high concentrations showed interference in cell aggregation for spheroid formation, slowing its growth. This was most likely caused by the blocking of EGFR on HT29 cells and depriving the

cells of growth factors; this exposure to phages was shown to result in less viable cells in the spheroid. With ongoing progress made in the discovery of phage-mammalian cell interactions, there is a tremendous potential for therapeutic applications of phages in cancer.

# Chapter 7: Future Research Objectives

Further controls are recommended in future experiments to supplement our findings. To confirm the role of EGF-displaying phages to enhance accumulation, internalization as well as slowing the growth of HT29 spheroid, experiments are recommended using the controls as outlined below:

1) Repeat all the experiments using cell lines that do not overexpress EGFR, such as NIH3T3, and other carcinoma cell lines that overexpress EGFR. Similar outcomes – higher accumulation of EGF-displaying phages, greater percentage of internalization and slowing of spheroid growth – are expected for EGFR-overexpressing spheroids. If such results are observed to a lesser degree in NIH3T3 spheroids and other cell lines with less EGFR expression, then the interactions observed in our studies may be specific to carcinoma cells. This will be therapeutically advantageous in vivo, as EGF-displaying phages will not harm normal cells and accumulate specifically in EGFR-expressing tumour cells.
2) Confirm the expression of EGFR on HT29 cells and quantify λ phages bound to EGFR via Western blot. Gene expression can be altered in cells in 3D culture. Conducting a Western blot will confirm that high EGFR expression is maintained at relatively high levels in HT29 spheroids. Additionally, a Western blot can confirm that the positive fluorescence observed with the confocal pictures is indeed, λ phages.
3) Repeat experiments using EGF as a control. EGF will bind competitively and preferentially to EGFR expressed on HT29 cells. This would reduce the number of EGF-displaying phages binding to HT29 cells. Less EGF-displaying phages would be retained in the spheroids as indicated by decrease in fluorescence by the confocal microscopy.

Cells are also expected to take on normal aggregation upon co-seeding with a high concentration of EGF-displaying phages. If EGFR is occupied by EGF, the treatment of spheroids with EGF-displaying phages would not lead to loose "gaps" between the intercellular spaces of spheroids, assuming that these gaps were caused by the infiltration of EGF-displaying phages. Additionally, there would be a smaller decrease in viability of HT29 cells in spheroids. This would confirm that the action of EGF-displaying phages observed in the performed experiments above was mediated specifically by the λ-EGF-EGFR interaction.

Other further studies include:

1) Constructing a λ phage-derived vector engineered to carry a mammalian transgene cassette expressing GFP. Fluorescent-tagging of this vector, then their application to spheroids and subsequent visualization of GFP-expressing cells provides an understanding of the infiltration and transfection efficiency of a λ- based vector. This allows us to assess phages as a delivery vehicle though a dense, 3D cell culture.
2) Perform RNA seq of HT29 cells in spheroids to determine differences in gene expression among untreated cells, cells in response to wildtype phages and EGF-displaying phages. This assay will elucidate the unknown mechanisms behind the cellular and molecular changes in response to phages. To date, the downstream pathways induced in response to EGF-displaying phages is unknown. It will be interesting to observe whether there are similarities in gene expression between cells treated with EGF-displaying phages and another inhibitor of the extracellular domain of EGFR, such as the mAb cetuximab.
3) Perform a Live/Dead Cell Staining. A commercially available kit can differentially label intracellular proteins of live cells with a green fluorescent probe and late apoptotic and

necrotic cells with a red fluorescent probe. The 3D cytotoxicity assay performed in this study can be further supplemented with this staining assay. This will determine the region of cells in spheroids that have been impacted by the treatment with EGF-displaying phages and indicate where phages have localized in the spheroid.

In the near future, we also hope to extend this study in vivo, applying EGF-displaying phages against human tumour xenograft in mice to observe effects of phages on tumour growth.

# References


Aalto, J., Pelkonen, S., Kalimo, H., & Finne, J. (2001). Mutant bacteriophage with non-catalytic endosialidase binds to both bacterial and eukaryotic polysialic acid and can be used as probe for its detection. *Glycoconjugate Journal*, *18*(10), 751–758.

Abbott, N. J., Rönnbäck, L., & Hansson, E. (2006). Astrocyte-endothelial interactions at the blood-brain barrier. *Nature Reviews Neuroscience*, *7*(1), 41–53.

Abedon, S. T., Kuhl, S. J., Blasdel, B. G., & Kutter, E. M. (2011). Phage treatment of human infections. *Bacteriophage*, *1*(2), 66–85.

Abeles, S. R., & Pride, D. T. (2014). Molecular bases and role of viruses in the human microbiome. *Journal of Molecular Biology*, *426*(23), 3892–3906.

Adams, G. P., Schier, R., McCall, A. M., Simmons, H. H., Horak, E. M., Alpaugh, R. K., Marks, J. D., Weiner, L. M. (2001). High affinity restricts the localization and tumor penetration of single-chain Fv antibody molecules. *Cancer Research*, *61*(12), 4750–4755.

Aggarwal, P., Hall, J. B., McLeland, C. B., Dobrovolskaia, M. A., & McNeil, S. E. (2009). Nanoparticle interaction with plasma proteins as it relates to particle biodistribution, biocompatibility and therapeutic efficacy. *Advanced Drug Delivery Reviews*, *61*(6), 428–437.

Alavi, M., Karimi, N., & Safaei, M. (2017). Application of various types of liposomes in drug delivery systems. *Advanced Pharmaceutical Bulletin*, *7*(1), 3–9.

Aldred, E. (2009). Bonds found in biological chemistry. In *Pharmacology* (pp. 11–19). Retrieved from https://www.sciencedirect.com/science/article/pii/B9780443068980000037

Arab, A., Behravan, J., Razazan, A., Gholizadeh, Z., Nikpoor, A. R., Barati, N., Jaafari, M. R. (2018). A nano-liposome vaccine carrying E75, a HER-2/neu-derived peptide, exhibits significant antitumour activity in mice. *Journal of Drug Targeting*, *26*(4), 365–372.

Ashelford, K. E., Norris, S. J., Fry, J. C., Bailey, M. J., & Day, M. J. (2000). Seasonal population dynamics and interactions of competing bacteriophages and their host in the rhizosphere. *Applied and Environmental Microbiology*, *66*(10), 4193–4199.

Aznavoorian, S., Stracke, M. L., Krutzsch, H., Schiffmann, E., & Liotta, L. A. (1990). Signal transduction for chemotaxis and haptotaxis by matrix molecules in tumor cells. *Journal of Cell Biology*, *110*(4), 1427–1438.

Bachmann, B. J. (1972). Pedigrees of some mutant strains of Escherichia coli K-12. *Bacteriological Reviews*, *36*(4), 525–557.

Baird, A. (2011). Gene transfer into mammalian cells using targeted filamentous bacteriophage. *Cold Spring Harbor Protocols*, *6*(8), 950–957.

Bakhshinejad, B., Karimi, M., & Sadeghizadeh, M. (2014). Bacteriophages and medical oncology: Targeted gene therapy of cancer. *Medical Oncology*, *31*(8), 1–11.

Bao, S., Ouyang, G., Bai, X., Huang, Z., Ma, C., Liu, M., Shao, R., Anderson, R. M., rich, J. N., Wang, X. F. (2004). Periostin potently promotes metastatic growth of colon cancer by augmenting cell survival via the Akt/PKB pathway. *Cancer Cell*, *5*(4), 329–339.

Barbone, D., Van Dam, L., Follo, C., Jithesh, P. V., Zhang, S. D., Richards, W. G., Bueno, R., Fennell, D. A., Broaddus, V. C. (2016). Analysis of gene expression in 3D spheroids highlights a survival role for ASS1 in mesothelioma. *PLoS ONE*, *11*(3).

Barbone, D., Yang, T. M., Morgan, J. R., Gaudino, G., & Broaddus, V. C. (2008). Mammalian target of rapamycin contributes to the acquired apoptotic resistance of human mesothelioma multicellular spheroids. *Journal of Biological Chemistry*, *283*(19), 13021–13030.

Barker, H. E., Paget, J. T. E., Khan, A. A., & Harrington, K. J. (2015). The tumour microenvironment after radiotherapy: Mechanisms of resistance and recurrence. *Nature Reviews Cancer*, *15*(7), 409–425.

Barr, J. J., Auro, R., Furlan, M., Whiteson, K. L., Erb, M. L., Pogliano, J., Stotland, A., Wolkowicz, R., Cutting, A. S., Doran, K. S., Salamon, P., Youle, M., Rohwer, F. (2013a). Bacteriophage adhering to mucus provide a non-host-derived immunity. *Proceedings of the National Academy of Sciences*, *110*(26), 10771–10776.

Barua, S., & Mitragotri, S. (2014). Challenges associated with penetration of nanoparticles across cell and tissue barriers: A review of current status and future prospects. *Nano Today*, Vol. 9, pp. 223–243.

Beghetto, E., & Gargano, N. (2011). Lambda-display: A powerful tool for antigen discovery. *Molecules*, *16*(4), 3089–3105.

Benlloch, S., Payá, A., Alenda, C., Bessa, X., Andreu, M., Jover, R., Castells, A., Llor, X., Aranda, F. I., Massutí, B. (2006). Detection of BRAF V600E mutation in colorectal cancer: Comparison of automatic sequencing and real-time chemistry methodology. *Journal of Molecular Diagnostics*, *8*(5), 540–543.

Berger, C., Madshus, I. H., & Stang, E. (2012). Cetuximab in combination with anti-human IgG antibodies efficiently down-regulates the EGF receptor by macropinocytosis. *Experimental Cell Research*, *318*(20), 2578–2591.

Berset, T. A., Hoier, E. F., & Hajnal, A. (2005). The C. elegans homolog of the mammalian tumor suppressor Dep-1/Scc1 inhibits EGFR signaling to regulate binary cell fate decisions. *Genes and Development*, *19*(11), 1328–1340.

Bilski, P., Daub, M. E., & Chignell, C. F. (2002). Direct detection of singlet oxygen via its phosphorescence from cellular and fungal cultures. *Methods in Enzymology*, *352*, 41–52.

Bloch, H. (1940). Experimental investigation on the relationships between bacteriophages and malignant tumors. *Archives of Virology*, *1*, 481–480.

BRAF GENE. (2015). BRAF B-Raf proto-oncogene, serine/threonine kinase [Homo sapiens (human)] - Gene - NCBI. Retrieved May 5, 2019, from Ncbi website: http://www.ncbi.nlm.nih.gov/gene/673

Breitbart, M., & Rohwer, F. (2005). Method for discovering novel DNA viruses in blood using viral particle selection and shotgun sequencing. *BioTechniques*, *39*(5), 729–736.

Bromberg, J. (2008). Stat proteins and oncogenesis. *Journal of Clinical Investigation*, *109*(9), 1139–1142.

Bruttin, A., & Brüssow, H. (2005). Human volunteers receiving Escherichia coli phage T4 orally: A safety test of phage therapy. *Antimicrobial Agents and Chemotherapy*, *49*(7), 2874–2878.

Bryce, N. S., Zhang, J. Z., Whan, R. M., Yamamoto, N., & Hambley, T. W. (2009). Accumulation of an anthraquinone and its platinum complexes in cancer cell spheroids: The effect of charge on drug distribution in solid tumour models. *Chemical Communications*, (19), 2673–2675.

Burotto, M., Manasanch, E. E., Wilkerson, J., & Fojo, T. (2015). Gefitinib and Erlotinib in Metastatic Non-Small Cell Lung Cancer: A Meta-Analysis of Toxicity and Efficacy of Randomized Clinical Trials. *The Oncologist*, *20*(4), 400–410.

Chattopadhyay, A., Vecchi, M., Ji, Q. S., Mernaugh, R., & Carpenter, G. (1999). The role of individual SH2 domains in mediating association of phospholipase C-γ1 with the activated EGF receptor. *Journal of Biological Chemistry*, *274*(37), 26091–26097.

Chauhan, V. P., Popović, Z., Chen, O., Cui, J., Fukumura, D., Bawendi, M. G., & Jain, R. K. (2011). Fluorescent nanorods and nanospheres for real-time in vivo probing of nanoparticle shape-dependent tumor penetration. *Angewandte Chemie - International Edition*, *50*(48), 11417–11420.

Chem, J. B., Opresko, L. K., Walsh, J., & Steven, H. (1990). Quantitative analysis of the endocytic system involved in hormone-induced receptor internalization . K A Lund , L K Opresko , C Starbuck , B J Walsh and H S Wiley Quantitative Analysis of the Endocytic System in Hormone-induced Receptor Internalization. *Journal of Biological Chemistry*, *265*(26), 15713–15723.

Choi, I.-K., Strauss, R., Richter, M., Yun, C.-O., & Lieber, A. (2013). Strategies to Increase Drug Penetration in Solid Tumors. *Frontiers in Oncology*, *3*, 193.

Ciardiello, F., Caputo, R., Bianco, R., Damiano, V., Pomatico, G., De Placido, S., Bianco, A. R., Tortora, G. (2000). Antitumor effect and potentiation of cytotoxic drugs activity in human cancer cells by ZD-1839 (Iressa), an epidermal growth factor receptor- selective tyrosine kinase inhibitor. *Clinical Cancer Research*, *6*(5), 2053–2063.

Citri, A., Skaria, K. B., & Yarden, Y. (2003). The deaf and the dumb: The biology of ErbB-2 and ErbB-3. In *The EGF Receptor Family: Biologic Mechanisms and Role in Cancer* (pp. 57–68).

Clark, J. R. (2015). Bacteriophage therapy: History and future prospects. *Future Virology*, *10*(4), 449–461.

Clokie, M. R. J., Millard, A. D., Letarov, A. V., & Heaphy, S. (2011). Phages in nature. *Bacteriophage*, *1*(1), 31–45.

Cordova, A., Deserno, M., Gelbart, W. M., & Ben-Shaul, A. (2003). Osmotic shock and the strength of viral capsids. *Biophysical Journal*, *85*(1), 70–74.

Cox, T. R., Bird, D., Baker, A. M., Barker, H. E., Ho, M. W. Y., Lang, G., & Erler, J. T. (2013). LOX-mediated collagen crosslinking is responsible for fibrosis-enhanced metastasis. *Cancer Research*, *73*(6), 1721–1732.

Curti, B. D., Urba, W. J., Alvord, W. G., Janik, J. E., Smith, J. W., Madara, K., & Longo, D. L. (1993).

Interstitial pressure of subcutaneous nodules in melanoma and lymphoma patients: changes during treatment. *Cancer Research*, *53*(10 Suppl), 2204–2207.

Dąbrowska, K., Miernikiewicz, P., Piotrowicz, A., Hodyra, K., Owczarek, B., Lecion, D., Kazmierczak, Z., Letarov, A., Górski, A. (2014). Immunogenicity studies of proteins forming the T4 phage head surface. *Journal of Virology*, *88*(21), 12551–12557.

Dabrowska, K., Opolski, A., Wietrzyk, J., Switala-Jelen, K., Boratynski, J., Nasulewicz, A., Lipinska, L., Chybika, A., Kujawa, M., Dolinska-Krajewska, B., Piasecki, E., Weber-Dabrowska B., Rybka, J., Salwa, J., Wojdat, E., Nowaczyk, M., Gorski, A. (2004). Antitumor activity of bacteriophages in murine experimental cancer models caused possibly by inhibition of β3 integrin signaling pathway. *Acta Virologica*, *48*(4), 241–248.

Dabrowska, K., Switała-Jelen, K., Opolski, A., Weber-Dabrowska, B., & Gorski, A. (2005). A review: Bacteriophage penetration in vertebrates. *Journal of Applied Microbiology*, *48*(4), 241-248.

Dabrowska, K., Wietrzyk, J., Switala-Jelen, K., Godlewska, J., Boratynski, J., Syper, D., Weber-Dabrowska, B., Gorski, A. (2004). Anticancer activity of bacteriophage T4 and its mutant HAP1 in mouse experimental tumour models. *Anticancer Research*, *24*(6), 3991–3995.

Dabrowska, Krystyna, Zembala, M., Boratynski, J., Switala-Jelen, K., Wietrzyk, J., Opolski, A., Szczaurska, K., Kujawa, M., Godlewska, J., Gorski, A. (2007). Hoc protein regulates the biological effects of T4 phage in mammals. *Archives of Microbiology*, *187*(6), 489–498.

Däster, S., Amatruda, N., Calabrese, D., Ivanek, R., Turrini, E., Droeser, R. A., Zajac, P., Fimognari, C., Spagnoli, G. C., Iezzi, G., Mele, V., Muraro, M. G. (2017). Induction of hypoxia and necrosis in multicellular tumor spheroids is associated with resistance to chemotherapy treatment. *Oncotarget*, *8*(1), 1725-1736.

De Jong, W. H., & Borm, P. J. A. (2008). Drug delivery and nanoparticles:applications and hazards. *International Journal of Nanomedicine*, *3*, 133–149.

De Roock, W., Claes, B., Bernasconi, D., De Schutter, J., Biesmans, B., Fountzilas, G., Kalogeras, K. T., Kotoula, V., Papamichael, D., Laurent-Puig, P., Penault-Llorca, F., Rougier, P., Vincenzi, B., Santini, D., Tonini, G., Cappuzzo, F., Frattini, M., Molinari, F., Saletti, P., De Dosso, S., Martini, M., Bardelli, A., Siena, S., Sartore-Bianchi, A., Tabernero, J., Macarulla, T., Di Fiore, F., Gangloff, A. O., Ciardiello, F., Pfeiffer, P., Qvortrup, C., Hansen, T.P., Van Cutsem, E., Piessevaux, H., Lambrechts, D., Delorenzi, M., Tejpar, S. (2010). Effects of KRAS, BRAF, NRAS, and PIK3CA mutations on the efficacy of cetuximab plus chemotherapy in chemotherapy-refractory metastatic colorectal cancer: A retrospective consortium analysis. *The Lancet Oncology*, *11*(8), 753–762.

Decuzzi, P., Godin, B., Tanaka, T., Lee, S. Y., Chiappini, C., Liu, X., & Ferrari, M. (2010). Size and shape effects in the biodistribution of intravascularly injected particles. *Journal of Controlled Release*, *141*(3), 320–327.

Desoize, B., & Jardillier, J. C. (2000). Multicellular resistance: A paradigm for clinical resistance? *Critical Reviews in Oncology/Hematology*, *36*(2-3), 193-207.

Dickson, R. P., & Huffnagle, G. B. (2015). The Lung Microbiome: New Principles for Respiratory Bacteriology in Health and Disease. *PLOS Pathogens*, *11*(7), e1004923.

Donnelly, A., Yata, T., Bentayebi, K., Suwan, K., & Hajitou, A. (2015). Bacteriophage mediates efficient gene transfer in combination with conventional transfection reagents. *Viruses*, *7*(12), 6476–6489.

Dreher, M. R., Liu, W., Michelich, C. R., Dewhirst, M. W., Yuan, F., & Chilkoti, A. (2006a). Tumor vascular permeability, accumulation, and penetration of macromolecular drug carriers. *Journal of the National Cancer Institute*, *98*(5), 335–344.

Dreher, M. R., Liu, W., Michelich, C. R., Dewhirst, M. W., Yuan, F., & Chilkoti, A. (2006b). Tumor Vascular Permeability, Accumulation, and Penetration of Macromolecular Drug Carriers. *JNCI: Journal of the National Cancer Institute*, *98*(5), 335–344.

Dubos, R. J., Straus, J. H., & Pierce, C. (1943). The Multiplication of Bacteriophage in vivo and Its Protective Effect Against an Experimental Infection with Shigella dysenteriae. *Journal of Experimental Medicine*, *78*(3), 161–168.

Emlet, D. R., Gupta, P., Holgado-Madruga, M., Del Vecchio, C. A., Mitra, S. S., Han, S. Y., Jensen, K. C., Vogel, H., Xu, L. W., Skirboll, S. S., Wong, A. J. (2014). Targeting a glioblastoma cancer stem-cell population defined by EGF receptor variant III. *Cancer Research*, *74*(4), 1238–1249.

Enmon, R., Yang, W. H., Ballangrud, Å. M., Solit, D. B., Heller, G., Rosen, N., Scher, H. I., Sgouros, G. (2003). Combination Treatment with 17-N-Allylamino-17-Demethoxy Geldanamycin and Acute Irradiation Produces Supra-Additive Growth Suppression in Human Prostate Carcinoma Spheroids. *Cancer Research*, *63*(23), 8393–8399.

Eriksson, F., Tsagozis, P., Lundberg, K., Parsa, R., Mangsbo, S. M., Persson, M. A. A., Harris, R. A., Pisa, P. (2009). Tumor-Specific Bacteriophages Induce Tumor Destruction through Activation of Tumor-Associated Macrophages. *The Journal of Immunology*, *182*(5), 3105–3111.

Fechner, H., Haack, A., Wang, H., Wang, X., Eizema, K., Pauschinger, M., Schoemaker, R., Veghel, R., Houtsmuller, A., Schultheiss, H. P., Lamers, J., Poller, W. (1999). Expression of Coxsackie adenovirus receptor and alpha(v)-integrin does not correlate with aconovector targeting in vivo indicating anatomical vector barriers. *Gene Therapy*, *6*(9), 1520–1535.

Ferretti, S., Allegrini, P. R., Becquet, M. M., & McSheehy, P. M. J. (2015). Tumor Interstitial Fluid Pressure as an Early-Response Marker for Anticancer Therapeutics. *Neoplasia*, *11*(9), 874–881.

Florence, A. T. (2012). "Targeting" nanoparticles: The constraints of physical laws and physical barriers. *Journal of Controlled Release*, *164*(2), 115–124.

French, A. R., Tadaki, D. K., Niyogi, S. K., & Lauffenburger, D. A. (1995). Intracellular trafficking of epidermal growth factor family ligands is directly influenced by the pH sensitivity of the receptor/ligand interaction. *Journal of Biological Chemistry*, *270*(9), 4334–4340.

Friedrich, J., Seidel, C., Ebner, R., & Kunz-Schughart, L. A. (2009a). Spheroid-based drug screen: considerations and practical approach. *Nature Protocols*, *4*(3), 309–324.

Gashaw, I., Ellinghaus, P., Sommer, A., & Asadullah, K. (2012). What makes a good drug target? *Drug Discovery Today*, *16*(23-24), 1037–1043.

Gavhane, N., Shete, S., Bhagat, K., Shinde, V., Bhong, K., Khairnar, G., & Yadav, V. (2011). Solid Tumors: Facts, Challenges and Solutions. *International Journal of Pharma Sciences and Research*

*(IJPSR*, *2*(1), 1–12.

Gavrilovskaya, I. N., Brown, E. J., Ginsberg, M. H., & Mackow, E. R. (1999). Cellular entry of hantaviruses which cause hemorrhagic fever with renal syndrome is mediated by beta3 integrins. *Journal of Virology*, *73*(5), 3951–3959.

Geier, M. R., & Merril, C. R. (1972). Lambda phage transcription in human fibroblasts. *Virology*, *47*(3), 638–643.

Geier, M. R., Trigg, M. E., Merril, C. R., Grier, M. R., Trigg, M. E., & Merril, C. R. (1973). Fate of bacteriophage lambda in non-immune germ-free mice. *Nature*, *246*(5430), 221–223.

Gerweck, L. E., Kozin, S. V, & Stocks, S. J. (1999). The pH partition theory predicts the accumulation and toxicity of doxorubicin in normal and low-pH-adapted cells. *British Journal of Cancer*, *79*(5–6), 838–842.

Giaccone, G., Ruiz, M. G., Le Chevalier, T., Thatcher, N., Smit, E., Rodriguez, J. A., Janne, ,P., Oulid-Aissa, D., Soria, J. C. (2006). Erlotinib for frontline treatment of advanced non-small cell lung cancer: A phase II study. *Clinical Cancer Research*, *12*(20 PART 1), 6049–6055.

Gilcrease, E. B., Winn-Stapley, D. A., Hewitt, F. C., Joss, L., & Casjens, S. R. (2005). Nucleotide sequence of the head assembly gene cluster of bacteriophage L and decoration protein characterization. *Journal of Bacteriology*, *187*(6), 2050–2057.

Gill, G. N., Kawamoto, T., Cochet, C., Le, A., Sato, J. D., Masui, H., Mcleod, C., Mendelsohn, J. (1984). Monoclonal anti-epidermal growth factor receptor antibodies which are inhibitors of epidermal growth factor binding and antagonists of epidermal growth factor-stimulated tyrosine protein kinase activity. *Journal of Biological Chemistry*, *259*(12), 7755–7760.

Gonzalez, J. M., Hamm-Alvarez, S., Tan, J. C. H., & Tan, J. C. H. (2013). Analyzing live cellularity in the human trabecular meshwork. *Investigative Ophthalmology & Visual Science*, *54*(2), 1039–1047.

Görlach, A., Herter, P., Hentschel, H., Frosch, P. J., & Acker, H. (1994). Effects of nIFN β and rifn γ on growth and morphology of two human melanoma cell lines: Comparison between two-and three-dimensional culture. *International Journal of Cancer*, *56*(2), 249–254.

Górski, A., Dąbrowska, K., Hodyra-Stefaniak, K., Borysowski, J., Międzybrodzki, R., & Weber-Dąbrowska, B. (2015). Phages targeting infected tissues: novel approach to phage therapy. *Future Microbiology*, *10*(2), 199–204.

Gorski, A., Dabrowska, K., Switala-Jeleń, K., Nowaczyk, M., Weber-Dabrowska, B., Boratynski, J., Wietrzyk J., Opolski, A. (2003). New insights into the possible role of bacteriophages in host defense and disease. *Medical Immunology (London, England)*, *2*(1), 2.

Gottesman, M. M. (2002). Mechanisms of Cancer Drug Resistance. *Annual Review of Medicine*, *53*(1), 615–627.

Governal, R. A., & Gerba, C. P. (1997). Persistence of MS-2 and PRD-1 bacteriophages in an ultrapure water system. *Journal of Industrial Microbiology and Biotechnology*, *18*(5), 297–301.

Grandis, J. R., Melhem, M. F., Gooding, W. E., Day, R., Holst, V. A., Wagener, M. M., Drening, S. D.,

Tweardy, D. J. (1998). Levels of TGF-α and EGFR protein in head and neck squamous cell carcinoma and patient survival. *Journal of the National Cancer Institute*, *90*(11), 824–832.

Graus-Porta, D., Beerli, R. R., Daly, J. M., & Hynes, N. E. (1997). ErbB-2, the preferred heterodimerization partner of all ErbB receptors, is a mediator of lateral signaling. *EMBO Journal*, *16*(7), 1647–1655.

Grill, J., Lamfers, M. L. M., van Beusechem, V. W., Dirven, C. M., Pherai, D. S., Kater, M., Van der Valk, P., Vogels, R., Vandertop, W. P., Pinedo, H. M., Curiel, D. T., Gerritsen, W. R. (2002). The organotypic multicellular spheroid is a relevant three-dimensional model to study adenovirus replication and penetration in human tumors in vitro. *Molecular Therapy : The Journal of the American Society of Gene Therapy*, *6*(5), 609–614.

Gu, G., Gao, X., Hu, Q., Kang, T., Liu, Z., Jiang, M., Miao, D., Song, Q., Yao, L., Tu, Y., Chen, H., Jiang, X., Chen, J. (2013). The influence of the penetrating peptide iRGD on the effect of paclitaxel-loaded MT1-AF7p-conjugated nanoparticles on glioma cells. *Biomaterials*, *34*(21), 5138–5148.

Haj, F. G., Markova, B., Klaman, L. D., Bohmer, F. D., & Neel, B. G. (2003). Regulation of receptor tyrosine kinase signaling by protein tyrosine phosphatase-1B. *Journal of Biological Chemistry*, *278*(2), 739–744.

Hajitou, A., Rangel, R., Trepel, M., Soghomonyan, S., Gelovani, J. G., Alauddin, M. M., Pasqualini, R., Arap, W. (2007). Design and construction of targeted AAVP vectors for mammalian cell transduction. *Nature Protocols*, *2*(3), 523–531.

Harada, H., Kizaka-Kondoh, S., & Hiraoka, M. (2005). Optical imaging of tumor hypoxia and evaluation of efficacy of a hypoxia-targeting drug in living animals. *Molecular Imaging*, *4*(3), 182–193.

Harding, J., & Burtness, B. (2005). Cetuximab: An epidermal growth factor receptor chimeric human-murine monoclonal antibody. *Drugs of Today*, *41*(2), 107.

Helmlinger, G., Yuan, F., Dellian, M., & Jain, R. K. (1997). Interstitial pH and pO 2 gradients in solid tumors in vivo: High-resolution measurements reveal a lack of correlation. *Nature Medicine*, *3*(2), 177–182.

Hendriks, B. S., Wiley, H. S., & Lauffenburger, D. (2003). HER2-mediated effects on EGFR endosomal sorting: Analysis of biophysical mechanisms. *Biophysical Journal*, *85*(4), 2732–2745.

Hendrix, R. W., & Duda, R. L. (1992). Bacteriophage λPaPa: Not the mother of all λ phages. *Science*, *258*(5085), 1145–1148.

Herbst, J. J., Opresko, L. K., Walsh, B. J., Lauffenburger, D. A., & Wiley, H. S. (1994). Regulation of postendocytic trafficking of the epidermal growth factor receptor through endosomal retention. *Journal of Biological Chemistry*, *269*(17), 12865–12873.

Hodyra-Stefaniak, K., Miernikiewicz, P., Drapała, J., Drab, M., Jonczyk-Matysiak, E., Lecion, D., … Dabrowska, K. (2015). Mammalian Host-Versus-Phage immune response determines phage fate in vivo. *Scientific Reports*, *5*, 14802.

Hosseinidoust, Z. (2017). Phage-Mediated Gene Therapy. *Current Gene Therapy*, *17*(2), 120–126.

Housman, G., Byler, S., Heerboth, S., Lapinska, K., Longacre, M., Snyder, N., & Sarkar, S. (2014). Drug resistance in cancer: an overview. *Cancers*, Vol. 6, pp. 1769–1792.

Howes, A. L., Chiang, G. G., Lang, E. S., Ho, C. B., Powis, G., Vuori, K., & Abraham, R. T. (2007). The phosphatidylinositol 3-kinase inhibitor, PX-866, is a potent inhibitor of cancer cell motility and growth in three-dimensional cultures. *Molecular Cancer Therapeutics*, *6*(9), 2505–2514.

Huang, K., Boerhan, R., Liu, C., & Jiang, G. (2017). Nanoparticles Penetrate into the Multicellular Spheroid-on-Chip: Effect of Surface Charge, Protein Corona, and Exterior Flow. *Molecular Pharmaceutics*, *14*(12), 4618–4627.

Huang, Z., & Bao, S. D. (2004). Roles of main pro- and anti-angiogenic factors in tumor angiogenesis. *World Journal of Gastroenterology*, *10*(4), 463–470.

Huh, H., Wong, S., St. Jean, J., & Slavcev, R. (2019). Bacteriophage interactions with mammalian tissue: Therapeutic applications. *Advanced Drug Delivery Reviews*, pii: S0169-409X(19)30003-1.

Inchley, C. J. (1969). The actvity of mouse Kupffer cells following intravenous injection of T4 bacteriophage. *Clinical and Experimental Immunology*, *5*(1), 173–187.

Ivanenkov, V. V., Felici, F., & Menon, A. G. (1999). Uptake and intracellular fate of phage display vectors in mammalian cells. *Biochimica et Biophysica Acta - Molecular Cell Research*, *1448*(3), 450–462.

Ivanenkov, V. V, & Menon, A. G. (2000). Peptide-Mediated Transcytosis of Phage Display Vectors in MDCK Cells. *Biochemical and Biophysical Research Communications*, *276*(1), 251–257.

Ivanovska, I., Wuite, G., Jonsson, B., & Evilevitch, A. (2007). Internal DNA pressure modifies stability of WT phage. *Proceedings of the National Academy of Sciences*, *104*(23), 9603–9608.

Jain, R. K. (1990). Vascular and interstitial barriers to delivery of therapeutic agents in tumors. *Cancer and Metastasis Review*, *9*(3), 253–266.

Jain, R. K. (2012). Delivery of molecular and cellular medicine to solid tumors. *Advanced Drug Delivery Reviews*, *46*(1–3), 149–168.

Jamali, F., Lemery, S., Ayalew, K., Robottom, S., Robie-Suh, K., Rieves, D., & Pazdur, R. (2009). Romiplostim for the treatment of chronic immune (idiopathic) thrombocytopenic purpura. *Oncology (Williston Park, N.Y.)*, *23*(8), 704–709.

Jepson, C. D., & March, J. B. (2004). Bacteriophage lambda is a highly stable DNA vaccine delivery vehicle. *Vaccine*, *22*(19), 2413–2419.

Juweid, M., Neumann, R., Paik, C., Perez-Bacete, M. J., Sato, J., van Osdol, W., & Weinstein, J. N. (1992). Micropharmacology of monoclonal antibodies in solid tumors: direct experimental evidence for a binding site barrier. *Cancer Research*, *52*(19), 5144–5153.

Karasseva, N. G., Glinsky, V. V., Chen, N. X., Komatireddy, R., & Quinn, T. P. (2002). Identification and characterization of peptides that bind human ErbB-2 selected from a bacteriophage display library. *Journal of Protein Chemistry*, *21*(4), 287–296.

Karlsson, H., Fryknäs, M., Larsson, R., & Nygren, P. (2012). Loss of cancer drug activity in colon cancer HCT-116 cells during spheroid formation in a new 3-D spheroid cell culture system. *Experimental Cell Research*, *318*(13), 1577–1585.

Kassner, P D, Burg, M. A., Baird, A., & Larocca, D. (1999). Genetic selection of phage engineered for receptor-mediated gene transfer to mammalian cells. *Biochemical and Biophysical Research Communications*, *264*(0006-291X), 921–928.

Kataoka, K., Harada, A., & Nagasaki, Y. (2012). Block copolymer micelles for drug delivery: Design, characterization and biological significance. *Advanced Drug Delivery Reviews*, *47*(1), 113–131.

Kaur, T., Nafissi, N., Wasfi, O., Sheldon, K., Wettig, S., & Slavcev, R. (2012). Immunocompatibility of Bacteriophages as Nanomedicines. *Journal of Nanotechnology*, *2012*, 1–13.

Khawar, I. A., Kim, J. H., & Kuh, H. J. (2015). Improving drug delivery to solid tumors: Priming the tumor microenvironment. *Journal of Controlled Release*, *201*, 78–89.

Kibria, G., Hatakeyama, H., Ohga, N., Hida, K., & Harashima, H. (2013). The effect of liposomal size on the targeted delivery of doxorubicin to Integrin alpha v beta 3-expressing tumor endothelial cells. *BIOMATERIALS*, *34*(22), 5617–5627.

Kim, A., Shin, T. H., Shin, S. M., Pham, C. D., Choi, D. K., Kwon, M. H., & Kim, Y. S. (2012). Cellular Internalization Mechanism and Intracellular Trafficking of Filamentous M13 Phages Displaying a Cell-Penetrating Transbody and TAT Peptide. *PLoS ONE*, *7*(12), e51813.

Kim, M.-S., Park, E.-J., Roh, S. W., & Bae, J.-W. (2011). Diversity and Abundance of Single-Stranded DNA Viruses in Human Feces. *Applied and Environmental Microbiology*, *77*(22), 8062–8070.

Kłosowska-Wardęga, A., Hasumi, Y., Burmakin, M., Åhgren, A., Stuhr, L., Moen, I., Reed, R. K., Rubin, K., Hellberg, C., Heldin, C.H. (2009). Combined Anti-Angiogenic Therapy Targeting PDGF and VEGF Receptors Lowers the Interstitial Fluid Pressure in a Murine Experimental Carcinoma. *PLoS ONE*, *4*(12), e8149.

Kolonin, M. G., Bover, L., Sun, J., Zurita, A. J., Do, K. A., Lahdenranta, J., … Pasqualini, R. (2006). Ligand-directed surface profiling of human cancer cells with combinatorial peptide libraries. *Cancer Research*, *66*(1), 34–40.

Kong, G., Braun, R. D., & Dewhirst, M. W. (2001). Characterization of the effect of hyperthermia on nanoparticle extravasation from tumor vasculature. *Cancer Research*, *61*(7), 3027–3032.

Kostarelos, K., Emfietzoglou, D., Papakostas, A., Yang, W. H., Ballangrud, Å., & Sgouros, G. (2004). Binding and interstitial penetration of liposomes within avascular tumor spheroids. *International Journal of Cancer*, *112*(4), 713–721.

Krumpe, L. R. H., & Mori, T. (2006). The use of phage-displayed peptide libraries to develop tumor-targeting drugs. *International Journal of Peptide Research and Therapeutics*, *12*, 79–91.

Kuh, H. J., Jang, S. H., Wientjes, M. G., Weaver, J. R., & Au, J. L. (1999). Determinants of paclitaxel penetration and accumulation in human solid tumor. *The Journal of Pharmacology and Experimental Therapeutics*, *290*(2), 871–880.

Kultti, A., Zhao, C., Singha, N. C., Zimmerman, S., Osgood, R. J., Symons, R., Jiang, P., Li, X., Thompson, C. B., Infante, J. R., Jacobetz, M. A., Tuveson, D. A., Frost, G. I., Shepard, H. M., Huang, Z. (2014). Accumulation of Extracellular Hyaluronan by Hyaluronan Synthase 3 Promotes Tumor Growth and Modulates the Pancreatic Cancer Microenvironment. *BioMed Research International*, *2014*, 1–15.

Kumari, S., Harjai, K., & Chhibber, S. (2011). Bacteriophage versus antimicrobial agents for the treatment of murine burn wound infection caused by Klebsiella pneumoniae B5055. *Journal of Medical Microbiology*, *60*(Pt 2), 205–210.

Lafrenie, R. M., Lee, S. F., Hewlett, I. K., Yamada, K. M., & Dhawan, S. (2002). Involvement of integrin alphavbeta3 in the pathogenesis of human immunodeficiency virus type 1 infection in monocytes. *Virology*, *297*(1), 31–38.

Lamaze, C., & Schmid, S. L. (1995). The emergence of clathrin-independent pinocytic pathways. *Current Opinion in Cell Biology*, *7*(4), 573–580.

Lankes, H. A., Zanghi, C. N., Santos, K., Capella, C., Duke, C. M. P., & Dewhurst, S. (2007). In vivo gene delivery and expression by bacteriophage lambda vectors. *Journal of Applied Microbiology*, *102*(5), 1337–1349.

Larocca, D, & Baird, A. (2001). Receptor-mediated gene transfer by phage-display vectors: applications in functional genomics and gene therapy. *Drug Discovery Today*, *6*(15), 793–801.

Larocca, David, Burg, M., & Baird, A. (2005). Evolving Phage Vectors for Cell Targeted Gene Delivery - An Update. *Medicinal Chemistry Reviews - Online*, *2*(2), 111–114.

Larocca, David, Jensen-Pergakes, K., Burg, M. A., & Baird, A. (2001). Receptor-Targeted Gene Delivery Using Multivalent Phagemid Particles. *Molecular Therapy*, *3*(4), 476–484.

Larocca, David, Witte, A., Johnson, W., Pierce, G. F., & Baird, A. (2008). Targeting Bacteriophage to Mammalian Cell Surface Receptors for Gene Delivery. *Human Gene Therapy*, *9*(16), 2393–2399.

Laskin, J. J., & Sandler, A. B. (2004). Epidermal growth factor receptor: A promising target in solid tumours. *Cancer Treatment Reviews*, *30*(1), 1–17.

Laurent-Puig, P., Cayre, A., Manceau, G., Buc, E., Bachet, J.-B., Lecomte, T., Rougier, P., Lievre, A., Landi, B., Boige, V., Ducreux, M., Ychou, M., Bibeau, F., Buche, O., Reid, J., Stone, S., Penault-Llorca, F. (2009). Analysis of *PTEN* , *BRAF* , and *EGFR* Status in Determining Benefit From Cetuximab Therapy in Wild-Type *KRAS* Metastatic Colon Cancer. *Journal of Clinical Oncology*, *27*(35), 5924–5930.

Lech, K., Reddy, K. J., & Sherman, L. A. (2004). Preparing Lambda DNA from Phage Lysates. In *Current Protocols in Molecular Biology*. John Wiley & Sons, Inc.

Lee, C. M., Tanaka, T., Murai, T., Kondo, M., Kimura, J., Su, W., Kitagawa, T., Ito, T., Matsuda, H., Miyasaka, M. (2002). Novel chondroitin sulfate-binding cationic liposomes loaded with cisplatin efficiently suppress the local growth and liver metastasis of tumor cells in vivo. *Cancer Research*, *62*(15), 4282–4288.

Lee, K. L., Hubbard, L. C., Hern, S., Yildiz, I., Gratzl, M., & Steinmetz, N. F. (2013). Shape matters: The

diffusion rates of TMV rods and CPMV icosahedrons in a spheroid model of extracellular matrix are distinct. *Biomaterials Science*, *1*(6), 581–588.

Lee, S. Y., Ferrari, M., & Decuzzi, P. (2009). Shaping nano-/micro-particles for enhanced vascular interaction in laminar flows. *Nanotechnology*, *20*(49), e495101.

Lehti, T. A., Pajunen, M. I., Skog, M. S., & Finne, J. (2017). Internalization of a polysialic acid-binding Escherichia coli bacteriophage into eukaryotic neuroblastoma cells. *Nature Communications*, *8*(1), 1915.

Lewandowska, M. A., Jóźwicki, W., & Żurawski, B. (2013). KRAS and BRAF mutation analysis in colorectal adenocarcinoma specimens with a low percentage of tumor cells. *Molecular Diagnosis & Therapy*, *17*(3), 193–203.

Li, B., Wang, Y., Zhu, H., Li, J., Hu, X., Wang, B., Hao, X. Z. Wang, L., Zhang, X. R., Shi, Y. (2011). Association of serum EGFR protein concentration with the efficacy of Gefitinib in the treatment of advanced non-small cell lung cancer. *Zhonghua Zhong Liu Za Zhi [Chinese Journal of Oncology]*, *33*(6), 431–435.

Li, Y., Macdonald-Obermann, J., Westfall, C., Piwnica-Worms, D., & Pike, L. J. (2012). Quantitation of the effect of ErbB2 on epidermal growth factor receptor binding and dimerization. *Journal of Biological Chemistry*, *287*(37), 31116–31125.

Li, Z. Y., Ni, S., Yang, X., Kiviat, N., & Lieber, A. (2004). Xenograft models for liver metastasis: Relationship between tumor morphology and adenovirus vector transduction. *Molecular Therapy*, *9*(5), 650–657.

Ma, H. L., Jiang, Q., Han, S., Wu, Y., Tomshine, J. C., Wang, D., Gan, Y., Zou, G., Liang, X. J. (2012). Multicellular tumor spheroids as an in vivo-like tumor model for three-dimensional imaging of chemotherapeutic and nano material cellular penetration. *Molecular Imaging*, *11*(6), 487–498.

Maeda, H., Sawa, T., & Konno, T. (2001). Mechanism of tumor-targeted delivery of macromolecular drugs, including the EPR effect in solid tumor and clinical overview of the prototype polymeric drug SMANCS. *Journal of Controlled Release*, *74*(1–3), 47–61.

Maeda, H., Tsukigawa, K., & Fang, J. (2016). A Retrospective 30 Years After Discovery of the Enhanced Permeability and Retention Effect of Solid Tumors: Next-Generation Chemotherapeutics and Photodynamic Therapy—Problems, Solutions, and Prospects. *Microcirculation*, *23*(3), 173–182.

Majewska, J., Beta, W., Lecion, D., Hodyra-Stefaniak, K., Kłopot, A., Kaźmierczak, Z., … Dąbrowska, K. (2015). Oral Application of T4 Phage Induces Weak Antibody Production in the Gut and in the Blood. *Viruses*, *7*(8), 4783–4799.

Malanchi, I., Santamaria-Martínez, A., Susanto, E., Peng, H., Lehr, H. A., Delaloye, J. F., & Huelsken, J. (2012). Interactions between cancer stem cells and their niche govern metastatic colonization. *Nature*, *481*(7379), 85–91.

Malumbres, M., & Barbacid, M. (2003). RAS oncogenes: the first 30 years. *Nature Reviews. Cancer*, *3*(6), 459–465.

Mancuso, F., Shi, J., & Malik, D. J. (2018). High throughput manufacturing of bacteriophages using

continuous stirred tank bioreactors connected in series to ensure optimum host bacteria physiology for phage production. *Viruses*, *10*(10), 1.

Martínez-Maqueda, D., Miralles, B., & Recio, I. (2015). HT29 Cell Line. In *The Impact of Food Bioactives on Health* (pp. 113–124). Retrieved from http://link.springer.com/10.1007/978-3-319-16104-4_11

Matsuo, T., Nishizuka, S. S., Ishida, K., Iwaya, T., Ikeda, M., & Wakabayashi, G. (2011a). Analysis of the anti-tumor effect of cetuximab using protein kinetics and mouse xenograft models. *BMC Research Notes*, *4*, 140.

Mattoon, D. R., Lamothe, B., Lax, I., & Schlessinger, J. (2004). The docking protein Gab1 is the primary mediator of EGF-stimulated activation of the PI-3K/Akt cell survival pathway. *BMC Biology*, *2*, 24.

Mehta, G., Hsiao, A. Y., Ingram, M., Luker, G. D., & Takayama, S. (2012). Opportunities and challenges for use of tumor spheroids as models to test drug delivery and efficacy. *Journal of Controlled Release : Official Journal of the Controlled Release Society*, *164*(2), 192–204.

Merril, C. R., Biswas, B., Carlton, R., Jensen, N. C., Creed, G. J., Zullo, S., & Adhya, S. (1996). Long-circulating bacteriophage as antibacterial agents. *Proceedings of the National Academy of Sciences*, *93*(8), 3188–3192.

Merril, C. R., Scholl, D., & Adhya, S. L. (2003). The prospect for bacteriophage therapy in Western medicine. *Nature Reviews Drug Discovery*, *2*(6), 489–497.

Miao, L., Newby, J. M., Lin, C. M., Zhang, L., Xu, F., Kim, W. Y., … Huang, L. (2016). The Binding Site Barrier Elicited by Tumor-Associated Fibroblasts Interferes Disposition of Nanoparticles in Stroma-Vessel Type Tumors. *ACS Nano*, *10*(10), 9243–9258.

Międzybrodzki, R., Kłak, M., Jonczyk-Matysiak, E., Bubak, B., Wójcik, A., Kaszowska, M., … Górski, A. (2017). Means to facilitate the overcoming of gastric juice barrier by a therapeutic staphylococcal bacteriophage A5/80. *Frontiers in Microbiology*, *8*, 467.

Mikawa, Y. G., Maruyama, I. N., & Brenner, S. (1996). Surface display of proteins on bacteriophage lambda heads. *J.Mol.Biol.*, *262*(0022–2836), 21–30.

Mikhail, A. S., Eetezadi, S., & Allen, C. (2013). Multicellular Tumor Spheroids for Evaluation of Cytotoxicity and Tumor Growth Inhibitory Effects of Nanomedicines In Vitro: A Comparison of Docetaxel-Loaded Block Copolymer Micelles and Taxotere®. *PLoS ONE*, *8*(4), e62630.

Milosevic, M., Fyles, A., Hedley, D., & Hill, R. (2004). The human tumor microenvironment: invasive (needle) measurement of oxygen and interstitial fluid pressure. *Seminars in Radiation Oncology*, *14*(3), 249–258.

Minchinton, A. I., & Tannock, I. F. (2006). Drug penetration in solid tumours. *Nature Reviews. Cancer*, *6*(8), 583–592.

Misinzo, G., Delputte, P. L., & Nauwynck, H. J. (2008). Inhibition of Endosome-Lysosome System Acidification Enhances Porcine Circovirus 2 Infection of Porcine Epithelial Cells. *Journal of Virology*, *82*(3), 1128–1135.

Mittler, F., Obeïd, P., Rulina, A. V., Haguet, V., Gidrol, X., & Balakirev, M. Y. (2017). High-Content Monitoring of Drug Effects in a 3D Spheroid Model. *Frontiers in Oncology*, *7*, 293.

Moran, Y., Fredman, D., Szczesny, P., Grynberg, M., & Technau, U. (2012). Recurrent horizontal transfer of bacterial toxin genes to eukaryotes. *Molecular Biology and Evolution*, *29*(9), 2223–2230.

Mueller-Klieser, W. (1997). Three-dimensional cell cultures: from molecular mechanisms to clinical applications. *The American Journal of Physiology*, *273*(4 Pt 1), 1109–1123.

Mueller-Klieser, Wolfgang. (1987). Multicellular spheroids - A review on cellular aggregates in cancer research. *Journal of Cancer Research and Clinical Oncology*, *113*(2), 101–122.

Nacev, A., Kim, S. H., Rodriguez-Canales, J., Tangrea, M. A., Shapiro, B., Emmert-Buck, M. R. (2011). A dynamic magnetic shift method to increase nanoparticle concentration in cancer metastases: a feasibility study using simulations on autopsy specimens. *International Journal of Nanomedicine*, *6*, 2907–2923.

Nadeem, A., & Lindi Wahl, S. M. (2016). *Bacteria-Phage Models with a Focus on Prophage as a Genetic Reservoir Graduate Program in Applied Mathematics* (University of Western Ontario).

Netti, P. A., Berk, D. A., Swartz, M. A., Grodzinsky, A. J., & Jain, R. K. (2000). Role of extracellular matrix assembly in interstitial transport in solid tumors. *Cancer Research*, *60*(9), 2497–2503.

Ni, C. Y., Murphy, M. P., Golde, T. E., & Carpenter, G. (2001). γ-secretase cleavage and nuclear locatization of ErbB-4 receptor tyrosine kinase. *Science*, *294*(5549), 2179–2181.

Nicastro, J., Sheldon, K., El-Zarkout, F. A., Sokolenko, S., Aucoin, M. G., & Slavcev, R. (2013). Construction and analysis of a genetically tuneable lytic phage display system. *Applied Microbiology and Biotechnology*, *97*(17), 7791–7804.

Nicastro, J., Wong, S., Khazaei, Z., Lam, P., Blay, J., & Slavcev, R. A. (2016). *Bacteriophage Applications - Historical Perspective and Future Potential*. Retrieved from http://link.springer.com/10.1007/978-3-319-45791-8

Oh, J., Byrd, A. L., Park, M., Kong, H. H., & Segre, J. A. (2016). Temporal Stability of the Human Skin Microbiome. *Cell*, *165*(4), 854–866.

Oliveira-Cunha, M., Newman, W. G., & Siriwardena, A. K. (2011). Epidermal growth factor receptor in pancreatic cancer. *Cancers*, *3*(2), 1513–1526.

Organization, W. H. (2018). WHO | Cancer. Retrieved March 11, 2018, from Who website: http://www.who.int/cancer/en/

Padera, T. P., Kadambi, A., Di Tomaso, E., Mouta Carreira, C., Brown, E. B., Boucher, Y., … Jain, R. K. (2002). Lymphatic metastasis in the absence of functional intratumor lymphatics. *Science*, *296*(5574), 1883–1886.

Pardridge, W. M. (2003). Blood-Brain Barrier Drug Targeting: the Future of Brain Drug Development. *Molecular Interventions*, *3*(2), 90–105.

Park, K., Cha, K. E., & Myung, H. (2014). Observation of inflammatory responses in mice orally fed with

bacteriophage T7. *Journal of Applied Microbiology*, *117*(3), 627–633.

Pasqualini, R., & Ruoslahti, E. (1996). Organ targeting in vivo using phage display peptide libraries. *Nature*, *380*(6572), 364–366.

Peles, E., Ben-Levy, R., Tzahar, E., Liu, N., Wen, D., & Yarden, Y. (1993). Cell-type specific interaction of Neu differentiation factor (NDF/heregulin) with Neu/HER-2 suggests complex ligand-receptor relationships. *The EMBO Journal*, *12*(3), 961–971.

Petter, J. G., & Vimr, E. R. (1993). Complete nucleotide sequence of the bacteriophage K1F tail gene encoding endo-N-acylneuraminidase (endo-N) and comparison to an endo-N homolog in bacteriophage PK1E. *Journal of Bacteriology*, *175*(14), 4354–4363.

Piersanti, S., Cherubini, G., Martina, Y., Salone, B., Avitabile, D., Grosso, F., … Saggio, I. (2004). Mammalian cell transduction and internalization properties of λ phages displaying the full-length adenoviral penton base or its central domain. *Journal of Molecular Medicine*, *82*(7), 467–476.

Pluen, A., Boucher, Y., Ramanujan, S., McKee, T. D., Gohongi, T., di Tomaso, E., … Jain, R. K. (2001). Role of tumor-host interactions in interstitial diffusion of macromolecules: Cranial vs. subcutaneous tumors. *Proceedings of the National Academy of Sciences*, *98*(8), 4628–4633.

Porayath, C., Salim, A., Palillam Veedu, A., Babu, P., Nair, B., Madhavan, A., & Pal, S. (2018). Characterization of the bacteriophages binding to human matrix molecules. *International Journal of Biological Macromolecules*, *110*, 608–615.

Poul, M.-A., Becerril, B., Nielsen, U. B., Morisson, P., & Marks, J. D. (2000). Selection of tumor-specific internalizing human antibodies from phage libraries. *Journal of Molecular Biology*, *301*(5), 1149–1161.

Poul, M. A., & Marks, J. D. (1999). Targeted gene delivery to mammalian cells by filamentous bacteriophage. *Journal of Molecular Biology*, *288*(2), 203–211.

Pride, D. T., Salzman, J., Haynes, M., Rohwer, F., Davis-Long, C., White, R. A., … Relman, D. A. (2012). Evidence of a robust resident bacteriophage population revealed through analysis of the human salivary virome. *The ISME Journal*, *6*(5), 915–926.

Priwitaningrum, D. L., Blondé, J. B. G., Sridhar, A., van Baarlen, J., Hennink, W. E., Storm, G., … Prakash, J. (2016). Tumor stroma-containing 3D spheroid arrays: A tool to study nanoparticle penetration. *Journal of Controlled Release*, *244*, 257–268.

Provenzano, P. P., Inman, D. R., Eliceiri, K. W., Knittel, J. G., Yan, L., Rueden, C. T., … Keely, P. J. (2008). Collagen density promotes mammary tumor initiation and progression. *BMC Medicine*, *6*, 11.

Przystal, J. M., Umukoro, E., Stoneham, C. A., Yata, T., O'Neill, K., Syed, N., & Hajitou, A. (2013). Proteasome inhibition in cancer is associated with enhanced tumor targeting by the adeno-associated virus/phage. *Molecular Oncology*, *7*,(1), 55–66.

Qiu, X. (2012). Heat Induced Capsid Disassembly and DNA Release of Bacteriophage λ. *PLoS ONE*, *7*(7), e39793.

Raja, J., Ludwig, J. M., Gettinger, S. N., Schalper, K. A., & Kim, H. S. (2018). Oncolytic virus immunotherapy: future prospects for oncology. *Journal for ImmunoTherapy of Cancer*, *6*(1), 140.

Rajkumar, T., & Gullick, W. J. (1994). The type I growth factor receptors in human breast cancer. *Breast Cancer Research and Treatment*, *29*(1), 3–9.

Ramnath, N., Dilling, T. J., Harris, L. J., Kim, A. W., Michaud, G. C., Balekian, A. A., … Arenberg, D. A. (2013). Treatment of stage III non-small cell lung cancer: Diagnosis and management of lung cancer, 3rd ed: American college of chest physicians evidence-based clinical practice guidelines. *Chest*, *143*(5 Suppl), e314S-e340S.

Rangel, R., Dobroff, A. S., Guzman-Rojas, L., Salmeron, C. C., Gelovani, J. G., Sidman, R. L., … Arap, W. (2013). Targeting mammalian organelles with internalizing phage (iPhage) libraries. *Nature Protocols*, *8*(10), 1916–1939.

Ranieri, G., Patruno, R., Ruggieri, E., Montemurro, S., Valerio, P., & Ribatti, D. (2006). Vascular endothelial growth factor (VEGF) as a target of bevacizumab in cancer: from the biology to the clinic. *Current Medicinal Chemistry*, *13*(16), 1845–1857.

Rau, D. C., Lee, B., Parsegian, V. A., & Evilevitch, A. (1984). Measurement of the repulsive force between polyelectrolyte molecules in ionic solution: hydration forces between parallel DNA double helices. *Proceedings of the National Academy of Sciences*, *81*(9), 2621–2625.

Razazan, A., Nicastro, J., Slavcev, R., Barati, N., Arab, A., Mosaffa, F., … Behravan, J. (2019). Lambda bacteriophage nanoparticles displaying GP2, a HER2/neu derived peptide, induce prophylactic and therapeutic activities against TUBO tumor model in mice. *Scientific Reports*, *9*, 2221.

Reyes, A., Haynes, M., Hanson, N., Angly, F. E., Heath, A. C., Rohwer, F., & Gordon, J. I. (2010). Viruses in the faecal microbiota of monozygotic twins and their mothers. *Nature*, *466*(7304), 334–338.

Ricciardelli, C., Mayne, K., Sykes, P. J., Raymond, W. A., McCaul, K., Marshall, V. R., & Horsfall, D. J. (1998). Elevated levels of versican but not decorin predict disease progression in early-stage prostate cancer. *Clinical Cancer Research*, *4*(4), 963–971.

Richter, M., & Zhang, H. (2005). Receptor-Targeted Cancer Therapy. *DNA and Cell Biology*, *24*(5), 271–282.

Riffle, S., & Hegde, R. S. (2017). Modeling tumor cell adaptations to hypoxia in multicellular tumor spheroids. *Journal of Experimental and Clinical Cancer Research*, *36*, 102.

Rizvi, S. A. A., & Saleh, A. M. (2018). Applications of nanoparticle systems in drug delivery technology. *Saudi Pharmaceutical Journal*, *26*(1), 64–70.

Roth, J. A., & Cristiano, R. J. (1997). Gene therapy for cancer: What have we done and where are we going? *Journal of the National Cancer Institute*, *89*(1), 21–39.

Rubin, B. A., Voronkov, L. A., & Zhivopistseva, I. V. (1975). [Adenine and pyridine nucleotides in forms of Verticillium dahliae Kleb. differing in pathogenicity]. *Doklady Akademii Nauk SSSR*, *224*(6), 1453–1455.

Russell, S., Wojtkowiak, J., Neilson, A., & Gillies, R. J. (2017). Metabolic Profiling of healthy and cancerous tissues in 2D and 3D. *Scientific Reports*, *7*(1), 15285.

Sacha, T. (2014). Imatinib in chronic myeloid leukemia: an overview. *Mediterranean Journal of Hematology and Infectious Diseases*, *6*(1), e2014007.

Santiago-Rodriguez, T. M., Ly, M., Bonilla, N., & Pride, D. T. (2015). The human urine virome in association with urinary tract infections. *Frontiers in Microbiology*, *6*, 14.

Santini, C., Brennan, D., Mennuni, C., Hoess, R. H., Nicosia, A., Cortese, R., & Luzzago, A. (1998). Efficient display of an HCV cDNA expression library as C-terminal fusion to the capsid protein D of bacteriophage lambda. *Journal of Molecular Biology*, *282*(1), 125–135.

Scaltriti, M., & Baselga, J. (2006). The epidermal growth factor receptor pathway: A model for targeted therapy. *Clinical Cancer Research*, *12*(18), 5268–5272.

Schwartz, A. L., Fridovich, S. E., & Lodish, H. F. (1982). Kinetics of internalization and recycling of the asialoglycoprotein receptor in a hepatoma cell line. *Journal of Biological Chemistry*, *257*(8), 4230–4237.

Scott, A. M., Wolchok, J. D., & Old, L. J. (2012). Antibody therapy of cancer. *Nat Rev Cancer*, *12*(4), 278–287.

Sen, A., Capitano, M. L., Spernyak, J. A., Schueckler, J. T., Thomas, S., Singh, A. K., … Repasky, E. A. (2011). Mild Elevation of Body Temperature Reduces Tumor Interstitial Fluid Pressure and Hypoxia and Enhances Efficacy of Radiotherapy in Murine Tumor Models. *Cancer Research*, *71*(11), 3872–3880.

Sevier, C. S., & Kaiser, C. A. (2002). Formation and transfer of disulphide bonds in living cells. *Nature Reviews Molecular Cell Biology*, *3*(11), 836–847.

Seynhaeve, A. L. B., Hoving, S., Schipper, D., Vermeulen, C. E., De Wiel-Ambagtsheer, G. A., Van Tiel, S. T., … Ten Hagen, T. L. M. (2007). Tumor necrosis factor a mediates homogeneous distribution of liposomes in murine melanoma that contributes to a better tumor response. *Cancer Research*, *67*(19), 9455–9462.

Shen, J., Ishii, Y., Xu, G., Dang, T. C., Hamashima, T., Matsushima, T., … Sasahara, M. (2012). PDGFR-B as a positive regulator of tissue repair in a mouse model of focal cerebral ischemia. *Journal of Cerebral Blood Flow and Metabolism*, *32*(2), 353–367.

Shi, F., Telesco, S. E., Liu, Y., Radhakrishnan, R., & Lemmon, M. A. (2010). ErbB3/HER3 intracellular domain is competent to bind ATP and catalyze autophosphorylation. *Proceedings of the National Academy of Sciences*, *107*(17), 7692–7697.

Shi, K., Zhou, J., Zhang, Q., Gao, H., Liu, Y., Zong, T., & He, Q. (2015). Arginine-Glycine-Aspartic Acid-Modified Lipid-Polymer Hybrid Nanoparticles for Docetaxel Delivery in Glioblastoma Multiforme. *Journal of Biomedical Nanotechnology*, *11*(3), 382–391.

Shimamoto, G., Gegg, C., Boone, T., & Quéva, C. (2012). Peptibodies: A flexible alternative format to antibodies. *MAbs*, *4*(5), 586–591.

Simonsen, T. G., Gaustad, J. V., Leinaas, M. N., & Rofstad, E. K. (2012). High interstitial fluid pressure is associated with tumor-line specific vascular abnormalities in human melanoma xenografts. *PLoS ONE*, *7*(6).

Sims, L. B., Curtis, L. T., Frieboes, H. B., & Steinbach-Rankins, J. M. (2016). Enhanced uptake and transport of PLGA-modified nanoparticles in cervical cancer. *Journal of Nanobiotechnology*, *14*(1).

Smith, T. L., Souza, G. R., Sidman, R. L., Arap, W., & Pasqualini, R. (2017). An AAVP-based solid-phase transducing matrix for transgene delivery: Potential for translational applications. *Cancer Gene Therapy*, *24*(8), 358–360.

Sokolenko, S., Nicastro, J., Slavcev, R., & Aucoin, M. G. (2012). Graphical analysis of flow cytometer data for characterizing controlled fluorescent protein display on ?? phage. *Cytometry Part A*, *81 A*(12), 1031–1039.

Solmi, R., Lauriola, M., Francesconi, M., Martini, D., Voltattorni, M., Ceccarelli, C., … Strippoli, P. (2008). Displayed correlation between gene expression profiles and submicroscopic alterations in response to cetuximab, gefitinib and EGF in human colon cancer cell lines. *BMC Cancer*, *8*.

Solomon, B. (2008). Filamentous bacteriophage as a novel therapeutic tool for Alzheimer's disease treatment. *J Alzheimers Dis*, *15*(2), 193–198.

Sonveaux, P., Copetti, T., De Saedeleer, C. J., Végran, F., Verrax, J., Kennedy, K. M., … Feron, O. (2012). Targeting the Lactate Transporter MCT1 in Endothelial Cells Inhibits Lactate-Induced HIF-1 Activation and Tumor Angiogenesis. *PLoS ONE*, *7*(3), e33418.

Soothill, J. S. (1994). *Bacteriophage prevents destruction of skin grafts by Pseudomonas aeruginosa* (Vol. 20). Retrieved from https://journals.scholarsportal.info/pdf/03054179/v20i0003/209_bpdosgbpa.xml

Sorkin, A. (2001). Internalization of the epidermal growth factor receptor: role in signalling. *Biochemical Society Transactions*, *29*(Pt 4), 480–484.

Souriau, C., Fort, P., Roux, P., Hartley, O., Lefranc, M. P., & Weill, M. (1997). A simple luciferase assay for signal transduction activity detection of epidermal growth factor displayed on phage. *Nucleic Acids Research*, *25*(8), 1585–1590.

Sriraman, S. K., Aryasomayajula, B., & Torchilin, V. P. (2014a). Barriers to drug delivery in solid tumors. *Tissue Barriers*, *2*(3), e29528-1-e29528-10.

Sternberg, N., & Hoess, R. H. (1995). Display of peptides and proteins on the surface of bacteriophage lambda. *Proceedings of the National Academy of Sciences of the United States of America*, *92*(5), 1609–1613.

Sternberg, N., & Weisberg, R. (1977). Packaging of coliphage lambda DNA. II. The role of the gene D protein. *Journal of Molecular Biology*, *117*(3), 733–759.

Su, J. L., Lai, K. P., Chen, C. A., Yang, C. Y., Chen, P. S., Chang, C. C., … Wei, L. H. (2005). A novel peptide specifically binding to interleukin-6 receptor (gp80) inhibits angiogenesis and tumor growth. *Cancer Research*, *65*(11), 4827–4835.

Subramanian, B. C., Moissoglu, K., & Parent, C. A. (2018). The LTB 4 –BLT1 axis regulates the polarized trafficking of chemoattractant GPCRs during neutrophil chemotaxis. *Journal of Cell Science*, *131*(18), jcs217422.

Sugahara, K. N., Braun, G. B., de Mendoza, T. H., Kotamraju, V. R., French, R. P., Lowy, A. M., … Ruoslahti, E. (2015). Tumor-Penetrating iRGD Peptide Inhibits Metastasis. *Molecular Cancer Therapeutics*, *14*(1), 120–128.

Svishchev, I. M., & Goncharov, V. V. (1990). Structure of water and aqueous solutions of nonelectrolytes, according to1H NMR data. II. Water-alcohol solutions. Topology of network of hydrogen bonds with low concentrations of alcohols, and bulk properties. *Journal of Structural Chemistry*, *31*(3), 432–437.

Taniguchi, H., Baba, Y., Sagiya, Y., Gotou, M., Nakamura, K., Sawada, H., … Baba, H. (2018). Biologic Response of Colorectal Cancer Xenograft Tumors to Sequential Treatment with Panitumumab and Bevacizumab. *Neoplasia (New York, N.Y.)*, *20*(7), 668–677.

Telesco, S. E., Shih, A. J., Jia, F., & Radhakrishnan, R. (2011). A multiscale modeling approach to investigate molecular mechanisms of pseudokinase activation and drug resistance in the HER3/ErbB3 receptor tyrosine kinase signaling network. *Molecular BioSystems*, *7*(6), 2066–2080.

Tong, R. T., Boucher, Y., Kozin, S. V., Winkler, F., Hicklin, D. J., & Jain, R. K. (2004). Vascular normalization by vascular endothelial growth factor receptor 2 blockade induces a pressure gradient across the vasculature and improves drug penetration in tumors. *Cancer Research*, *64*(11), 3731–3736.

Toole, B. P., & Slomiany, M. G. (2008). Hyaluronan: A constitutive regulator of chemoresistance and malignancy in cancer cells. *Seminars in Cancer Biology*, *18*(4), 244–250.

Torchilin, V. P. (2005). Recent advances with liposomes as pharmaceutical carriers. *Nature Reviews. Drug Discovery*, *4*(2), 145–160.

Tredan, O., Galmarini, C. M., Patel, K., & Tannock, I. F. (2007). Drug Resistance and the Solid Tumor Microenvironment. *JNCI Journal of the National Cancer Institute*, *99*(19), 1441–1454.

Urbanelli, L., Ronchini, C., Fontana, L., Menard, S., Orlandi, R., & Monaci, P. (2001). Targeted gene transduction of mammalian cells expressing the HER2/neu receptor by filamentous phage. *Journal of Molecular Biology*, *313*(5), 965–976.

Vainshtein, I., Roskos, L. K., Cheng, J., Sleeman, M. A., Wang, B., & Liang, M. (2015). Quantitative Measurement of the Target-Mediated Internalization Kinetics of Biopharmaceuticals. *Pharmaceutical Research*, *32*(1), 286–299.

Van Belleghem, J. D., Dąbrowska, K., Vaneechoutte, M., Barr, J. J., & Bollyky, P. L. (2019). Interactions between bacteriophage, bacteria, and the mammalian immune system. *Viruses*, *11*(1), e10.

Van Cutsem, E., Köhne, C.-H., Hitre, E., Zaluski, J., Chang Chien, C.-R., Makhson, A., … Rougier, P. (2009). Cetuximab and Chemotherapy as Initial Treatment for Metastatic Colorectal Cancer. *New England Journal of Medicine*, *360*(14), 1408–1417.

Varde, N. K., & Pack, D. W. (2004). Microspheres for controlled release drug delivery. *Expert Opinion*

*on Biological Therapy*, *4*(1), 35–51.

Vaupel, P. (2004). Tumor microenvironmental physiology and its implications for radiation oncology. *Seminars in Radiation Oncology*, *14*(3), 198–206.

Vaupel, P., Kallinowski, F., & Okunieff, P. (1989). Blood Flow, Oxygen and Nutrient Supply, and Metabolic Microenvironment of Human Tumors: A Review. *Cancer Research*, *49*(23), 6449–6465.

Venook, A. P., Niedzwiecki, D., Lenz, H. J., Innocenti, F., Fruth, B., Meyerhardt, J. A., … Blanke, C. (2017). Effect of first-line chemotherapy combined with cetuximab or bevacizumab on overall survival in patients with KRAS wild-type advanced or metastatic colorectal cancer a randomized clinical trial. *Journal of the American Medical Association*, *317*(23), 2392–2401.

Vermeulen, L., Todaro, M., de Sousa Mello, F., Sprick, M. R., Kemper, K., Perez Alea, M., … Medema, J. P. (2008). Single-cell cloning of colon cancer stem cells reveals a multi-lineage differentiation capacity. *Proceedings of the National Academy of Sciences*, *105*(36), 13427–13432.

Vlahovic, G., Rabbani, Z. N., Herndon, J. E., Dewhirst, M. W., & Vujaskovic, Z. (2006). Treatment with Imatinib in NSCLC is associated with decrease of phosphorylated PDGFR-β and VEGF expression, decrease in interstitial fluid pressure and improvement of oxygenation. *British Journal of Cancer*, *95*(8), 1013–1019.

Vukovic, V., & Tannock, I. F. (1997). Influence of low pH on cytotoxicity of paclitaxel, mitoxantrone and topotecan. In *British Journal of Cancer*, *75*(8), 1167–1172.

Walker, K. A., Murray, T., Hilditch, T. E., Wheldon, T. E., Gregor, A., & Hann, I. M. (1988). A tumour spheroid model for antibody-targeted therapy of micrometastases. *British Journal of Cancer*, *58*(1), 13–16.

Wan, P. T. C., Garnett, M. J., Roe, S. M., Lee, S., Niculescu-Duvaz, D., Good, V. M., … Cancer Genome Project. (2004). Mechanism of activation of the RAF-ERK signaling pathway by oncogenic mutations of B-RAF. *Cell*, *116*(6), 855–867.

Wang, Q., Villeneuve, G., & Wang, Z. (2005). Control of epidermal growth factor receptor endocytosis by receptor dimerization, rather than receptor kinase activation. *EMBO Reports*, *6*(10), 942–948.

Wang, T. H., Hsia, S. M., & Shieh, T. M. (2017). Lysyl oxidase and the tumor microenvironment. *International Journal of Molecular Sciences*, *18*(1), 62.

Waterman, H., Sabanai, I., Geiger, B., & Yarden, Y. (1998). Alternative intracellular routing of ErbB receptors may determine signaling potency. *Journal of Biological Chemistry*, *273*(22), 13819–13827.

Weber-Dabrowska, B., Zimecki, M., & Mulczyk, M. (2000). Effective phage therapy is associated with normalization of cytokine production by blood cell cultures. *Archivum Immunologiae et Therapiae Experimentalis*, *48*(1), 31–37.

Wieduwilt, M. J., & Moasser, M. M. (2008). The epidermal growth factor receptor family: biology driving targeted therapeutics. *Cellular and Molecular Life Sciences : CMLS*, *65*(10), 1566–1584.

Wiley, H. S. (1988). Anomalous binding of epidermal growth factor to A431 cells is due to the effect of

high receptor densities and a saturable endocytic system. *Journal of Cell Biology*, *107*(2), 801–810.

Willett, C. G., Boucher, Y., di Tomaso, E., Duda, D. G., Munn, L. L., Tong, R. T., … Jain, R. K. (2004). Direct evidence that the VEGF-specific antibody bevacizumab has antivascular effects in human rectal cancer. *Nature Medicine*, *10*(2), 145–147.

Wong, S. F. (2005). Cetuximab: An epidermal growth factor receptor monoclonal antibody for the treatment of colorectal cancer. *Clinical Therapeutics*, *27*(6), 684–694.

Xie, Y. M., & Hung, M. C. (1994). Nuclear localization of P185neu Tyrosine kinase and its association with transcriptional transactivation. *Biochemical and Biophysical Research Communications*, *203*(3), 1589–1598.

Xu, C. F., & Solomon, E. (1996). Mutations of the BRCA1 gene in human cancer. *Seminars in Cancer Biology*, *7*(1), 33–40.

Xu, H., Yu, Y., Marciniak, D., Xu, H., Yu, Y., & Marciniak, D. (2005). Epidermal growth factor receptor ( EGFR ) − related protein inhibits multiple members of the EGFR family in colon and breast cancer cells Epidermal growth factor receptor ( EGFR )– related protein inhibits multiple members of the EGFR family in colon and. *Molecular Cancer Therapeutics*, *3*(12), 435–442.

Yang, C. H., Wu, P. C., Huang, Y. Bin, & Tsai, Y. H. (2004). A new approach for determining the stability of recombinant human epidermal growth factor by thermal fourier transform infrared (ftir) microspectroscopy. *Journal of Biomolecular Structure and Dynamics*, *22*(1), 101–110.

Yang, J. L., Qu, X. J., Russell, P. J., & Goldstein, D. (2004). Regulation of epidermal growth factor receptor in human colon cancer cell lines by interferon α. *Gut*, *53*(1), 123-9.

Yao, K., Gietema, J. A., Shida, S., Selvakumaran, M., Fonrose, X., Haas, N. B., … O'Dwyer, P. J. (2005). In vitro hypoxia-conditioned colon cancer cell lines derived from HCT116 and HT29 exhibit altered apoptosis susceptibility and a more angiogenic profile in vivo. *British Journal of Cancer*, *93*(12), 1356–1363.

Yata, T., Lee, E. L. Q., Suwan, K., Syed, N., Asavarut, P., & Hajitou, A. (2015). Modulation of extracellular matrix in cancer is associated with enhanced tumor cell targeting by bacteriophage vectors. *Molecular Cancer*, *14*, 110.

Ying, X., Wen, H., Lu, W. L., Du, J., Guo, J., Tian, W., … Zhang, Q. (2010). Dual-targeting daunorubicin liposomes improve the therapeutic efficacy of brain glioma in animals. *Journal of Controlled Release*, *141*(2), 183–192.

Yoshida, T., Okamoto, I., Okabe, T., Iwasa, T., Satoh, T., Nishio, K., … Nakagawa, K. (2007a). Matuzumab and cetuximab activate the epidermal growth factor receptor but fail to trigger downstream signaling by Akt or Erk. *International Journal of Cancer*, *122*(7), 1530–1538.

Yoshida, T., Okamoto, I., Okabe, T., Iwasa, T., Satoh, T., Nishio, K., … Nakagawa, K. (2007b). Matuzumab and cetuximab activate the epidermal growth factor receptor but fail to trigger downstream signaling by Akt or Erk. *International Journal of Cancer*, *122*(7), 1530–1538.

Yu, D., & Hung, M. C. (2000). Overexpression of ErbB2 in cancer and ErbB2-targeting strategies. *Oncogene*, *19*(53), 6115–6121.

Yuan, F., Leunig, M., Kun Huang, S., Berk, D. A., Papahadjopoulos, D., & Jam, R. K. (1994). Microvascular Permeability and Interstitial Penetration of Sterically Stabilized (Stealth) Liposomes in a Human Tumor Xenograft' reveal heterogeneous distribution of liposomes in tumor interstitium. *Cancer Research*, *54*(13), 3352-3356.

Yue, B. (2014). Biology of the extracellular matrix: An overview. *Journal of Glaucoma*, *23*(8), S20–S23.

Yuen, S. T., Davies, H., Chan, T. L., Ho, J. W., Bignell, G. R., Cox, C., … Wooster, R. (2002). Advances in Brief Similarity of the Phenotypic Patterns Associated with BRAF and KRAS Mutations. *Cancer Resarch*, *62*, 6451–6455.

Zakharova, M. Y., Kozyr, A. V., Ignatova, A. N., Vinnikov, I. A., Shemyakin, I. G., & Kolesnikov, A. V. (2005). Purification of filamentous bacteriophage for phage display using size-exclusion chromatography. *BioTechniques*, *38*(2), 194–198.

Zanoni, M., Piccinini, F., Arienti, C., Zamagni, A., Santi, S., Polico, R., … Tesei, A. (2016). 3D tumor spheroid models for in vitro therapeutic screening: a systematic approach to enhance the biological relevance of data obtained. *Scientific Reports*, *6*(1), 19103.

Zhang, Q., Xiao, H., Jin, F., Li, M., Luo, J., & Wang, G. (2018). Cetuximab improves azd6244 antitumor activity in colorectal cancer ht29 cells in vitro and in nude mice by attenuating her3/akt pathway activation. *Oncology Letters*, *16*(1), 326-334.

Zhao, B., Wang, L., Qiu, H., Zhang, M., Sun, L., Peng, P., … Yuan, X. (2017). Mechanisms of resistance to anti-EGFR therapy in colorectal cancer. *Oncotarget*, *8*(3), 3980–4000.

Zong, T., Mei, L., Gao, H., Cai, W., Zhu, P., Shi, K., … He, Q. (2014). Synergistic dual-ligand doxorubicin liposomes improve targeting and therapeutic efficacy of brain glioma in animals. *Molecular Pharmaceutics*, *11*(7), 2346–2357.